LA-UR- 94-2892
C.1

LA-UR-94-2892
C. 1

THE LOS ALAMOS ARZAMAS-16 HIGH MAGNETIC FIELD SHOT SERIES, ANCHO CANYON SITE, DECEMBER, 1993

by

C. M. Fowler and B. L. Freeman

DX-15 Shock Wave Physics Group

Los Alamos National Laboratory
Los Alamos, New Mexico 87544

DX-15:GR-94-2

August, 1994

With appended contributions from:

M. G. Sheppard, et al., X-5
J. M. Christian, DX-15
L. R. Veeser, P-14
B. R. Marshall, EG&G, Santa Barbara
W. D. Zerwekh, DX-15
J. D. Goettee, et al., DX-15 (post doctoral appointee)
V. V. Druzhinen, et al., Arzamas-16, Russia

Distribution listed on page 27

LOS ALAMOS NATIONAL LABORATORY
3 9338 00202 8784

DO NOT CIRCULATE

PERMANENT RETENTION

TABLE OF CONTENTS

		PAGE NUMBER
	TABLE OF CONTENTS	i
	PHOTOGRAPH OF RUSSIAN VISITORS	ii
	PREFACE	1
I.	INTRODUCTION	4
II.	THE MC-1 GENERATOR	4
III.	FIRING COMPATIBILITY	6
	3.1 The Explosive System	6
	3.2 Electrical Compatibility	9
IV.	FIELD AND CURRENT MEASUREMENTS	10
V.	HTSC MEASUREMENTS	12
	5.1 Earlier Los Alamos Studies at Lower Fields	13
	5.2 Microwave Diagnostics	17
	5.3 Compilation of Data	18
VI.	NON-LINEAR FARADAY ROTATION IN CdS	20
	6.1 Early Los Alamos Experiments	20
	6.2 The CdS Add-on Experiment	22
	6.3 Further Data	23
	GROUP PHOTOGRAPH	24
	REFERENCES	25
	DISTRIBUTION LIST	27
	APPENDIX, (contains Refs. 2,3,4,6,10,11,12,19,21,23)	28




rooms
Welcome
Pajarito Pl

PREFACE

An historic collaboration took place at Los Alamos during the last few weeks of 1993. A group of eight Russians from Arzamas 16 joined a team of Los Alamos and other U.S. people to conduct a series of high magnetic field explosive shots at Ancho Canyon Site (TA-39), a Los Alamos Security area.

The test series was built around the MC-1 high magnetic field generators developed by Pavlovskii *et al.*[1] This explosive-driven cylindrical flux compressor develops magnetic fields in the vicinity of 1000 T (10 MG).

As detailed later, the exercise first required testing and adapting Los Alamos explosives to Russian hardware and carrying out magneto hydrodynamic calculations that guided several aspects of the program. The use of different kinds of explosives in the first two shots helped benchmark some of these codes. Following these system characterization shots, subsequent solid-state investigations using the remaining assemblies led to the value of the low-temperature upper-critical magnetic field for the high-temperature super-conductor YBCO, and to new information on the non-linear Faraday effect in CdS. Considerable effort went into the preparation of the super-conductor samples and to various assemblies for Faraday rotation measurements. Finally, a microwave (94-GHz) system was developed and used to detect the superconducting transition.

We have organized this report in the following way: background material pertinent to the collaboration and to the makeup of the shot series is given in Sec. 1, while details of the MC-1 high-magnetic field generators are given in Sec. 2. Details of the explosive system and compatibility test are given in Sec. 3. Magnetic field and current measurements are discussed in Sec. 4. Included here are results of the benchmarking tests. The high-temperature super-conductor shots are treated in Sec. 5 and the CdS Faraday rotation experiment is discussed in Sec. 6.

The authors found it a difficult task to adequately acknowledge the outstanding contributions made by a large number of people, all of whom were required to make the program successful. We decided to associate the American people with more or less specific program activities, although in many cases their activities were considerably more extensive.

• Russian Delegation. Our Russian visitors are shown in the photograph facing this page. From left to right they are Alexander Bykov, head of the delegation, Mikhail Dolotenko, Olga Tatsenko, Nikolai Kolokolchikov, Elena Gerdova, Yuri Kudasov, Vadim Platonov and Elena Panevkina.

• Administrative Support. The international aspects of the collaboration were spearheaded by Stephen Younger (ADNWT), Irvin Lindemuth (X-5), and Robert Reinovsky (DX-DO). Bob had many additional responsibilities since he was the Group Leader of DX-15 at this time. He handled these duties in exemplary fashion.

Many other support functions involving safety, secretarial, security, logistics, etc., were expertly handled by Emmanuel Lopez, Janet Neff, Kathryn Smith, Samia Davis, Tony Valerio, and Pita Valencia (DX-15), and Eva Roybal (NWT/ICF).

• Interpreters. The demanding task of Russian-English translation was ably handled by Elena Gerdova and Elena Panevkina (two of our Russian visitors), and by Eugene Kutyreff (NIS-10). Additionally, Wilfred Lewis (EG&G, Santa Barbara) supplemented his primary scientific activities by often serving as an interpreter.

• The fabrication and testing of the required explosives were overseen by J. M. Christian. The following people played key roles in this crucial part of the exercise: Michael Christian and Stanley Marsh (DX-15); John Horne and Robert Montoya (DX-16); Larry Hatler, Doug Hemphill, Jack Markham, and Bart Olinger (ESA-2).

• Overall Shot Assembly and Firing. James King served as the Firing Point Supervisor for the entire series. The DX-15 Firing Point Team included James King, Dennis Herrera, Tommy Herrera, Kerry Sowder, and David Torres. Besides assembling and firing the systems, they also ensured the safety of personnel at the firing site.

• Magneto Hydrodynamic Modeling and Calculations. As noted earlier, these calculations often served as an experimental guide. They were carried out by John Brownell, Carl Lund, and Maurice Sheppard (X-5).

• Faraday Samples. Faraday sample assemblies were furnished by Wilfred Lewis, Bruce Marshall, and Guy Leach (EG&G, Santa Barbara). Included were quartz and crown glass field diagnostic assemblies and CdS samples for the non-linear Faraday rotation studies.

• B-dot Probes. B-dot probes are the primary magnetic field diagnostic used at Los Alamos. Several of these probes for each shot were constructed and calibrated by Bruce Freeman and Kerry Sowder (DX-15).

• Microwave System. The microwave system was the primary diagnostic tool used in the YBCO experiments. The system was designed and assembled by William Zerwekh (DX-15) and Bill Papatheofanis (P-14).

• YBCO Samples. Availability of good samples was a key factor in the successful YBCO studies. These samples were made and characterized by Fernando Garzon, Robert Houlton, Catherine Mombourquette, and David Reagor (MTL-11) and by Quanxi Jia and Xin Di Wu (MTL-STC).

• Cryogenic Setup and Control. Control and measurement of the sample temperatures was a key requirement in the YBCO studies. Jeffrey Goettee (DX-15 Post-Doc) and James King (DX-15) handled this part of the program.

• Optical and Microwave Data Recording. Data from fiber-optic current belts, Faraday field sensors, and microwaves were recorded (and partly installed in the shot assemblies) by Lynn Veeser, George Allred, Donald Bartram, Bill Papatheofanis, and Patrick Rodriguez (P-14); and William Zerwekh (DX-15). The near-perfect acquisition of these data was a key element to the success of the program.

• Russian Activities. The Russian people were interested and helpful observers and eager to pitch in where help was needed. Nikolai Kolokolchikov was invaluable to the Firing Point team, in particular with generator assembly and probe placement. Vadim Platonov and Yuri Kudasov contributed greatly to the YBCO experiments, both in assembling the system and in the microwave diagnostic and temperature control aspects of the experiments. Olga Tatsenko was particularly helpful in the Faraday rotation work and in preliminary analysis of the solid-state data. Mikhail Dolotenko served as a right-hand man to Bruce Freeman in the overall coordination of the shots. Additionally, he spent a considerable fraction of his time with the X-5 calculation team. Alexander Bykov assured the appropriate meshing of the Russian team with the Los Alamos group, and maintained an overall perspective of the program. We considered the excellent cooperation achieved by the American and Russians teams to be a major highlight of the collaboration.

• The Tallahassee Meeting. At the close of the program, it was agreed that we would meet again in a few months to go over the data acquired with the aim of publishing some of the results. Dr. Jack Crow, head of the National High Magnetic Field Laboratory (NHMFL) in Tallahassee, FL, kindly made Laboratory facilities available to us for this meeting, that took place May 23–27, 1994. He was a most gracious and helpful host. Dwight Rickel, of the Los Alamos branch of the NHMFL handled the demanding task of organizing the meeting in expert fashion.

Various subjects of interest to the high-magnetic field community were discussed at this meeting. Among them were some considerations of MG-VII, to be hosted by ARZAMAS-16 in 1996, plans for a meeting of theorists to explore possible applications of multimegagauss fields; ways to better acquaint the scientific community with this branch of physics; and ways to encourage wider participation in future high-field experiments.

The analysis and compilation of data led to two papers to be presented at International Conferences (attached to this report) and near completion of a third paper. Plans were made for a more extensive YBCO review paper and a study of the influence of HE type on the MC-1 performance pending continued high magnetic field collaboration.

I. INTRODUCTION

The origin of this program had its roots in general discussions, held at various Megagauss conferences, about the possibility of developing 20-MG and higher systems. These discussions were followed somewhat later by a letter from Alexander Pavlovskii[2] proposing a joint collaboration to try to develop such a system.* It was not possible at that time to consider such a collaboration. However, a couple of years later, such arrangements were being widely discussed, and a collaboration agreement was suggested.[3] Eventually, a wider ranging collaboration[4] was negotiated that included the purchase of five sets of MC-1 hardware. As a first step toward the high-field collaboration, it was agreed that some joint high-field, solid-state experiments would also be undertaken, in addition to code bench-marking experiments with these systems that would aid in the future design of the 20-MG system. As originally planned, about a year before the joint exercise was done, the five MC-1 assemblies were to be used as follows.

1. Two of the generators would be used to characterize the system dynamics by using two different drive explosives, Composition B and PBX-9501. The experimental flux compression dynamics would be compared to those predicted by the codes.

2. The other three generators would be used to measure the low-temperature, critical magnetic field of the high-temperature superconductor $YBa_2Cu_3O_7$ (YBCO).

Both the Arzamas 16 and Los Alamos groups have had significant prior interest in both these topics, as noted later.

It was understood at the outset that the main explosive charges (15–20 kg) would be made at Los Alamos. An additional complication arose, because of shipping restrictions, when it turned out that Los Alamos would also have to load the initiation systems, even though they required only very small amounts of explosives.

An additional experiment was carried out in the last shot, the measurement of the Faraday rotation in CdS to investigate the previously observed magnetic field dependence of the Verdet coefficient at high magnetic fields.

II. THE MC-1 GENERATOR

The most recent overview of the MC-1 generator is given by Pavlovskii.[5] From this overview and earlier articles by the Pavlovskii team, Sheppard *et al.*[6] have summarized the main features of the generators most pertinent to the present program. The descriptions that follows is essentially a verbatim quote from the section of their report entitled "MC-1 Description." A complete copy of this report is attached.

A diagram of the MC-1 system is presented in Fig. 1. Figures 2 and 3 are photographs of this basic assembly and some of the components used in the experiments. The HE cylinder, which in the Russian experiments has been composed of a 50/50 RDX/TNT mix, is detonated simultaneously on its outer diameter by a ring of ten block initiators.

---

*Copies of Refs. 2, 3 and 4 are attached to this report.

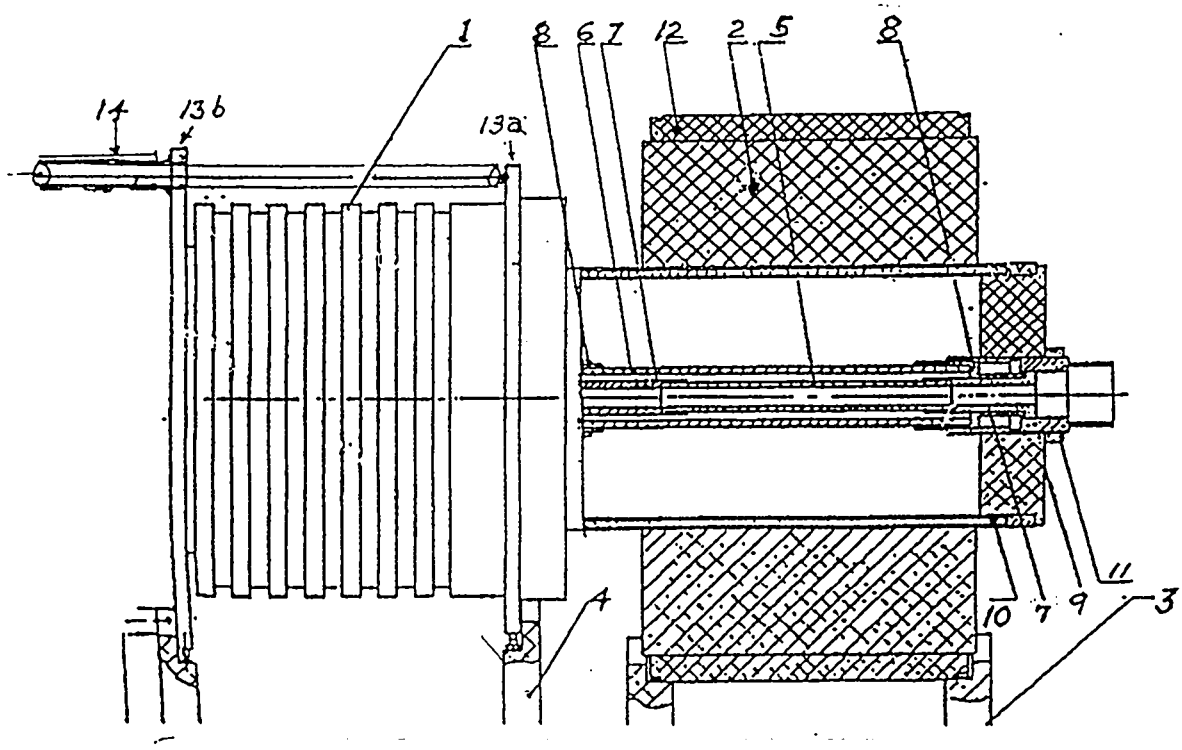


Fig. 1. MC-1 generator with three cascades. 1-insulated current feed for solenoid, 2-explosive charge, 3,4- support stands. 5-3rd cascade, 6-2nd cascade,7,8,9-foam support cradles for cascades,10-solenoid (first cascade),11- assembley nut, 12-initiator block, 13a,b-ring electrodes to which solenoid cascade wires are connected. The solenoid wires are connected to a while the return wires, parallel to the cylinder axis, are connected to b. 14-one of the coaxial cables (usually twenty-four) connecting the capacitor bank to the solenoid. The center core of the cable is connected to 13a, the ground braid to 13b.

Inside the HE of Fig. 1 are three concentric cylindrical shells, known as cascades in the Russian literature, made of a unique copper-epoxy composite. These shells successively take on the role of armature during implosion. The shells are made of hundreds of 0.25-mm diameter, enamel-coated, copper threads arranged side by side in layers and secured in a casting of epoxy. The 500 copper threads of the outer cascade are wound in a two-turn solenoid and then brought back along the outside diameter, parallel with the cylindrical axis, to complete the return current path. As noted on Fig. 1, the many solenoid input wires are connected to the ring electrode (13a) while the outer return wires are connected to the other ring electrode (13b). The solenoid cascade is impregnated with epoxy and cured. The outside diameters of all three cascades, which are cast with a thicker layer of epoxy, are machined smooth to inhibit hydrodynamics instabilities. An initial magnetic field, of up to 220 kG (typically 130-160 kG), is created by discharging a capacitor through the first cascade. Coaxial cables from the capacitor bank are connected to the outer cascade as noted in Fig. 1 (14). The discharge is timed so that peak field is achieved just as the HE detonation wave reaches the first cascade. Upon contact the HE shock breaks down the

insulation between the solenoid threads and transforms the first cascade into a conducting cylinder—trapping and then compressing the initial field as the shell begins to move.

The second and third cascades are similarly constructed except that all of the copper threads are laid parallel to the axis. Before a cascade is contacted and shocked from outside, it cannot conduct current in the solenoidal direction. Hence, it is transparent to the axial field that is being compressed by the preceding shell. On contact, however, the cascade is transformed by the shock into a conducting cylinder, which traps the field inside as the new cascade becomes the new armature.

The use of multiple cascades serves two important functions. The first benefit of multiple cascades is the velocity enhancement that is derived from collisions of heavy outer shells with lighter inner shells. The second (and more crucial) benefit is related to implosion stability. As the outer cascade compresses flux, magnetic and hydrodynamic instabilities tend to disrupt the shell. These instabilities are made worse by the inherent perturbations associated with the copper-epoxy composite. The inner cascades are strategically placed to recollect and smooth out the perturbations before the outer cascade is disrupted. The loss of flux that is incurred during the transition is offset by achieving a more stable and reproducible implosion

In the early systems developed by Fowler, Garn, and Caird,[7] initial field coils were also placed under the explosive charge. While very large fields were obtained (up to 14 MG), performance was erratic. The use of additional Pavlovskii cascades would presumably have led to better reproducibility. An alternative approach to controlling the instability was investigated by Caird *et al.*[8,9] They placed the solenoid outside of the HE and used a single stainless steel armature. On the timescales of the initial capacitor discharge, the stainless steel armature allowed magnetic flux to diffuse inside the cylinder; but on the short timescale of the implosion, the flux was essentially trapped and compressed. However, the poorer coupling of the initial coils with the armature results in substantially lower initial and, therefore, also final compressed fields.

Figure 2 is a photograph of the MC-1 generator (with a mockup explosive charge) before the second and third cascades have been installed. The two electrode rings, to which the capacitor bank cables will be installed, are clearly evident. The second and third cascades are shown in Fig. 3. Mounting disks that center the cascades are shown for the second, larger cascade, but not for the smaller, third cascade. The highest magnetic fields are obtained when all three cascades are used. However, fields of several megagauss are still obtained when only the first two cascades are used. The third item shown in Fig. 3 (right) is a Styrofoam cryostat that fits inside the second cascade. The cryostat was used in the high temperature superconductor experiments and is described later.

III. FIRING COMPATIBILITY

The successful transfer of MC-1 technology to Ancho Canyon required adapting our explosive systems and our capacitor bank to their hardware.

3.1 The Explosive System

Most of the following comments are extracted, some almost verbatim, from a report by Christian,[10] a copy of which is attached to this document.

The MC-1 generator's first stage (see Fig. 1) uses ten foam blocks loaded with extrudable explosive to initiate the surface of an HE-ring (300-mm OD × 150-mm ID × 183-mm high), which in turn implodes the first cascade.

The impracticality of rapidly shipping anything but inert parts from Russ[illegible] Los Alamos dictated that we not only fabricate the main cylindrical ring charges at Los Alamos, but also load the Russian Initiation Blocks (RIBs) here.

The Russian HE is a mix of equal parts of RDX and TNT, somewhat less energetic than our Comp B variety, which is 60% RDX and 40% TNT, the explosive we intended to use for most of the subsequent tests, (as noted later, PBX-9501 HE was used for one of the charges).

Finally, we note that the Russians connect the RIB detonators in series and therefore use a high-voltage (60-kV) firing unit, whereas we employ a 2.5-kV firing unit, but fire the detonators in parallel.

These technical differences provided the impetus for us to verify by test that the Los Alamos HE substitutes would be hydrodynamically acceptable. Although a number of test alternatives were considered, we decided on a simple framing camera experiment as an ideal way to check the performance of the system. A number of strategically placed arrival time pins were also deployed in the test system.

Rather than using an entire HE cylinder, it was decided that only half of a cylinder would be adequate for the test and that, further, only the three central RIBs would be adequate, (instead of the five that would cover half a cylinder). As customary here, the RIBs detonators were fired in parallel. The first cascade, made of fine copper wire and epoxy in the actual systems, was simulated by a 7-mm-thick annealed 6061 aluminum liner, curved to fit the inside HE diameter.

Many technical details dealing with the test and other aspects of the explosive system are available in Ref. 10. Here, however, we present only the conclusions:

Conclusions

The combination of the XTX-8003-loaded RIBs and the closely fitted Comp B charge functioned very effectively as a large-area cylindrical lens with stable convergent flow characteristics ideally suited for MC-1 generator applications. On the strength of these test results, cylindrical HE charges (four Comp B and one PBX-9501) and hand-loaded RIBs were ordered for the entire shot series, with every confidence of proper performance. The RIB detonators were fired in parallel for this experiment, as is customary here. The favorable outcome reinforced our assertion that the ten RIBs in the final assemblies would perform satisfactorily when fired in parallel, although the Russians typically fire them in series using a high-voltage (60-kV) firing unit.

3.2 Electrical Compatibility

For most of their experiments, the Russians put an initial current of approximately 2 MA into the first cascade to generate the initial required flux.

The capacitor bank used at Arzamas-16 to supply the current, stored considerably more energy than two modules of the Los Alamos bank. However, owing to a very large

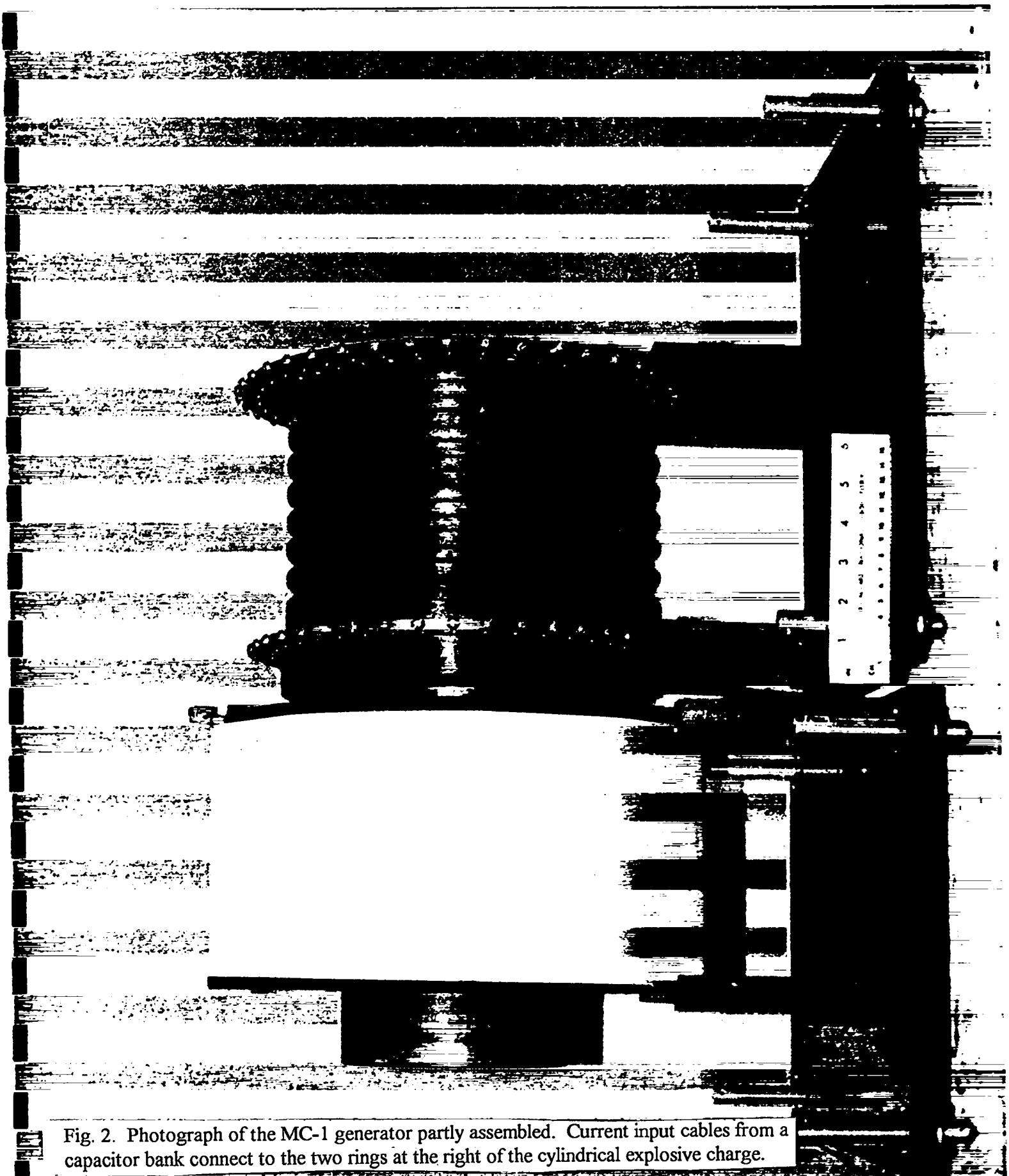


Fig. 2. Photograph of the MC-1 generator partly assembled. Current input cables from a capacitor bank connect to the two rings at the right of the cylindrical explosive charge.

Los Alamos
Los Alamos National Laboratory
Los Alamos, New Mexico 87545
Photography

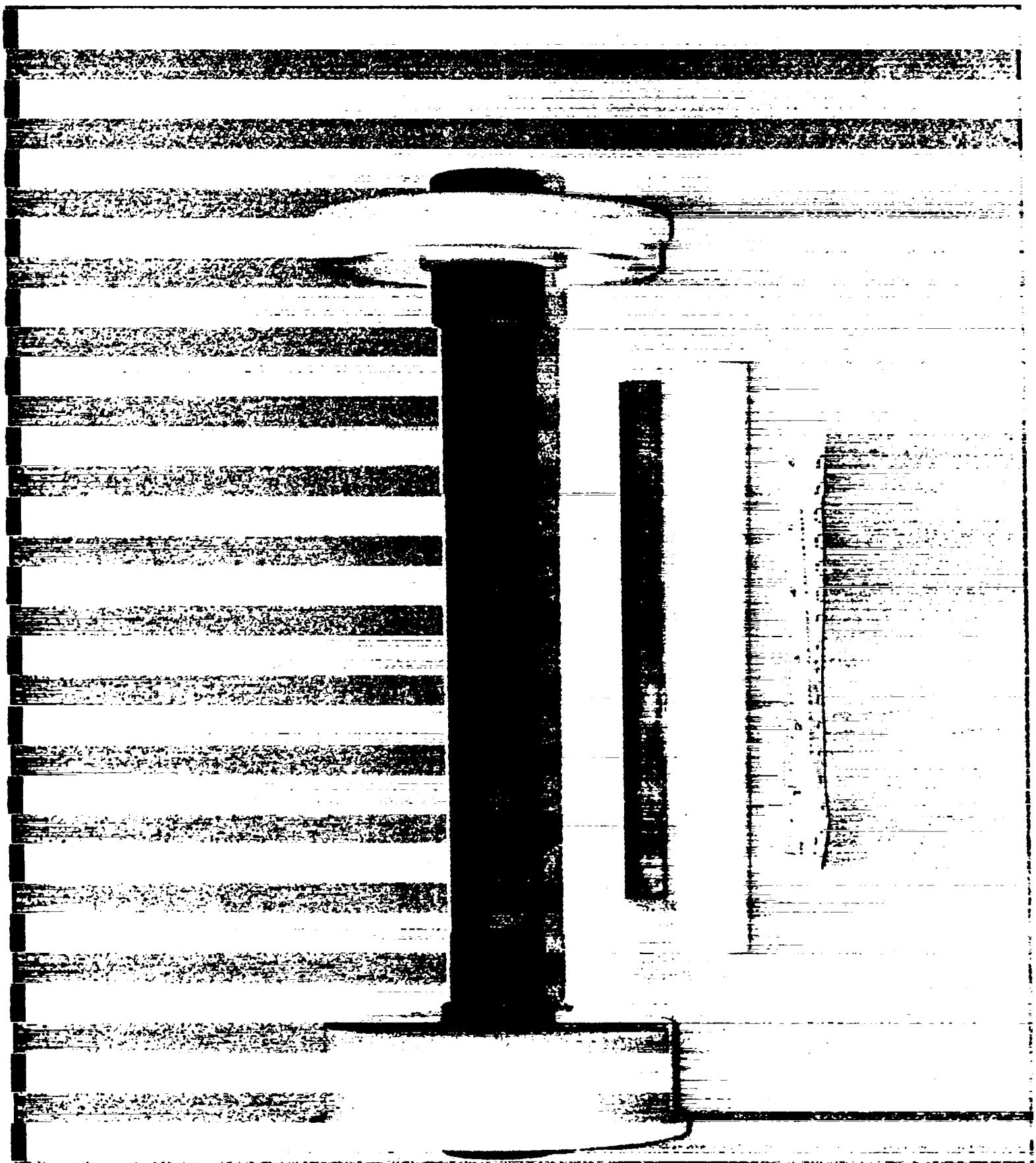


Fig. 3. Inner cascades for the MC-1 generator. The small, third cascade is used to produce the highest fields. The lower object is a foam cryostat used for some of the solid state experiments. It fits inside the second cascade.

Los Alamos
Los Alamos National Laboratory
Los Alamos, New Mexico 87545
Photography

source inductance in their bank (at least by our standards), the time required to generate this current is considerably longer at Arzamas 16, with two consequences: the fraction of the bank voltage across the coil is considerably smaller at Arzamas 16, but the potential for disrupting and ruining the field coil from magnetic forces (first cascade) is increased. The latter point did not concern us, since our faster current source would make firing at Los Alamos even safer. The higher voltage that would be developed across the first cascade, however, was a point of considerable concern to us. Our Russian colleagues did not share our worry in this matter. They proved to be right, for no problems were encountered from this source in any of the five shots.

IV. FIELD AND CURRENT MEASUREMENTS

Magnetic fields were determined in two ways.

1. Integration of voltages obtained from calibrated $\dot{B}$ probes.
2. Measurement of the Faraday rotation of plane, polarized light through a standard material.

The first method has been used at Los Alamos for decades. Probe calibrations are obtained from a special capacitor bank-coil system set up for this purpose. Both the probe of unknown area and a standard probe whose area is accurately known, are placed inside the coil. Comparison of the signals obtained when the capacitor bank is fired gives the area of the probe under calibration in terms of the standard probe area.

On the other hand, the Russian team generally uses the Faraday rotation method.[1] This measurement is often supplemented with $\dot{B}$ probe measurements, but the Faraday measurement is the primary one. Their standard arrangement employs He-Ne laser light ($0.6328\text{-}\mu$m) and a standard, heavy flint glass as the optically active medium.

We used the same system here for the Faraday measurements. Standard flint glass cylinders were furnished by the Russian team. Light from a He-Ne laser was transported to and from the standard flint glass cylinder assemblies by fiber optics. Details of the system, gathering and analysis of the data are given by Veeser[11] in a supplement to this report.

The actual Faraday rotation packages are rather complicated. The flint glass cylinder lengths are accurately measured, appropriate light polarizers are placed on both ends of the glass cylinder, and special lenses then couple the fiber optic pipes to the assembly. These assemblies were then placed in protective ceramic tubes supplied by the Russian team. The Faraday packages were fabricated at the EG&G Santa Barbara office. Details of the fabrication technique are given by Marshall[12] in a supplement to this report.

As noted earlier, $\dot{B}$ probes were used to give independent field measurements. Additionally, in a few shots the current flowing through the imploding liners was measured using Faraday rotation of polarized light in fiber optic "Rogowski" belts linking the current carriers. This technique, now in standard use at Los Alamos, is also described by Veeser in his supplement[11] and, in more detail, in Ref. 13.

The first two MC-1 shots fired, MC-1-1 and MC-1-2, were field characterization shots, and contained only magnetic field and current measuring diagnostics. The first shot used

a Comp B explosive charge, while the second shot used PBX-9501 explosive. Both shots used all three cascades to produce the highest fields.

Shot MC-1-1, was heavily diagnosed, since it was our first shot with this system. The diagnostics included a conventional Rogowski loop for initial current measurement, a Faraday Rogowski belt for large current measurements, twelve $\dot{B}$ probes, with various areas designed for field measurements at various stages of the entire field history and, finally, three Faraday rotation probes. Figure 4 gives an enlarged cross-sectional view of the third cascade and the various probes used for the field measurements.

The three Faraday assemblies were housed in ceramic tubes, 4-mm OD and 2-mm ID, shown crosshatched. Two of the Faraday cylinders were quartz, the other being the standard flint glass supplied by the Russian team. $\dot{B}$ probes, wound on 1-mm forms and protected with shrink tubing, and the Faraday fiber optic Rogowski belt are shown in the figure in a close-packed configuration with the ceramic tubes. As would be expected, the heavily protected Faraday probes survived longest before being hit by the imploding cascade, while the $\dot{B}$ probes were destroyed earliest. Figure 1 of Veeser's report[11] compares the magnetic fields obtained from quartz and flint glass Faraday measurements for the shot. In general, the values agreed quite well, showing only a few percent difference at the highest fields. Figure 2 of that report gives a plot of the current carried in the imploding liner vs. time. The peak current reached about 85 MA at the time the fiber optic belt was destroyed, about 150 ns before the peak field registered by the Faraday probes.

Figure 5 compares the magnetic fields obtained from MC-1 and MC-2. The time scales are normalized from the start of flux compression by the outer cascade. We were gratified to observe the expected result, that a higher field was produced by the more powerful explosive. In further shots, we intend to use PBX-9501 explosive, although the remainder of the shots in this series used Comp B.

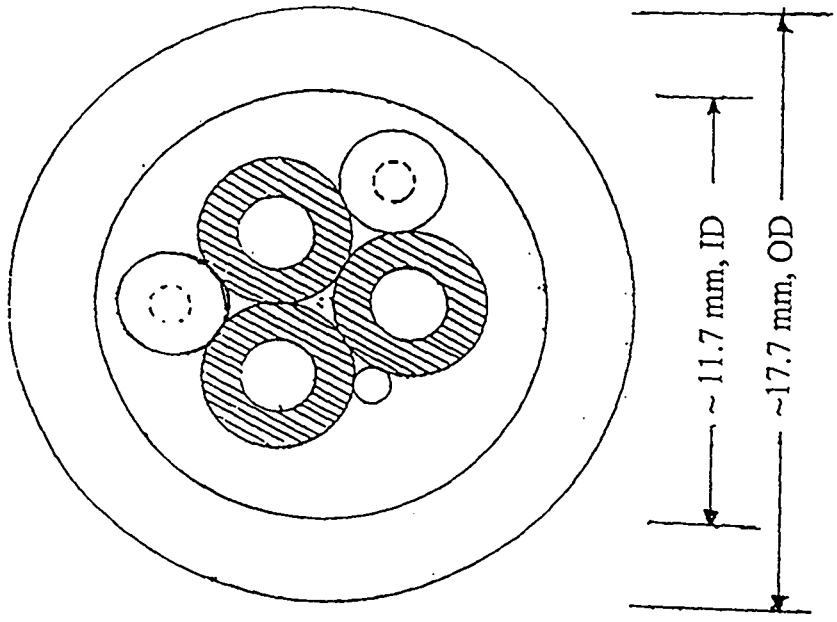


Fig. 4. Enlarged sketch showing the location of various diagnostics inside the third cascade.

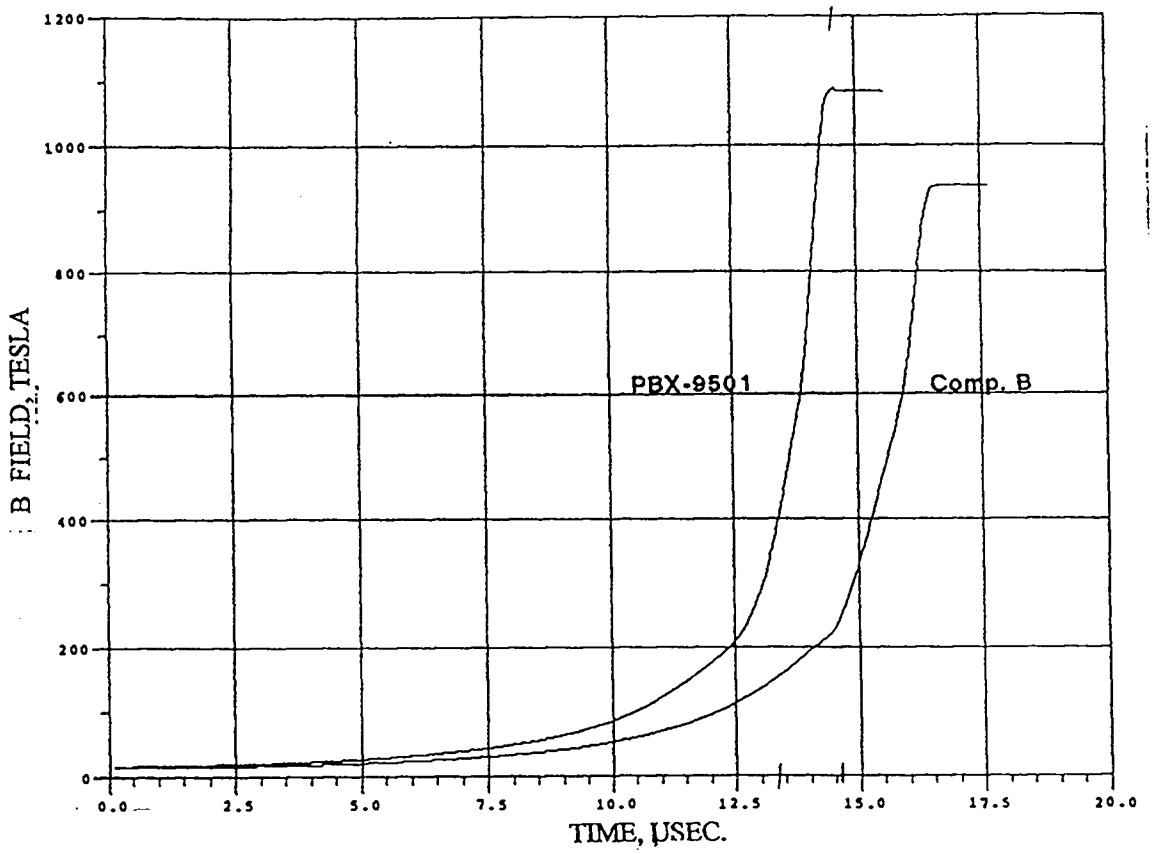


Fig. 5. Magnetic field vs. time traces obtained for two different shots, one with a Composition B explosive charge, the other with a PBX 9501 charge. Time scales are adjusted so that zero time corresponds to the onset of flux compression.

V. HTSC MEASUREMENTS

The decision to use three of the MC-1 assemblies for HTSC experiments was motivated by the uncertainty in the value of the low-temperature critical magnetic field for the high-temperature superconductor YBCO. All superconductors have the property that a high enough magnetic field, at any temperature (below the zero field—critical temperature) will quench the superconductivity. The highest magnetic field at which superconductivity persists is at the lowest temperature. For YBCO, and other HTSCs, the field dependency is reasonably flat at low temperatures. Therefore, near maximum field values should be obtained at liquid helium temperatures, since the zero field critical temperature is in the neighborhood of 90 K.

The crystalline form of this material has a c-axis length considerably different form those in the a-b plane, with the result that the limiting (low-temperature) critical field is different for the two orientations of the crystal c-axis, i.e., parallel or perpendicular to the magnetic field. We think that the critical magnetic field for the parallel orientation is in the neighborhood of 130 T. However, the critical field for the perpendicular orientation has been in considerable doubt, with estimates ranging from about 200 to 900 T!

5.1 Earlier Los Alamos Studies at Lower Fields

Megagauss field studies on YBCO have been carried out previously by a Japanese team, in addition to Russian and American teams. Many of the Russian and American scientists involved in these earlier studies also took part in these experiments.

Several different techniques have been used to study HTSC properties in megagauss fields. Figure 6 illustrates one of the techniques.[14,15] A meander-line pattern of YBCO was coated on a substrate with the c-axis perpendicular to the substrate, terminating in the diagnostic lead tabs. The sample was then characterized by measuring its resistance vs. temperature. Figure 7 is a typical curve. As seen from the heavy line, the sample starts to lose resistance at about 92 K, and is completely superconducting at 88 K. The dash line, continuing from the onset of superconductivity (92 K, 6.6 kΩ) to the origin, gives an estimate of what the resistance would be if the YBCO became a normal conductor, as a sufficiently high magnetic field would cause it to be. When the sample is placed in the high-magnetic field coil with the substrate plane lined up with the magnetic field, the sample c-axis is then perpendicular to the magnetic field.

A standard four-terminal technique is used to obtain the sample resistance as a function of the magnetic field. A pulser sends a known constant current pulse through the sample just before the magnetic field pulse is delivered to the coil. The sample resistance is then determined from the voltage measured across the sample.

Resistances so determined are shown on Fig. 8 for samples initially at temperatures of 70, 74 and 83 K. As noted on Fig. 7, from the dashed line, only the 83-K sample reached a magnetic field high enough to drive the sample normal. From this figure, the normal value should be about 6 K. That value was achieved at about 115 T, according to Fig. 8. This point (83 K, 115 T) is plotted on Fig. 14.

Two other features are noted on Fig. 8. First, the samples at 70 and 74 K required much larger fields before saturating. Second, in the 83-K experiment, the resistance remained at zero until about 45 T, when it suddenly started to rise more rapidly. This behavior is thought to arise from the sudden onset of fluxoid motion. The locus of such points as a function of temperature is called the "reversibility line." Evidence now indicates that the location of this line depends upon the risetime of the magnetic field, the field onset values being higher for faster risetime fields. We mention this because we think that some earlier papers erroneously interpreted reversibility line fields as the upper critical, or saturation, fields.

The data point (83 K, 115 T) of Fig. 14 led to our first rough estimate of the upper critical field. According to a model of Werthamer, Helfand, and Hohenberg,[16] the upper critical field, at zero temperature, is related to the slope of the saturation curve at Tc.

$$B(T=0) \doteq 0.7\left(\frac{dB}{dT}\right)_{T=Tc} \times Tc \ .$$

Here, Tc = 91 K and, very roughly using a straight line slope, dB/dT$\doteq$ ΔB/Δ T = 115 T/8 K. Thus,

$$B(T=0) \doteq 0.7 \times (115/8) \times 91 \doteq 900T \ !$$

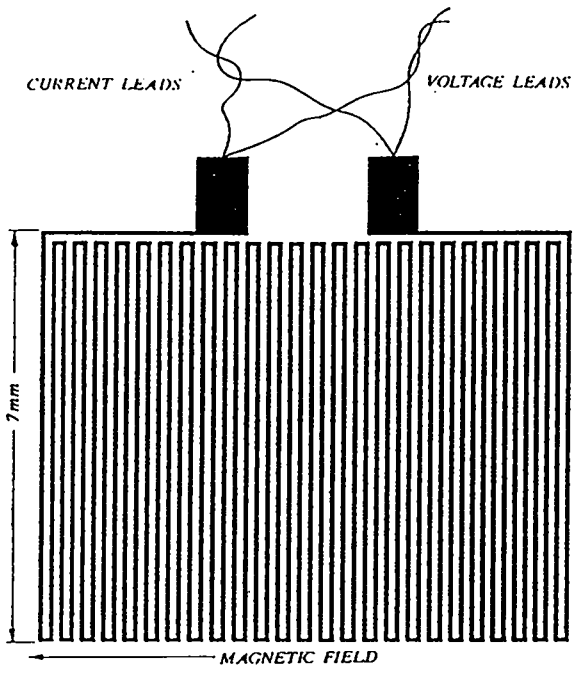


Fig. 6. Sketch of YBCO meander line sample showing electrical connections used to obtain the onset and saturation of resistance as a function of magnetic field.

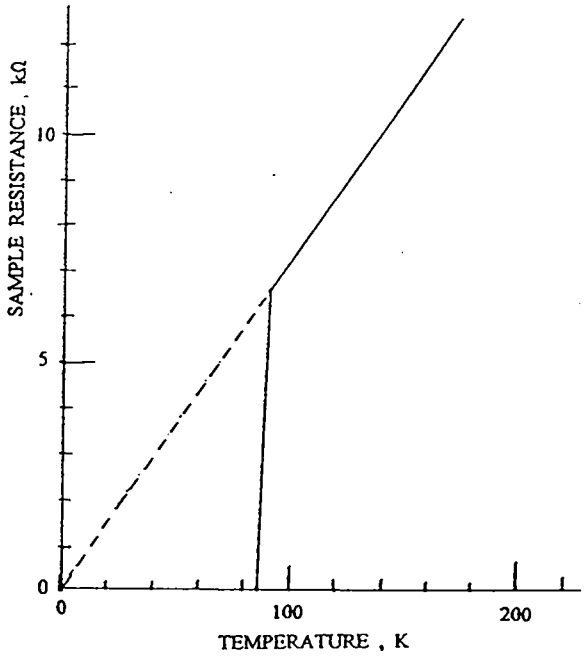


Fig. 7. Idealized resistance vs. temperature for a superconductor. The extrapolated dash line is taken to be the sample resistance if the material goes normal at a temperature in this range.

While it was thought that this value was too large, we did feel that the critical field could be in the neighborhood of 500 T, a field readily accessible with the MC-1 generators, but not with the high-field systems presently used at Los Alamos. It was for this reason that we selected a study of the high-temperature superconductors as the major solid-state experiments with the MC-1's.

Two kinds of high-field, flux compressors were used in the Los Alamos experiments: a single-stage "strip" generator for fields up to 150 T, and a two-stage system for fields up to and exceeding 200 T. The two-stage system is shown schematically on Fig. 9. The first stage consists of two single-stage or strip generators connected in series with the second stage but fired in parallel. We describe first the strip generators since, as noted above, they are used individually to generate fields up to 150 T. For these generators, the load coils are normally made from 51-mm square brass bar stock, 76-mm long. A hole of the appropriate diameter is drilled through the block. The output ends of the generator plates are connected to the load by soldering then to the faces formed by machining a slot from one side of the block to the hole. The explosive layers consist of two sheets each of DuPont Detasheet C-8. The sheets are about 340-mm long and 95-mm wide, into the plane of the figure, with a combined mass of approximately 1.6 kg. The angled copper plates are 1.6-mm thick, 340-mm long and are separated by 100 mm at the current input end. To enhance the structural strength of the plates they are bent upwards about 20 mm on the long sides to form troughs that, in turn, hold the explosive strips. The inside dimensions of the troughs are about 100 mm.

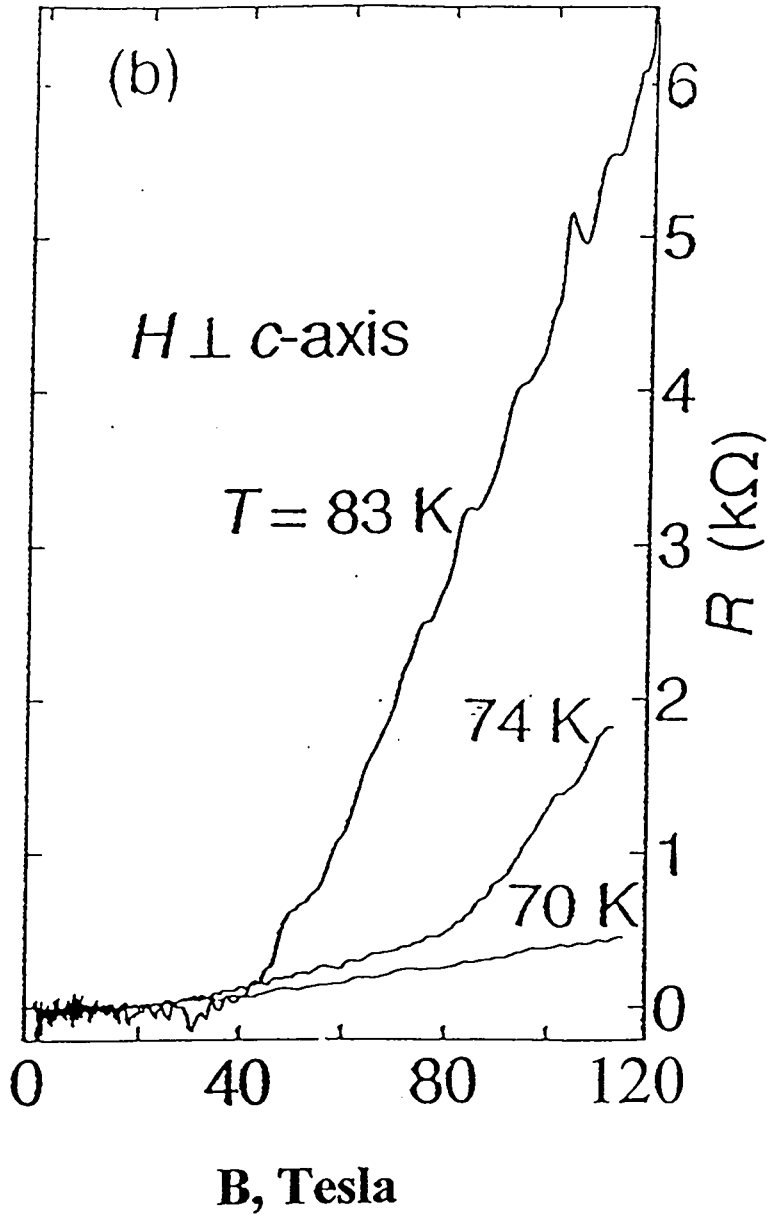


Fig. 8. Resistance vs. field obtained from samples (as in Fig. 6.) tested at different temperatures. Only the sample at 83 K reached the saturation resistance. The magnetic fields were not high enough to drive the lower temperature samples to the normal state.

In the two-stage system, the second stage and load coil are machined form a single piece of brass bar stock, usually 76-mm deep into the plane of the paper, 180-mm wide and 76-mm high. The triangular cavity, or second stage, is normally about 150-mm wide and 32-mm high at the triangle apex. Initial magnetic fields are supplied by a capacitor bank and fill both first and second-stage cavities as well as the cylindrical load coil. The second stage is initiated at such a time as to continue flux compression into the load coil

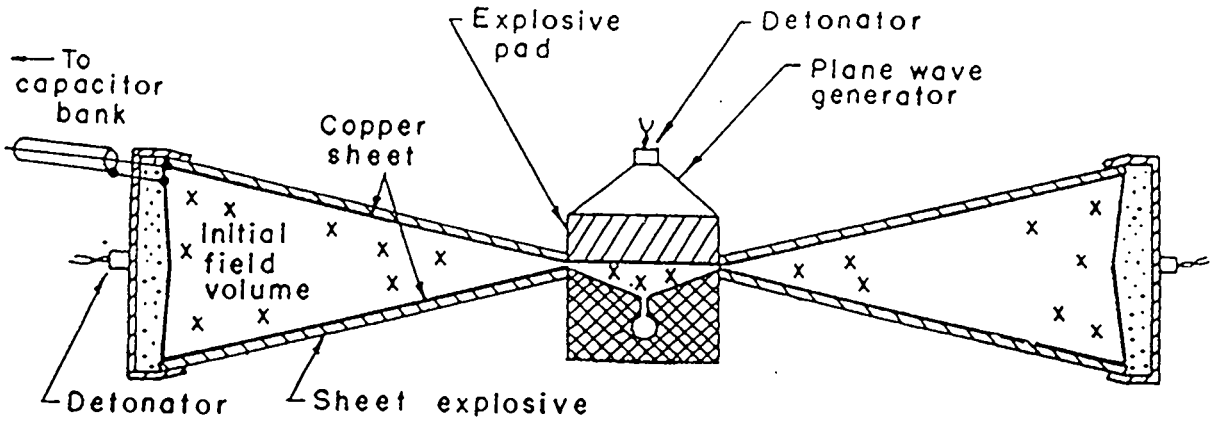


Fig. 9. Schematic drawing of a two stage high field generator.

at the end of the first-stage compression. The second-stage explosive system consists of a plane-wave initiator and a high-explosive pad, normally 76-mm deep and 155-mm long. The explosive used most often is the plastic bonded type, PBX-9501.

The peak magnetic fields obtained in the systems depend upon the load coil diameters. For 16-mm diameter load coils, the single-stage system develops a field of 125–130 T, while fields of 200–220 T are developed in the two-stage system. Field vs. time plots are shown In Fig. 10 for a single-stage system with load coil diameter of 12.7 mm and for a two-stage system with a load coil diameter of 28 mm. As noted later, this large diameter is the same as the inner diameter of the MC-1 second cascade that housed the YBCO experiments. Rather coincidentally both peak fields were about 147 T.

When making electrical measurements in these fields, one of the chief problems is managing unwanted electrical pulses generated by the changing magnetic fields. As can be seen from Fig. 10, values of dB/dT achieve peak values of 15 T/μs, a few microseconds before peak field. This gives rise to an inductive voltage at this time of 15 V around each square millimeter of area perpendicular to the field. While this sensitivity is fine for field measuring probes, it demands great care in making samples and in connecting leads (as in Fig. 6) so as to minimize projected area perpendicular to the field. Many true electrical signals are less than a volt, so such unwanted sample projected areas should be less than 0.1 mm.^{2} In spite of this difficulty, we have been able to make reasonably good measurements in such fields, by being very painstaking in preparing and mounting the samples and leads.

For implosion-produced fields, such as those of the MC-1, the situation is far worse. As seen in Fig. 5, dB/dt values get as large as 1000 T/μs. Thus, areas as small as 1-mm^2 normal to the field develop a peak voltage of 1 KV. We felt that good resistance measurement would be impossible in this environment and decided, instead, to use the microwave diagnostic described below.

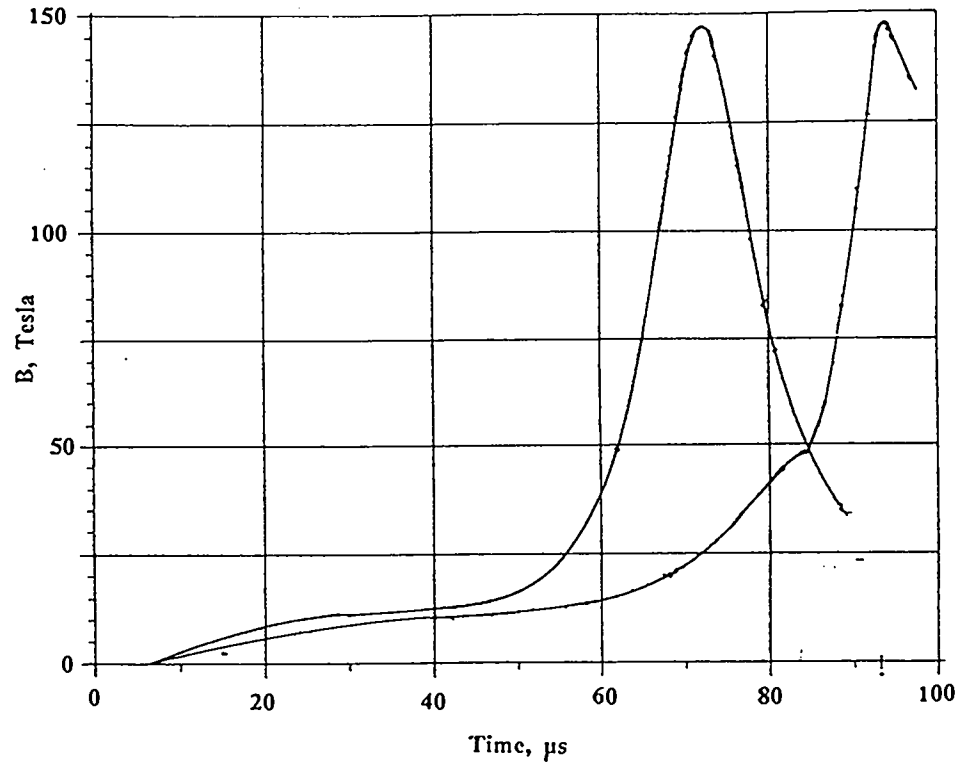


Fig. 10. Magnetic field vs. time plots from a single stage flus compressor (12.7 mm D load coil) and a two-stage compressor (28 mm D load coil).

5.2 Microwave Diagnostics

Microwave diagnostics were first used by a team from the P. N. Lebedev Physical Institute and Arzamas-16, as reported by Golovashkin *et al.*[17] The principle of the technique is straightforward. Figure 11 shows the styrofoam cryostat and sample holder used in these experiments. The overall diameter is approximately 28 mm, the inside diameter of the second cascade. The YBCO sample is placed between two diclectric wave guides. When the sample is completely superconducting, no signal is transmitted through the sample. As the sample starts to show resistance, such as at the onset of flux flow, microwaves are transmitted through it.

The YBCO samples used here were typically 1500 ± 500-nm thick and were deposited on a sapphire substrate with the c-axis perpendicular to the substrate. (A thin layer of CeO was deposited on the substrate first, a requirement for deposition of a good film on this material). Since the magnetic fields are paralleled to the cryostat axis, as is the substrate plane, the YBCO c-axis is perpendicular to the field.

A related diagnostic was used first by Sakakibara, Goto, and Miura.[18] Here, the sample, oriented as in Fig. 11, it was estimated that was sandwiched between two coils, one of which transmitted radio frequency signals of 20 MHz, the other serving as a receiver. The coil planes were parallel to the sample, thus minimizing B pickup. When the sample started to become resistive, the receiving coil began to show a signal. In both the microwave and

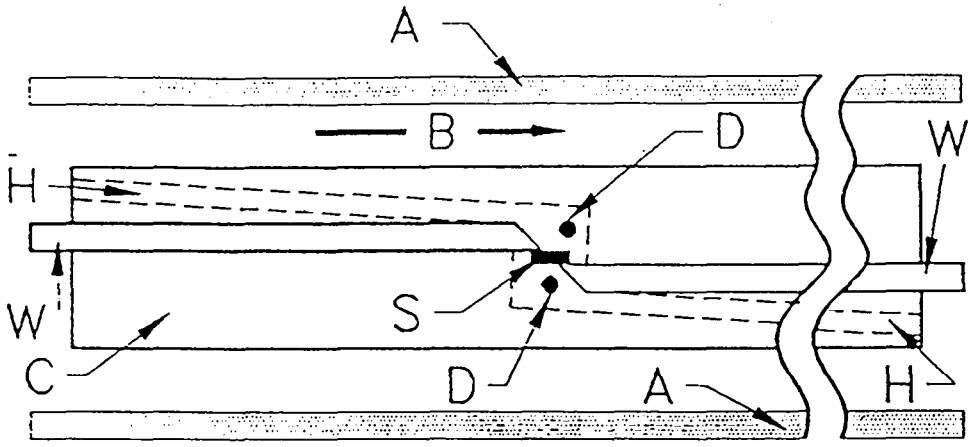


Fig. 11. Schematic of the diagnostics inside the MC-1 generator. A is the imploding liner, B is the magnetic field direction, C is the cryostat, D's are the temperature sensing diodes, H is the helium cooling channel, S is the sample, and W is the dielectric waveguide. The inductive and Faraday magnetic field probes are near D.

20-MHz systems, the super-conducting to normal state transition was considered complete when resistiveness derived from the signals became saturated.

While the radio frequency technique is appealing, it should be noted that in one cycle, 0.05 μs at 20 MHz, the magnetic field could change as much as 50 T (0.05 μs $\times$ 1000 T/μs)!

The transmission characteristics of the dielectric waveguide are affected by conductors and even by other insulators if they are too close to the waveguide. We decided that we needed unambiguous data to at least 500 T. With use of 4-mm waveguide, as shown in Fig. 11, it was estimated that the shock wave developed in the cryostat, from the imploding cascade, could reach a radius of about 6 mm before disturbing the microwave signal. Calculations dealing with this point are given in Ref. 6. In Fig. 7 of that reference, it is noted that a field of about 600 T is reached before the shock wave reaches the Styrofoam radius of 6 mm.

The entire microwave diagnostic system permitted measurement of both in phase and quadrature signals for both transmitted and reflected radiation. A brief description of the system together with schematic drawings is given in the attached report by Zerwekh.[19]

5.3 Compilation of Data

Four YBCO shots were fired in all. The first shot was fired at about 5 K below the zero field critical temperature (88 K) using a Los Alamos two-stage system. It was fired, primarily, as a general all-around checkout of all diagnostics, before doing the much more expensive MC-1 experiments; we were gratified that not only did all systems perform well, but we also got a saturation point (83 K, 45 T) on our final B vs. T curve, Fig. 14.

In the MC-1 shots, the initial YBCO temperatures were $\sim$30 K, 4 K and $\sim$60 K, respectively for MC-1 shots 3, 4, and 5. Unfortunately, the microwave signals were lost for the MC-1 Shot 5 experiment.

Figure 12 shows the microwave signal replotted against magnetic field for the MC-1 Shot 4 ($T_o = 4$ K). Quadrature signals are given for both transmitted and reflected signals. From these signals, as shown by Basovich, *et al.*,[20] the real and imaginary parts of the conductivity may be calculated from both the reflected and transmitted signals. Values so obtained are shown on Fig. 13. We take the upper critical field to be that value of B at which the imaginary part of the conductivity vanishes, as argued by Basovich, *et al.* From Fig. 14,, we place this value at 340 ± 40 T. This point is plotted on Fig. 14 at 9 K ± 5 K to reflect the possibility of sample heating during the experiment. A rough calculation gave a temperature rise of 10 K as an upper limit. No appreciable heating was calculated for the other experiments. This calculation, as well as a discussion of the complex conductivity analysis, will be discussed in more detail in a summary paper in preparation.

Figure 14 shows the data points we have obtained so far, and a tentative phase line (dashed line). A paper describing the experiments is nearing the final proofing stage, and a more extensive review paper is under preparation. In the meantime, a short, post-deadline survey paper by Goettee, *et al.*,[21] was presented at the recent *Fourth International Conference on Materials and Mechanisms of Superconductivity, High Temperature Superconductors.* (July 5–9, 1994) at Grenoble, France. A copy of this paper is attached.

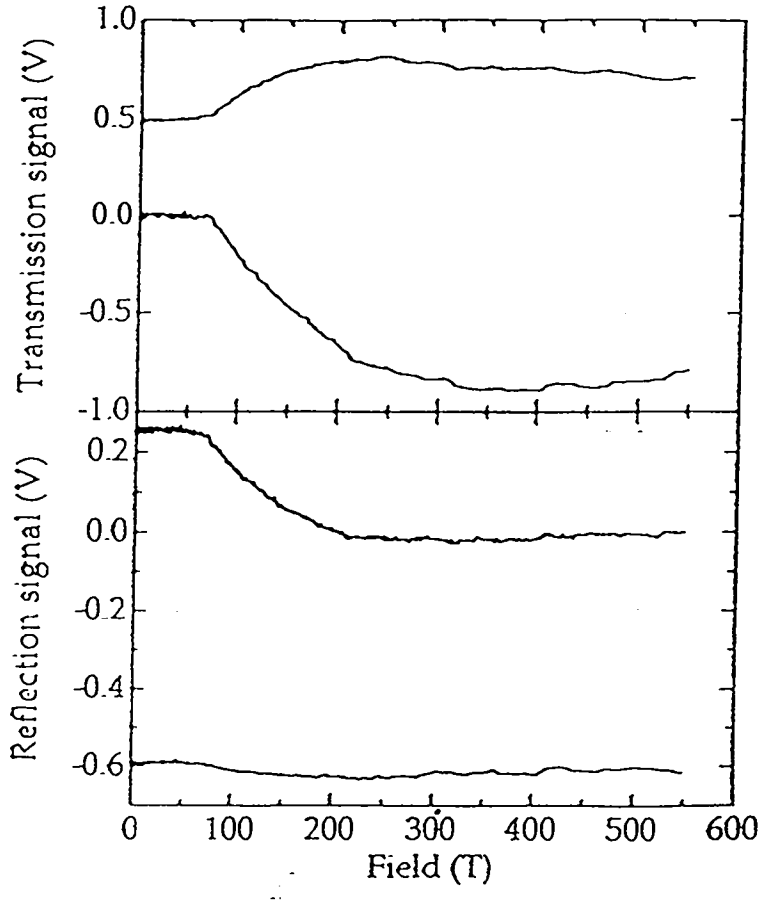


Fig. 12. Measured microwave transmission and reflection signals from the 4 K experiment plotted against magnetic field.

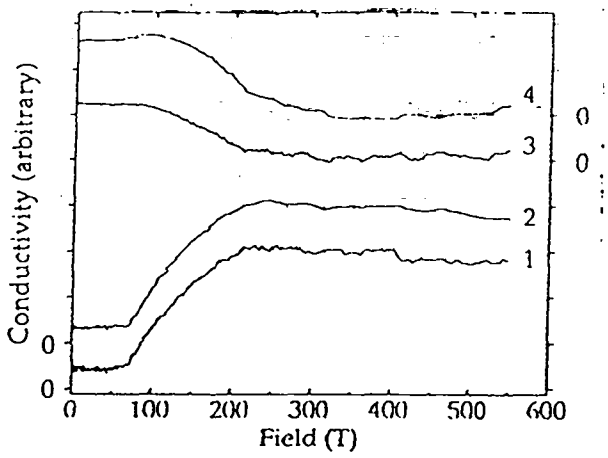


Fig. 13. Curves (1) and (3) show real and imaginary conductivities determined from the reflection signals of Fig. 12. Curves (2) and (4) give values from the transmission signals.

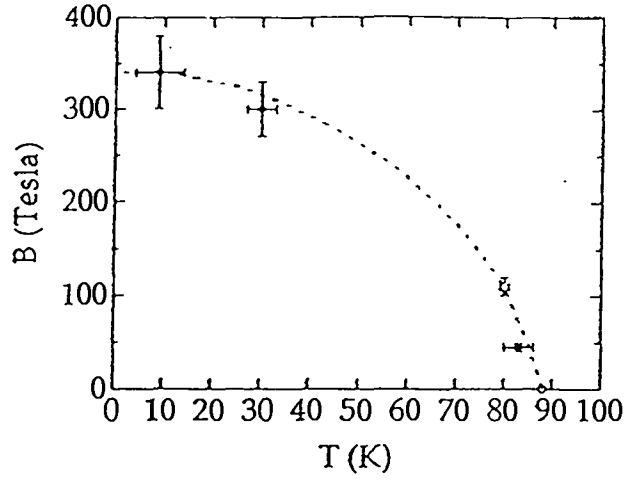


Fig. 14. Measured values of B, the upper critical magnetic field, vs. temperature for YBCO. The point at 80 K is from earlier work.

VI. NON-LINEAR FARADAY ROTATION IN CdS

Optical transmission studies on CdS in megagauss fields were carried out at Los Alamos nearly 25 years ago. Non-linear Faraday rotation was observed, particularly at shorter wavelengths. The peak field in these studies was about 180 T. The non-linearity was small at longer wavelengths. Consequently we decided to add on an experiment to the YBCO experiment on MC-1-5 in which a longer wavelength would be used to probe the Faraday rotation in CdS at substantially higher magnetic fields.

6.1 Early Los Alamos Experiments

In these early experiments, the CdS samples were at ~6.5 K, and a continuous wavelength light source allowed signal detection from the CdS absorption cutoff wavelength of ~490 nm to about 640 nm. Investigations were made in both the Faraday mode, and in straight light transmission.

In the Faraday mode, polarizers were placed on each side of the sample and the transmitted light was recorded on film after passing through a ruled grating onto a rotating mirror streak camera. The time position on the film is correlated with that of probe signals that furnish the magnetic field. Figure 15 shows one of the records obtained where the time axis on the right has been converted to magnetic field. An exploding bridgewire spectrum is displayed across the top of the film. The well-known spectral lines are mainly from gold, lead, and indium, components of the bridgewire and solder. The explanation of the unusual character of Fig. 15 can best be obtained by following a particular wavelength of the white light spectrum across the photograph. The alternate light and dark regions then correspond to 90° rotations of the polarization plane of the light of that particular

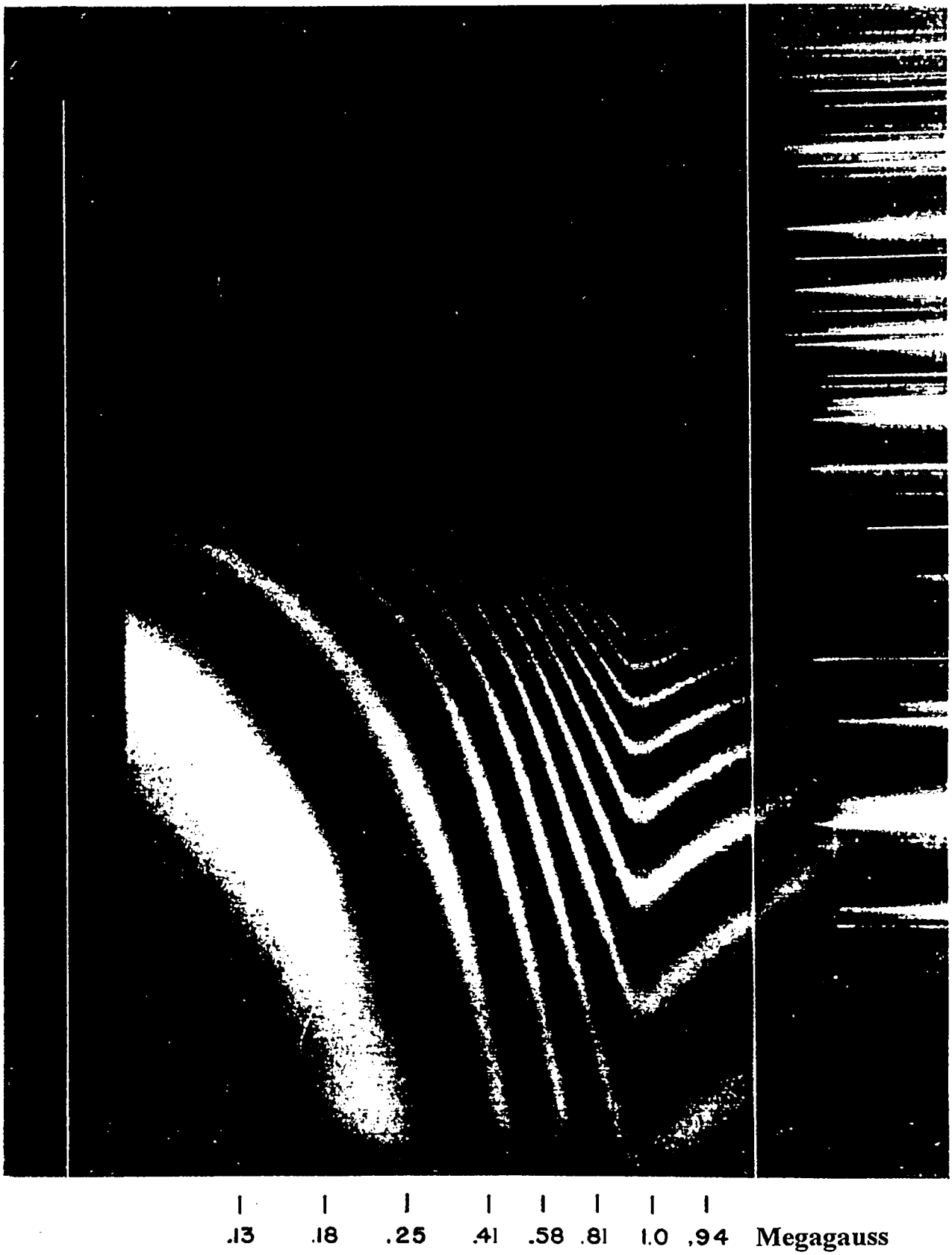


Fig. 15. Faraday rotation spectrum of CdS at 6.5 K. The absorption edge at~ 490 nm is clearly evident

wavelength as the field increases. The sudden leftward deflection of the light and dark streaks occurs at peak field. Beyond this point the field begins to drop, but at a slower rate than the rise near peak. For the longer wavelengths, the rotation up to 1 MG is practically linear with the magnetic field. For wavelengths near the absorption edge, the amount of rotation increases enormously and is no longer linear with the field. This experiment was repeated at higher fields, and the results showed that deviations from rotation linearity with field begin to occur at longer wavelengths but that experiments at higher fields would be very useful.

One straight transmission experiment was done on CdS at 6.5 K in a field rising to about 190 T. A shift of the absorption cutoff edge at high fields was quite evident, the cutoff wavelength moving about 60 A towards the violet at the field peak. Details of the experimental arrangements for these experiments and the CdS results are given by Fowler.[22]

6.2 The CdS Add-On Experiment

In the last MC-1 experiment, the flint glass Faraday probe normally used by the Russians for field measurement was replaced by a CdS crystal. The magnetic field was determined from B-dot probes. The Faraday assembly was made by EG&G, Santa Barbara, as described by Marshall in attached Ref. 12. Light was supplied by a HeNe laser operating at 543 nm. Faraday rotation measurements were done as noted earlier and described by Veeser in attached Ref. 11.

The Faraday rotation angle vs. magnetic field is plotted on Fig. 16 to 480 T. The non-linearity is clearly evident. Comparison of this data with earlier data is shown on Fig. 17. Data at 517, 558, and 608 nm are taken from Ref. 22. The data from the shot at 543 nm are highlighted by dots. These latter data were taken at an estimated temperature of 100 K as opposed to 6.5 K for the other data. The rotation angles were also normalized to the same crystal length.

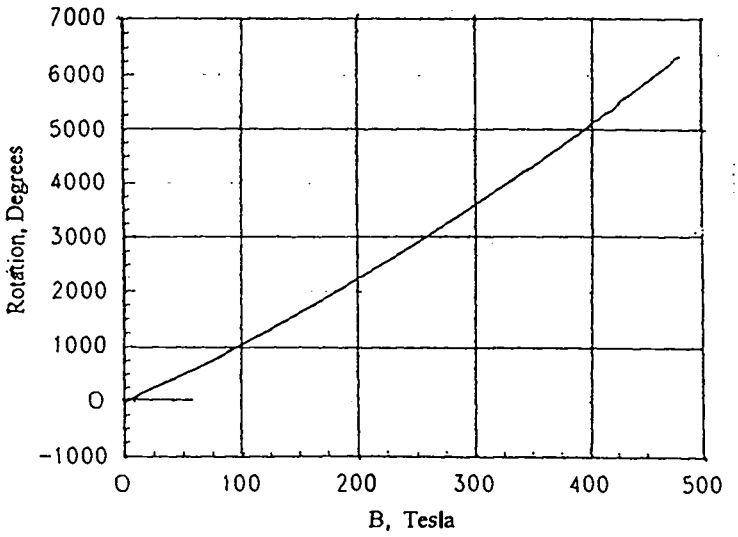


Fig. 16. Faraday rotation angle for 543 nm light in CdS as a function of magnetic field.

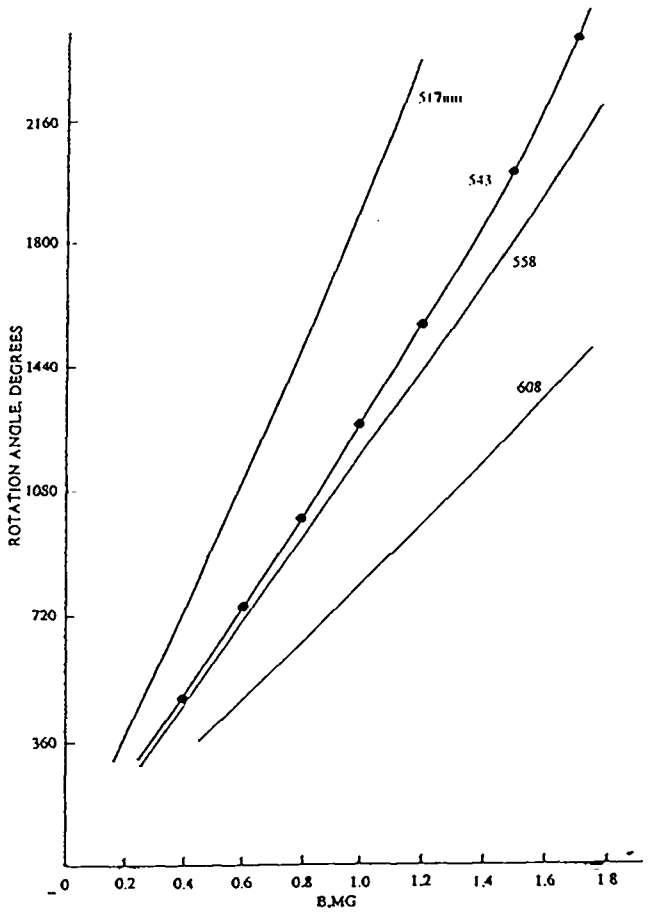


Fig. 17. Comparison of Faraday rotation data from Fig. 16 with earlier data to 170 T.

6.3 Further Data

A CdS crystal from the same batch used in the experiments here was taken to Russia, where a Faraday shot was fired at 300 K using a HeNe laser wavelength of 633 nm. Significant non-linearity was observed starting from about 400 T and increasing to the peak field of ~700 T.

A paper[23] surveying this work and offering an explanation of the non-linear effects is expected to be given by O. M. Tatsenko at the forthcoming, *Fourth International Symposium on Research in High Magnetic Fields*, to be held at Nijmegen, the Netherlands, August 29-31, 1994. Some of the theory, however, is still under discussion. A copy of the paper is attached to this report.

Group Photograph

The following photo shows most of the people who took part in the firing-site activities admiring our first fully-assembled MC-1 generator.

REFERENCES

1. A. I. Pavlovskii, N. P. Kolokolchikov, O. M. Tatsenko, A. I. Bykov, M. I. Dolotenko, and A. A. Karpikov, "Reproducible Generation of Multimegagauss Magnetic Fields," *Megagauss Physics and Technology*, P. J. Turchi, ed., Plenum Press, (New York and London, 1980), 627.

2. Letter from A. I. Pavlovskii to C. M. Fowler, June 30, 1989 (copy attached).

3. Letter to A. I. Pavlovskii from C. M. Fowler and J. H. Brownell containing a proposal by C. M. Fowler, B. L. Freeman, J. H. Brownell, and M. G. Sheppard, Document X-5-OU-92-23, February 6, 1992. (copy attached)

4. I. R. Lindemuth, "VNIIEF Collaboration Documents," report X-1(IRL)2/93-7, February 16, 1993. This report contains various documents relevant to our VNIIEF collaborations, including the original agreement of June 26, 1992 "Record of the Meeting ..." that included plans to purchase MC-1 high-field generators. (Partial copy attached).

5. A. I. Pavlovskii, "Ultrahigh Magnetic Fields Cumulation," *Megagauss Fields and Pulsed Power Systems*, eds., V. M. Titov and G. A. Shvetsov (Nova Science Publications, Inc., New York, 1990), 1.

6. M. G. Sheppard, C. M. Fowler, and B. L. Freeman, "Generation of Ultra-High Magnetic Fields for AGEX." Los Alamos document, LA 12773, Aug. 1994 (copy attached).

7. C. M. Fowler, W. B. Garn, and R. S. Caird, "Production of Very High Magnetic Fields by Implosions." J. Appl. Phys 31, 588 (1960).

8. R. S. Caird, W. B. Garn, D. B. Thomson, and C. M. Fowler, "An Explosive-Driven High-Field System for Physics Applications." J. Appl. Phys. 35, 781 (1964).

9. R. S. Caird, W. B. Garn, D. B. Thomson, and C. M. Fowler, "A Cylindrical Explosive Flux Compression System." in "Megagauss Field Generation by Explosives and Related Experiments," eds. H. Knoepfel and F. Herlach. (Euratom, Brussels, 1966), 101.

10. J. M. Christian, "Hydrotest H-1668: Test of an Extex Initiator and Comp-B Driver for the Russian MC-1 Flux Compression Generator." Los Alamos report DX-15:GR-94 1, February 1, 1994 (copy attached).

11. L. R. Veeser, "Faraday Magnetic Field and Current Measurements." Informal Los Alamos Group P-14 Report. (copy attached)

12. B. R. Marshall, "Report on Faraday Sensors Supplied to P-14 for Magnetic Field Compression Experiments, November–December 1993." Informal report from EG&G, Santa Barbara. (copy attached)

13. L. R. Veeser, R. S. Caird, C. M. Fowler, and D. J. Erickson, "A Fiber Optic sensor for Measuring Multi-Megampere Currents." in "28th. Proc. of SPIE. 506, 1984, 103.

14. J. L. Smith, J. S. Brooks, C. M. Fowler, B. L. Freeman, J. D. Goettee, W. L. Hults, J. C. King, P. M. Mankiewich, E. I. DeObaldia, M. L. O'Malley, D. G. Rickel, and W. J. Skocpol, "High Field Measurements on YBCO," J. Low Temp. Phys 95, (1994), 75

15. J. D. Goettee, J. S. Brooks, D. G. Rickel, B. L. Freeman, C. M. Fowler, J. C. King, P. M Mankiewich, W. J. Skocpol, E. I. DeObaldia, M. L. O'Malley, and J. L. Smith, "Megagauss Exploration of the Field-Temperature Phase Diagram of $YBa_2Cu_3O_7$ Epitaxial Films." in "Megagauss Field Generation and Pulsed Power Applications," eds. M. Cowan and R. B. Spielman, (Nova Sciences, NY, 1994) in press.

16. N. R. Werthamer, E. Helfand, and P. C. Hohenberg, "Temperature and Purity Dependence of the Superconducting Critical Field, H_{C2}. III Electron Spin and Spin-Orbit Effects." Phys. Rev. 147. (1966), 295

17. A. I. Golovashkin, O. M. Ivanenko, Yu. B. Kudasov, K. V. Mitsen, A. I. Pavlovskii, V. V. Platonov and O. M. Tatsenko, "Low Temperature Measurements of H_{C2} in HTSC Using Megagauss Fields." Physica B 177, (1992), 105.

18. T. Sakakibara, T. Goto, and N. Miura, "Technique for Contactless Transport Measurement in Very High magnetic Fields – A Challenge to Determine $HC^2(O)$ of High-Tc Superconductors in the Megagauss Range." Physica B 155, (1989), 189.

19. W. D. Zerwekh, "A 94-GHz Microwave System for Diagnostics in Multi-Megagauss Fields." Informal Los Alamos, Group DX-15 report. (copy attached)

20. A. J. Basovich, S. V. Gaponov, E. B. Kluenkov, N. P. Kolokolchikov, Yu. B. Kudasov, I. M. Markevtsev, A. I. Pavlovskii, V. V. Platonov, O. M. Tatsenko, and S. A. Voronov, *Phys. Lett.* **A163**, 322 (1992).

21. J. D. Goettee, Yu. B. Kudasov, W. D. Zerwekh, A. I. Bykov, M. I. Dolotenko, C. M. Fowler, B. L. Freeman, J. C. King, N. P. Kolokolchikov, W. Lewis, B. R. Marshall, B. Papatheofanis, V. V. Platonov, P. J. Rodriguez, M. G. Sheppard, O. M. Tatsenko, and L. R. Veeser, "Complex Microwave Conductivity of Magnetic Fields up to 500 T," Los Alamos Report LA-UR 94-2197, to be published in Physica C, (copy attached).

22. C. M. Fowler, "Megagauss Physics," *Science* **180**, pp. 261–267 (1973), and "Magnetic Field Applications," Los Alamos Scientific Laboratory Report LA-5065-MS, October 1972, pp. 64–77.

23. V. V. Druzhinin, O. M. Tatsenko, A. I. Bykov, M. I. Dolotenko, N. P. Kolokolchikov, Yu. B. Kudasov, V. V. Platonov, C. M. Fowler, B. L. Freeman, J. D. Goettee, J. C. King, W. Lewis, B. R. Marshall, B. J. Papatheofanis, P. J. Rodriguez, L. R. Veeser, and W. D. Zerwekh, "Nonlinear Faraday Effect in CdS Semiconductor in an Ultrahigh Magnetic Field." (copy attached)

DISTRIBUTION:

J. Immele, NWT, MS A105
S. M. Younger, NWT, MS F630
C. A. Ekdahl, AGEX-2, MS E529
D. M. Parkin,, CM-CMS, MS K765
L. Campbell, CM-CMS, MS E536
F. M. Mueller, CM-STC, MS K763
J. L. Smith/W. L. Hults, CM-STC, MS K763
R. H. Day, DX-DO, MS P915
R. E. Reinovsky, DX-DO, MS E527
J. M. Christian, DX-15, MS C970
W. D. Zerwekh, DX-15, MS C970
J. D. Goettee, DX-15, MS E536
L. A. Stretz/L. E. Hatler, ESA-2, MS C930
H. T. Hawkins, DDNIS, MS F650
E. Kutyreff, NIS-10, MS B230
F. H. Garzon/R. J. Houlton/C. B. Mombourquette/D. W. Reagor, MST-11, MS D429
Q. Jia, CM-STC, MST-11, MS G755
X. D. Wu, CM-STC, MS K763
J. D. Thompson, MTL-10, MS K764
J. S. Ladish, P-1, MS E526
M. Y. Hockaday, P-14, MS D410
G. D. Allred/D. E. Bartram/P. Rodriguez, P-14, MS D410
B. J. Papatheofanis, P-14, MS D410
L. R. Veeser, P-14, MS D410
J. S. Cohen, T-4, MS B212
L. A. Collins, T-4, MS B212
R. B. Schultz, X-DO, MS B218
I. R. Lindemuth, X-1, MS F645
J. H. Brownell, X-5, MS B259
C. M. Lund, X-5, MS B259
M. G. Sheppard, X-5, MS B259
W. Lewis/EG&G, Santa Barbara, CA
B. R. Marshall, Santa Barbara, CA
J. Crow, NHMFL, Tallahassee, FL
V. Selimir, VNIIEF, Arzamas 16, Russia
B. L. Freeman, DX-15, MS C970
C. M. Fowler, DX-15, MS C970

APPENDIX

This appendix contains material referenced in the text that is not available in the public literature. Included are copies of References 2, 3, 4, 6, 10, 11,12, 19, 21 and 23. Most of these references are informal reports from participants in the shot series. References 6 and 10 are major reports that deal with earlier tests and calculations necessary to define the subsequent test series. References 21 and 23 are copies of papers to be given at major conferences.

Dear Dr. C. M. Fowler.

Owing to circumstances over which I have no control we shouldn't meet at the conference "Megagauss – 5". I feel somewhat unhealthy and doctors don't recommend me to go to Novosibirsk. I'm getting well now.

In spite of this unforeseen situation the preparation of the book shouldn't be delayed.

If you've managed to compilate a variant of plan–prospect of a future book, I ask you to send it with Dr. G. A. Shvetsov and to inform about the adress of correspondence.

There is one more question for discussion. During the last years the evolution of explosive method for superhigh fields obtaining by coaxial shells system magnetic flux compression allows to obtain a field with intensity of about 16 MOe. On this way it seems real to achieve the fields reproducibility of 20 – 30 MOe during the next few years. The reports concerning these problems will be made at the conference. The experiment with such facilities will be both expensive and complicated enough. It seems that it is high time to think about a joint program of works on both superhigh magnetic fields cumulation and experiments setting in such fields. What's your opinion?

Dear Dr. C. M. Fowler, I wish to thank you once more for organization of such a wonderful trip across the USA, which deeply impressed me. I send you the book "The Problems of Modern Experimental and Theoretical Physics", involving the articles on magnetic cumulation, and a small souvenir – a box with your portrait in memory of our first meetings in Novosibirsk. The painter used a photograph of year 1983, that is why it was difficult to reproduce the versatility as a feature of your character. But his main effort to depict you full of strength and energy I share completely and wish you health and durable creative activities.

I hope for a successful work on the book, scientific contacts expanding and meetings with you. I ask you to give my sincere thanks to your wife for warm reception. My wife thanks you for souvenirs.

Sincerely yours,

A.I. Pavlovskii.

30.06.89.

Reference 3

Los Alamos
Los Alamos National Laboratory
Los Alamos, New Mexico 87545

DATE: February 6, 1992
MAIL STOP: B259
IN REPLY REFER TO: X-5-OU-92-23
TELEPHONE: (505) 667-7780

Prof. A. I. Pavlovsky
Head of Dept. of Fundamental and Applied Research
All-Union Scientific Research Institute of
Experimental Physics
Arzamas, Gorki Region, 607200
Russia
Telex: 1151109, ARSA, SU

Dear Dr. Pavlovsky:

Shortly after your visit to Los Alamos we discussed the possibility of a joint project with you and your laboratory. We decided that your suggestion to collaborate on a high field experiment was an excellent one. We have formulated a brief statement of our thoughts and have enclosed it in this letter. We would like to have your critical comments and your opinion on how to proceed.

We very much look forward to a collaboration and hope to hear from you in the near future.

Sincerely,
C. M. Fowler/JHB
J. H. Brownell

C. M. Fowler
J. H. Brownell

Enc: Proposal

cy: CRM-4, MS A150
C. Fowler, M-6, J970
X-5 File

An Equal Opportunity Employer/Operated by University of California

PROPOSAL

We propose to explore the feasibility of obtaining institutional support and funding for a collaboration between Dr. A. I. Pavlovsky of the All Union Institute of Experiment Physics of the Soviet Union and the researchers indicated below of the Los Alamos National Laboratory on a high magnetic field experiment. The ultimate goal of this work is to produce high fields for physics studies, and the first step will be to produce fields considerabely higher than have been achieved before. Specifically, we propose to reach amplitudes equal to or greater than 20 megagauss using flux compression generators, perhaps of the cascade type. Availability of such large magnetic fields would significantly extend the range of fields now available. Los Alamos and the All Union Institute would design the system collaboratively using existing data bases at both laboratories and extrapolate them using appropriate design techniques including hydrodynamic and magnetohydrodynamic computer codes.

C. M. Fowler, B. L. Freeman
Dynamic Testing Division

J. H. Brownell, M. G. Sheppard
Applied Theoretical Physics Division

pv pss-16 9-16-94 Reference 4

~~OFFICIAL U.S. ONLY~~

Los Alamos

memorandum

Los Alamos National Laboratory
Los Alamos, New Mexico 87545

To: C. Ekdahl, P-14, MS-D410
D. Erickson, DAD/NWT, MS-A105
M. Fowler, M-6, MS-J970
J. Goforth, M-6, MS-J970
J. Parker, P-DO, MS-E526
R. Reinovsky, M-6, MS-J970
S. Younger, NWT/ICF-AGEXII, MS-E527

Date: February 16, 1993

From: Irv Lindemuth

Telephone/FAX: 7-7844/5-3389

Symbol: X-1(IRL)2/93-7

Mail Stop: F645

Subject: VNIIEF Collaboration Documents

There are now quite a few documents which are relevant to our collaboration with VNIIEF, and so I thought it might be a good idea to have them all in one place for easy reference. The documents attached are:

I. The original collaboration agreement signed in June, 1992 (the "Record of the Meeting").

II. The memorandum of understanding signed in November, 1992; this agreement defines the conditions for our purchase of a DEMG experiment at VNIIEF and the 4 MC-1's for experiments at LANL.

III. The LDRD ERDI (Exploratory Research and Development Initiative) proposal which was funded at the $450k level in late December, 1992 (program code XL80); staffing requirements were guestimates which clearly need refining as the joint experiments become more well-defined.

IV. A P-14 request (memo P-14-U-93-023) for LDRD capital equipment funds (M-6: any requests from you appropriate?).

V. The "Purchase Request" generated by B. Donham, NWT/ICFA.

VI. A "Cost Analysis for Purchase of Ultra-high Magnetic Field Generators" (memo NWT/ICFA:BJD-92-459, generated by B. Donham).

VII. A "Sole Source Justification for Purchase of Ultra-high Magnetic Field Generators" (memo NWT/ICFA:BJD-92-464, generated by B. Donham).

VIII. The LANL $200k purchase order to VNIIEF for the joint experiments (I didn't know that this would actually cost our ERDI account $230k because of a 4% X-Division tax and a 10.7% MAT-Division tax); I note that the purchase order inadvertantly omitted reference to the MOU (item II above) and does not mention the DEMG experiment, but the MAT-7 buyer (J. Jefferis) assures me that this should cause no problems because the MOU was attached to the PO.

THE RECORD OF THE MEETING OF THE REPRESENTATIVES OF THE ALL RUSSIAN INSTITUTE OF EXPERIMENTAL PHYSICS AND THE LOS ALAMOS NATIONAL LABORATORY ON THE TOPIC OF COLLABORATION ON ULTRAHIGH MAGNETIC FIELDS AND PULSED POWER APPLICATIONS

Arzamas-16
June 22-26, 1992

The purpose of this meeting was to define specific areas of collaboration between the All Russian Institute of Experimental Physics (VNIIEF) and the Los Alamos National Laboratory in the areas of ultrahigh magnetic fields and pulsed power applications.

Attending the meeting from Los Alamos were:

Dr. C. Maxwell Fowler
Dr. Irvin R. Lindemuth
Dr. Robert E. Reinovsky
Dr. Stephen M. Younger (Leader of US Delegation)

Academician Alexander I. Pavlovskii led the discussions on the Russian side. Leading scientists of VNIIEF dr. V.K. Chernyshov, dr. V.N. Mokhov, dr. R.Z. Ludaev, dr. M.I. Dolotenko and others in the discussions participated.

In addition to detailed technical discussions, tours of selected facilities were provided for the US visitors.

In opening discussions on June 22, Director V.A. Belugin of VNIIEF described the meeting as primarily technical in nature, with the intention of precisely identifying a collaborative program of research between the two laboratories. It was agreed that these discussions would concentrate on direct collaboration between VNIIEF and Los Alamos, rather than on the preparation of proposals for submission to external organizations.

During the discussions eight technical areas were identified as suitable for detailed technical collaboration.

In the area of ultrahigh magnetic fields:

I. It was agreed that VNIIEF and Los Alamos would both perform detailed theoretical calculations on high magnetic field generators developed by VNIIEF with the aim of improving the theoretical understanding of these devices. Specifically, calculations will be performed on simple prototype configurations to check the basic physics in the models and on more complex systems which are capable of producing very high fields.

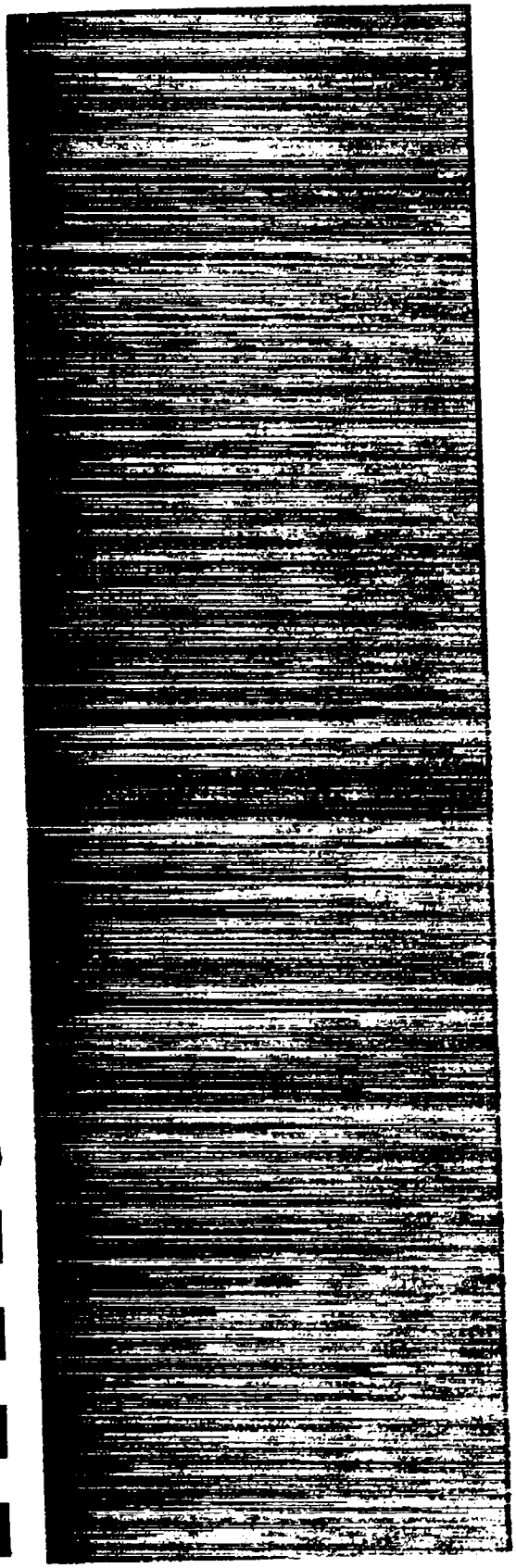
Investigations of ultrahigh magnetic field diffusion into metals were defined as a sphere of mutual interest, a theoretical part (calculations) of which could be accomplished by LANL with further VNIIEF experimental verification.

VNIIEF action: Theoretical calculations, experiments and providing of necessary data for Los Alamos calculations.
Los Alamos action: Theoretical calculations.

II. VNIIEF agreed to provide a price quote to Los Alamos for the delivery of ultrahigh magnetic field generators. This will allow Los Alamos to take advantage of technical developments at VNIIEF and for VNIIEF to extend the use of their generators to other facilities with different experimental capabilities for applications. It is anticipated that the acquisition of these devices will allow additional collaboration in the future on the development of even higher field generators. It is understood that upon receipt of an acceptable quote from VNIIEF, Los Alamos will institute purchase procedures.

VNIIEF action: Provide quote to Los Alamos

LA-12773



Generation of Ultra-High Magnetic Fields for AGEX

Los Alamos
NATIONAL LABORATORY

Los Alamos National Laboratory is operated by the University of California for the United States Department of Energy under contract W-7405-ENG-36.

Edited by Patricia W. Mendius, CIC-1
Prepared by Clara DeMaria, X-DO

An Affirmative Action/Equal Opportunity Employer

This report was prepared as an account of work sponsored by an agency of the United States Government. Neither The Regents of the University of California, the United States Government nor any agency thereof, nor any of their employees, makes any warranty, express or implied, or assumes any legal liability or responsibility for the accuracy, completeness, or usefulness of any information, apparatus, product, or process disclosed, or represents that its use would not infringe privately owned rights. Reference herein to any specific commercial product, process, or service by trade name, trademark, manufacturer, or otherwise, does not necessarily constitute or imply its endorsement, recommendation, or favoring by The Regents of the University of California, the United States Government, or any agency thereof. The views and opinions of authors expressed herein do not necessarily state or reflect those of The Regents of the University of California, the United States Government, or any agency thereof.

LA-12773

UC-741 and UC-700
Issued: August 1994

Generation of Ultra-High Magnetic Fields for AGEX

Maurice G. Sheppard
C. Max Fowler
Bruce L. Freeman

Los Alamos
NATIONAL LABORATORY
Los Alamos, New Mexico 87545

GENERATION OF ULTRA-HIGH MAGNETIC FIELDS FOR AGEX

by

Maurice G. Sheppard, C. Max Fowler, and Bruce L. Freeman

ABSTRACT

Generation of ultra-high magnetic fields of 10-25 MG (0.4-2.5 MJ/cm^3) using high-explosive-driven magnetic flux-compression is one approach which could enhance the U.S. Above Ground EXperimental (AGEX) capability. The beginnings of a U.S.-Russian collaboration to generate 20 MG by extending flux-compression technology are described. The first joint experiments, planned for November 1993 at Los Alamos, will test the Russian MC-1 10 MG generator and will be followed by several high-temperature superconductor experiments. Equation-of-state experiments involving isentropic compression at pressures of several megabars are being considered as follow-on joint experiments. Magnetohydrodynamic (MHD) calculations of the MC-1 experiments using the 1D MHD code RAVEN are presented, including comparisons and benchmarks against previous Russian experiments and calculations. The first joint experiments will use Russian hardware and U.S. high-explosive. Gaining practical experience with the MC-1 and benchmarking the RAVEN predictions for the performance of the modified generator are important first steps towards reaching the 20 MG goal.

Introduction

Energy densities associated with magnetic fields of 10-25 MG (0.4-2.5 J/cm^3) represent a potential energy source for Above Ground EXperiments (AGEX). Possible relevant uses for ultra-high magnetic fields include magnetically driven liner implosions for x-ray production, adiabatic (isentropic) compression of materials at pressures exceeding 10 Mb for equation-of-state studies, neutron production through fusion plasma confinement or compression, and high-power microwave production.

Scientists from Los Alamos National Laboratory and the Russian nuclear weapons laboratory at Arzamas-16 are collaborating on ultra-high magnetic field experiments using explosive pulsed power. This collaboration, made possible for the first time by the end of the Cold War, will allow the scientific exchange of unclassified knowledge, data, and experience which has been inaccessible to the general scientific community because of its proximity to each country's nuclear weapons program. The first series of experiments will use the Russian MC-1 flux-compression generator (FCG), designed and perfected by the late A. I. Pavlovskii and his colleagues.[1] The MC-1 was assembled with U.S. high-explosives (HE) and diagnostics to measure the upper critical field transition,

$H_{c2}(T)$, of the high-temperature superconductor (HTSC), $YBa_2Cu_3O_7$ (YBCO), at temperatures of 4 K and higher. Experiments should commence in November 1993 at Los Alamos.

The scope of this paper is limited to a presentation of 1D MHD simulations of the MC-1 with the Lagrangian RAVEN code; this paper is not intended to be a complete report of the U.S.-Russian collaboration. A general discussion of ultra-high magnetic field generation in the next section is followed by a description of the MC-1 FCG and a review of the Russian experience with this generator. The fourth section gives details of RAVEN calculations with different types of HE and varying initial fields. These calculations are compared with Russian calculations and experimental results. Preshot calculations for the HTSC experiments and possible isentropic compression experiments for equation-of-state studies are also included.

Generation of Ultra-High Magnetic Fields

Generating 10 MG magnetic fields, or greater, in volumes large enough for diagnostics and macroscopic experiments presents special challenges associated with high energies, high energy densities, very large magnetic pressures, and magnetic induced plasma instabilities. The primary mechanism for creating such fields is explosively-driven magnetic flux-compression. A seed field is first generated and trapped in a volume which is surrounded by electrical conductors. Then, a conducting armature, driven by HE, wipes out the volume while doing work against the trapped field -- thus amplifying it. An excellent review of flux-compression fundamentals appears in Fowler, Caird, and Garn.[2]

To illustrate the magnitude of the challenge presented by ultra-high fields, consider the following discussion. The energy density associated with 10 MG is 0.4 MJ/cm^3, whereas the chemical energy released upon HE detonation is only 9×10^{-3} MJ/cm^3. Furthermore, the magnetic pressure associated with 10 MG is 4 Mb -- an order of magnitude above typical HE pressures. Since energies and pressures scale as the square of the magnetic field, the difficulty of the task and the richness of the payoff skyrocket with higher fields. The trick is to efficiently convert large amounts of HE chemical energy into kinetic energy of an armature. The armature must then wipe out the high inductance volume in a short enough time that the trapped magnetic field neither diffuses out of nor destroys its confining walls. At the 10 MG level, and slightly higher, the Russian scientists at Arzamas-16 have demonstrated repeatable and reliable performance with the MC-1.[3,4]

MC-1 Description

A diagram of the Russian three-cascade MC-1 FCG is presented in Fig. 1. The HE cylinder, which in the Russian experiments has been composed of a 50/50 RDX/TNT mix, is detonated simultaneously on its outer diameter surface by a ring of 10 polystyrene block initiators.

Inside the HE are 3 concentric cylindrical shells (known as cascades in the Russian literature), made of a unique copper-epoxy composite. These shells successively take on the role of armature during implosion. The shells are made of hundreds of 0.25-mm diameter, enamel-coated, copper threads arranged side-by-side in layers and secured in a casting of epoxy. The 500 copper threads of the outer cascade are wound in a 2-turn solenoid and then brought back along the outside diameter, parallel with the cylindrical axis, to complete the return current path. The solenoid cascade is impregnated with epoxy and cured. The outside diameters of all 3 cascades, which are cast with a thicker layer of epoxy, are machined smooth to inhibit hydrodynamic instabilities. An initial magnetic field of up to 220 kG (typically 130-160 kG) is created by discharging a capacitor through the first cascade. The discharge is timed so that peak field is achieved just as the HE detonation wave reaches the first cascade. Upon contact the HE shock breaks down the insulation between the solenoid threads and transforms the first cascade into a conducting cylinder — trapping and then compressing the initial field as the shell begins to move.

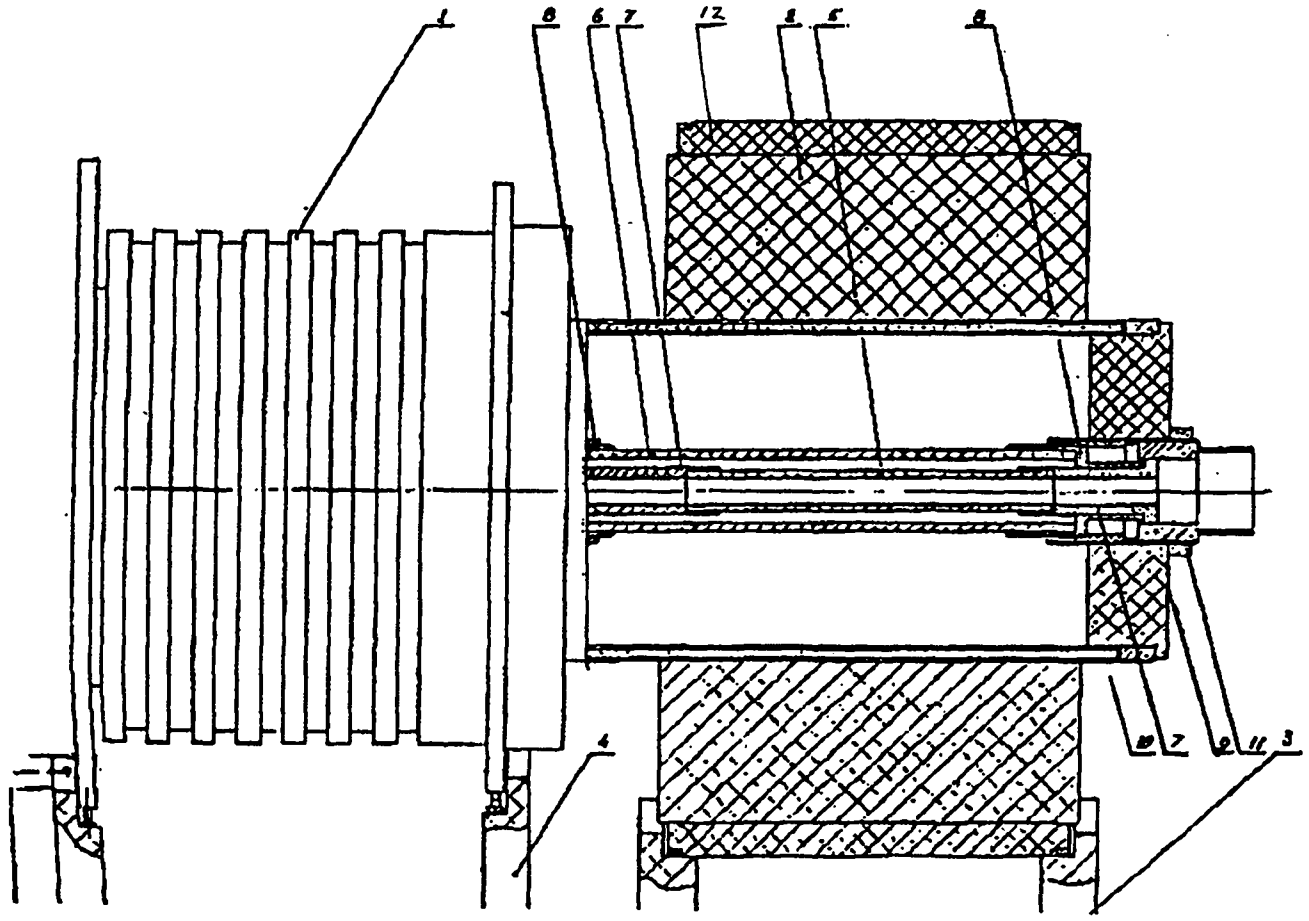


Fig. 1. Russian 3-cascade MC-1 FCG. Labels are identified as follows: 1 - insulated current feed for solenoid; 2 - explosive charge; 3, 4 - support stands; 5 - 3rd cascade; 6 - 2nd cascade; 7, 8, 9- insulating foam assembly cradles for cascades; 10 - solenoid; 11 - assembly nut; 12 - initiator

The second and third cascades are similarly constructed except that all of the copper threads are laid parallel to the axis. Before a cascade is contacted and shocked from outside, it will only conduct current in the axial direction. Hence, it is transparent to the axial field which is being compressed by the preceding shell. On contact, however, the cascade is transformed by the shock into a conducting cylinder, which traps the field inside as the new cascade becomes the new armature.

The use of multiple cascades serves two important functions. The first benefit of multiple cascades is the velocity enhancement which is derived from collisions of heavy outer shells with lighter inner shells. The second (and more crucial) benefit is related to implosion stability. As the outer cascade compresses flux, magnetic and hydrodynamic instabilities tend to disrupt the shell. These instabilities are made worse by the inherent perturbations associated with the copper-epoxy composite. The inner cascades are strategically placed to recollect and smooth out the perturbations before the outer cascade is disrupted. The loss of flux which is incurred during the transition is offset by achieving a more stable and reproducible implosion.

In the early systems developed by Fowler, Garn, and Caird,[5] initial field coils were also placed under the explosive charge. While very large fields were obtained (up to 14 MG), performance was erratic. The use of additional Pavlovskii cascades would presumably have led to better reproducibility. An alternative approach to controlling the instabilities was investigated by Caird et al.[6,7] They placed the solenoid outside of the HE and used a single stainless steel armature. On the timescales of the initial capacitor discharge, the stainless steel armature allowed magnetic flux to diffuse inside the cylinder; but on the short timescale of the implosion, the flux was essentially trapped and compressed. However, the poorer coupling of the initial coils with the armature results in substantially lower initial, and, therefore, also final compressed fields.

Details for the First Experimental Series

The first of 5 tests of the MC-1 will be a proof test of the 3-cascade generator using COMP-B HE instead of the Russian 50/50 mix. COMP-B is slightly more energetic by virtue of its 60/40 RDX/TNT composition. The generator will be preloaded to 160 kG using the capacitor bank at Point 88 in Ancho Canyon. Assuming successful validation of the MC-1 performance in the first shot, the next 3 tests are designed to measure the critical field transition of YBCO. Finally, if everything goes as planned, the last experiment of this series will be another test of the 3-cascade system using PBX-9501 -- a dramatically higher energy HE. Results of these tests will be compared with the preshot calculations described in the next section. Benchmarking of the RAVEN code at these high fields is a first step towards pursuing the 20 MG goal.

In the HTSC experiments, the third cascade will be removed, and the volume inside the second cascade will be occupied by a 0.15 g/cm^3 foam cryostat. The YBCO sample, which occludes a 4-mm dielectric microwave waveguide, and Faraday rotation diagnostics will be bathed in liquid helium via channels in the foam. As the field strength increases during the compression, the YBCO film will undergo the H_{c2} transition and become resistive. Before the transition occurs, 94 GHz diagnostic microwaves, which will be focused into one end of the waveguide, will be largely reflected by the superconducting film. After the transition, the microwaves will be increasingly transmitted and detected.

1D MHD RAVEN Calculations

Simulations of the MC-1 have been conducted with the 1D Lagrangian MHD code RAVEN utilizing SESAME equations of state (EOS) and electrical conductivities.[8,9] Cascades were modeled as sandwiched layers of copper and epoxy. The number of layers used for each cascade matches the actual number of layers of copper thread in each cascade, and the thickness of the layers was adjusted to match the reported average density of each cascade while fixing the total sandwich thickness. This approach differs from the Russian computational models,[3] which use a mixed copper-epoxy EOS and only one layer per cascade shell. The Russians scaled a standard copper resistivity model by a factor of 5 to use for the mixed EOS. The RAVEN calculations treated each copper shell with an unscaled resistivity and each epoxy layer as an insulator. To allow the axial magnetic field to pass freely through the cascades until they were shocked in the calculations, the standard copper resistivity in each zone was multiplied by a step function which remained zero until the zone density first exceeded 1% above normal density; subsequently the step function stayed equal to one for the remainder of the simulation.

3-Cascade MC-1 Simulations

Calculations of the 3-cascade MC-1 with an initial field of 160 kG were done with JWL HE models for the 50/50 mix, COMP-B and PBX-9501. Radius vs. time plots for the cascade interfaces, from the 50/50 mix calculations, are shown in Fig. 2. Plots of the on-axis field vs. time are shown in Fig. 3 for these calculations.

Similar Russian calculations and experimental results from one test are also compared with our calculation in Fig. 3. The measured peak field for the 50/50 mix, averaged over 100's of tests, is reported as 9.5 ± 0.5 MG,[10] which is in excellent agreement with the RAVEN simulation. The Russian calculation underestimates the measured peak field. Using higher energy explosives, like COMP-B and PBX-9501, gives a higher peak field by transferring more kinetic energy (velocity) to the cascades but at the expense of a smaller minimum radius. Peak fields predicted for 50/50, COMP-B, and PBX-9501 are 10 MG, 11 MG, and 13.5 MG while the radii at which the inner surfaces of the third cascade are stopped by the compressed field are 4.4 mm, 4.2 mm, and 3.6 mm respectively. The combination of higher velocity and higher peak field, coming from the use of more energetic HE, results in significantly higher time derivatives for the field. For the 50/50 mix, RAVEN predicts a derivative of 12.5 MG/μs, whereas the prediction for PBX-9501 is a factor of 2 higher.

Operation of the MC-1 is illustrated in Figs. 4-6, which show various quantities as a function of radius at 3 different times for the COMP-B simulation. Figure 4 shows density and magnetic field of the second and third cascades at 21 μs, before the outer cascade has made contact. Note the alternating copper and epoxy layers in the cascades and their transparency to the magnetic field. At 23.5 μs, Fig. 5 shows the second cascade already turned into a conductor, moving at 5.5-mm/μs and compressing the field through the still transparent third cascade. Finally at 24.6 μs, in Fig. 6, the third cascade is beginning to be slowed by the magnetic back-pressure on-axis. Notice that between the two cascades, the magnetic field is acting as a staging fluid to continuously transfer kinetic energy from the second to the third cascade while keeping them somewhat separated.

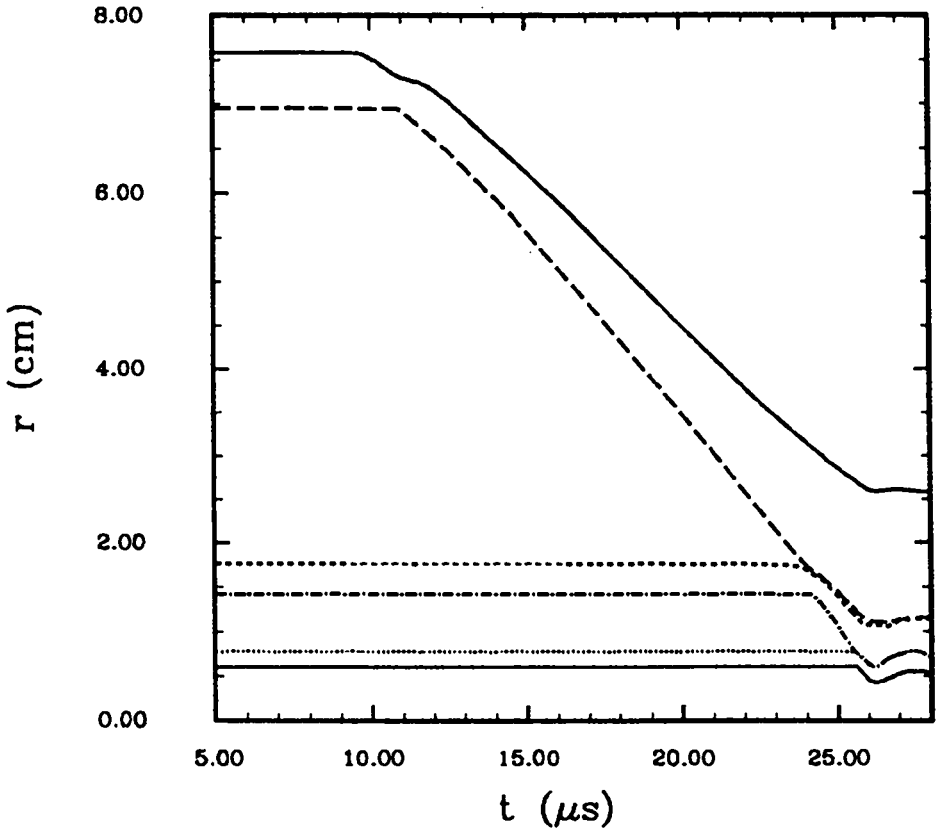


Fig. 2. Cascade interface positions from the RAVEN simulation of a 3-cascade MC-1 driven by 50/50 mix HE. Time is relative to HE detonation.

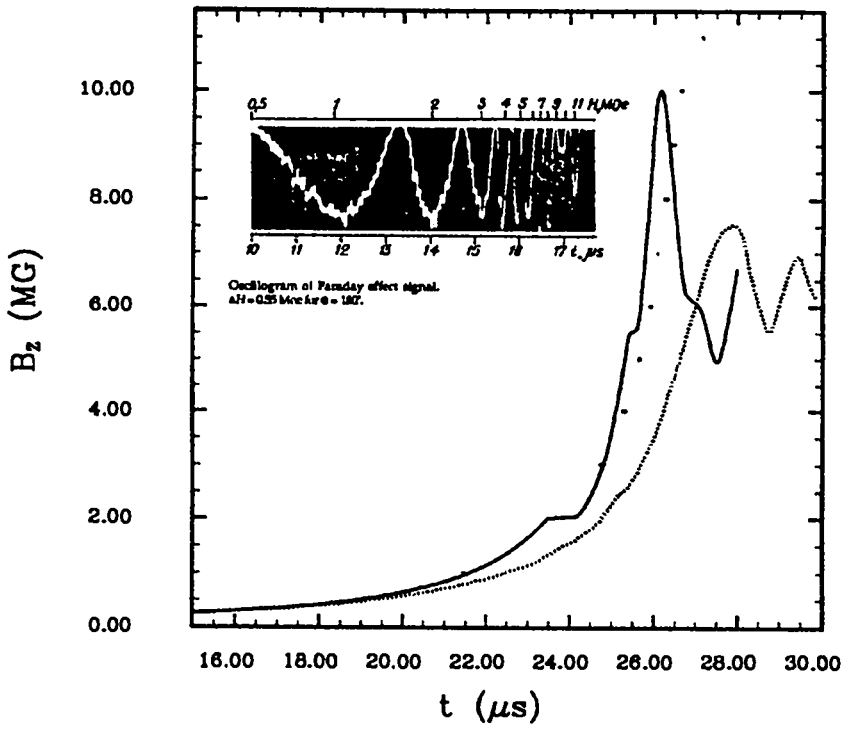


Fig. 3. Axial magnetic field for 3-cascade MC-1 with 160 kG initial field. The solid line is from the RAVEN simulation of Fig. 2, the dotted line is from ID Russian simulations provided by Dolotenko, and the points are experimental data from Ref. 1.

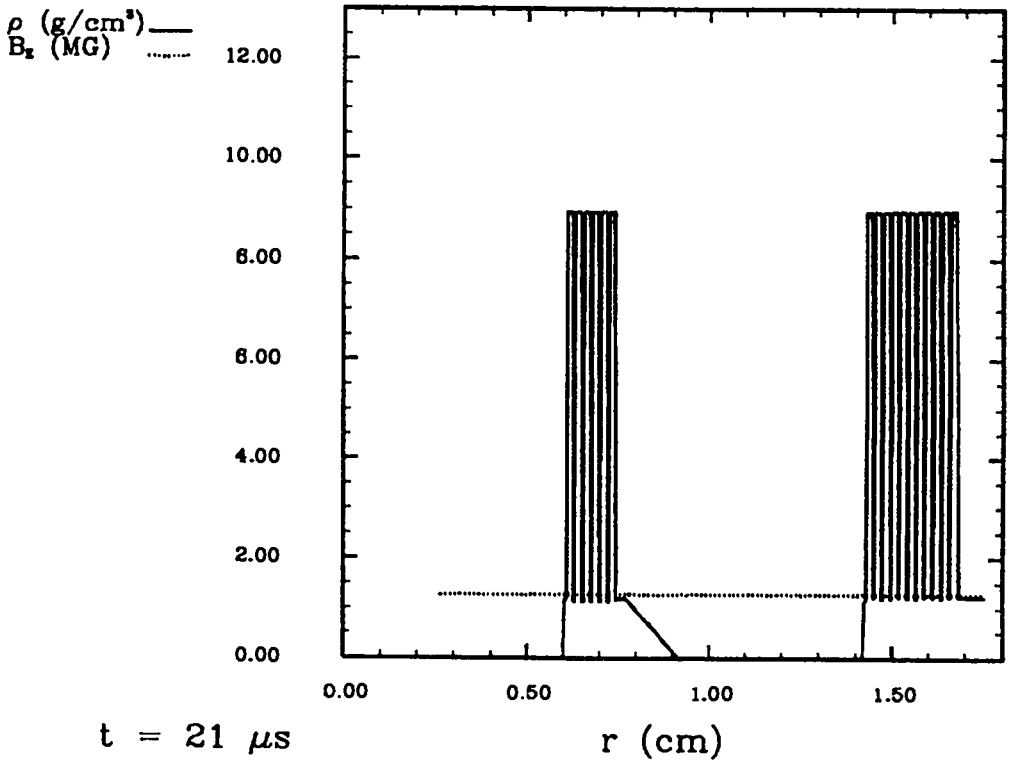


Fig. 4. Density and magnetic field profiles through the 2nd and 3rd cascades from RAVEN simulations of the MC-1 driven by COMP-B at 21 μs after HE detonation.

Another way to achieve higher fields (up to a point) in the MC-1, is to use a smaller initial field. This change allows the armature to implode further before the field gets high enough to stop and turn it around. This has the effect of raising the time-derivative of the field and reducing the central field volume. If the initial field gets too small, the integrity of the central volume is destroyed by instabilities, or the diagnostics are destroyed before peak field is reached. Calculations with COMP-B at initial fields of 160 kG, 130 kG, and 100 kG predicted peak fields of 11 MG, 12 MG and 13.2 MG with minimum radii of 4.2 mm, 3.7 mm, and 3.2 mm, respectively.

2-Cascade MC-1 Simulations

Simulations of the 2-cascade MC-1 were done with COMP-B and a 0.15 g/cm^3 polystyrene cryostat in preparation for the HTSC experiments. Figure 7 shows selected Lagrangian zone boundaries in the cryostat plotted with the predicted magnetic field and its derivative. The

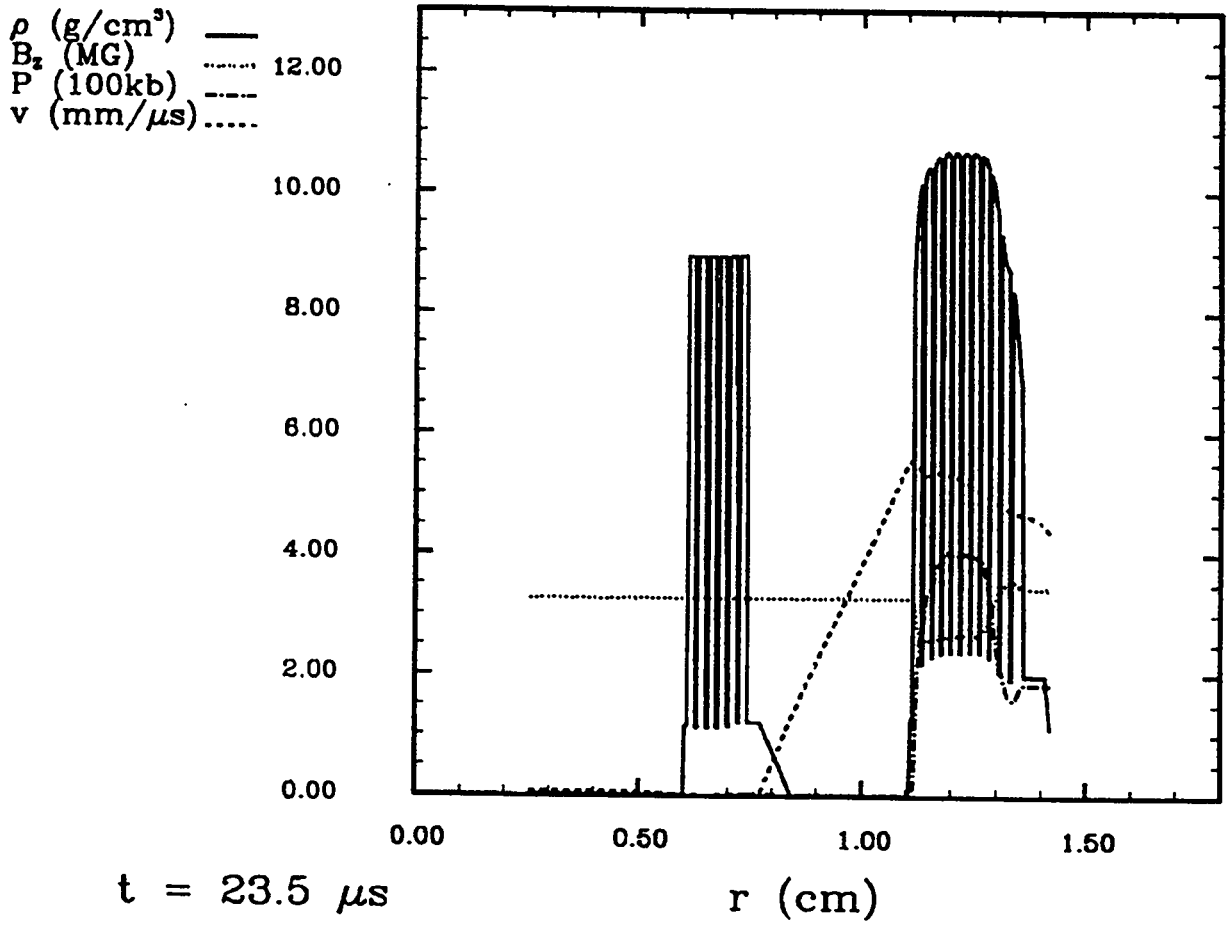


Fig. 5. Profiles through the 2nd and 3rd cascades from RAVEN simulations of the MC-1 driven by COMP-B at 23.5 μs after HE detonation.

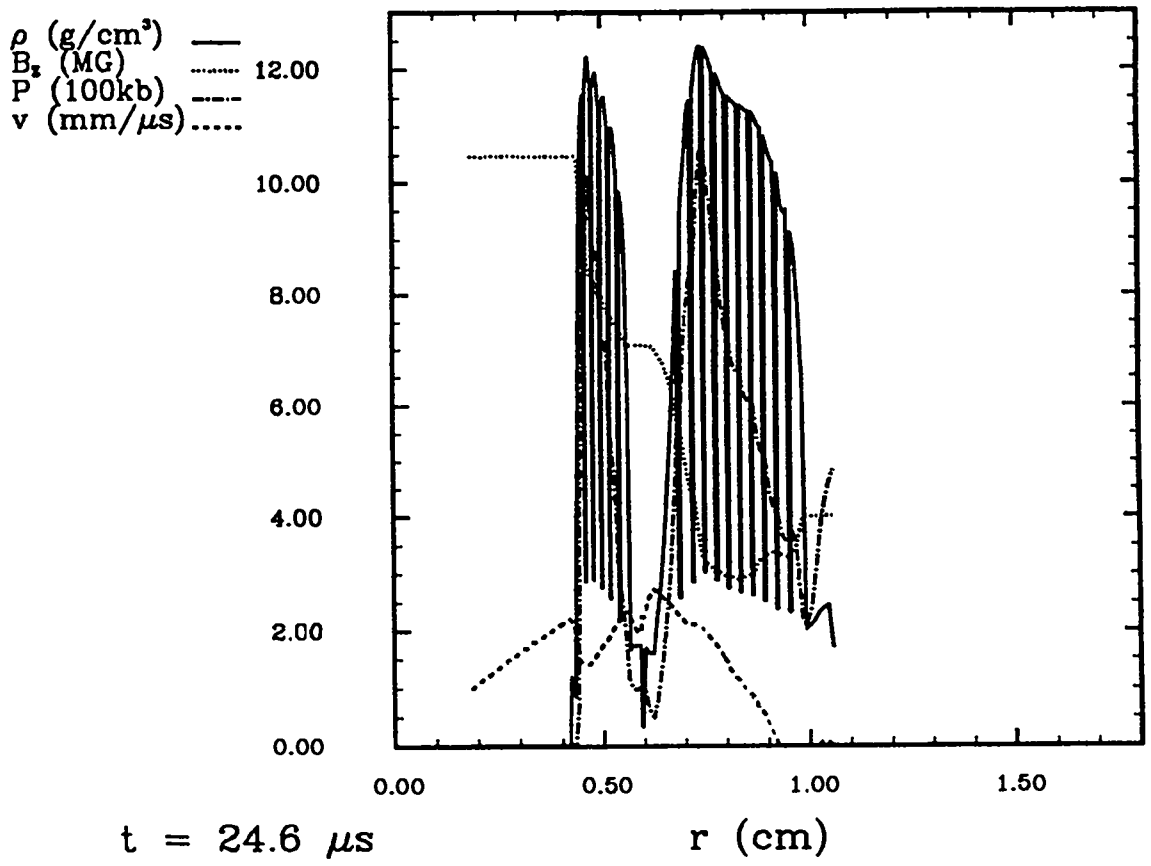


Fig. 6. Profiles through the 2nd and 3rd cascades from RAVEN simulations of the MC-1 driven by COMP-B at 24.6 μs after HE detonation.

experimental volume required to contain the YBCO film, dielectric waveguide, and field diagnostics is 6 mm in radius. Figure 8, taken from the same simulation, shows the zone boundary nearest 6 mm with the zonal density, pressure, and velocity plotted on the same graph as the field and its derivative. RAVEN predicts that the MC-1 should produce 5 MG before destructive signals reach the 6 mm level. Unfortunately, this prediction must be considered optimistic because RAVEN cannot account for shell instabilities and azimuthal asymmetries which could easily generate signals that precede the 1D simulation estimate. Furthermore, accurately modeling the hydrodynamics of shocked foams (with 3D voids throughout) with a simple EOS is a difficult proposition.

Simulations of Isentropic Compression Experiments using the MC-1

Isentropic compression experiments can potentially give valuable EOS data at high pressures and low temperatures. These conditions are reachable through magnetic compression of a cryogenically cooled capsule at the center of a high-field flux-compression system. A recent paper by Fowler et al.[11] surveys efforts in this area. In a system designed by Pavlovskii et al.[12] employing a 2-cascade MC-1, the cryostat consists of two concentric stainless steel tubes surrounding a tubular copper sample holder. The stainless steel tubes form channels for liquid helium. The central volume contains a

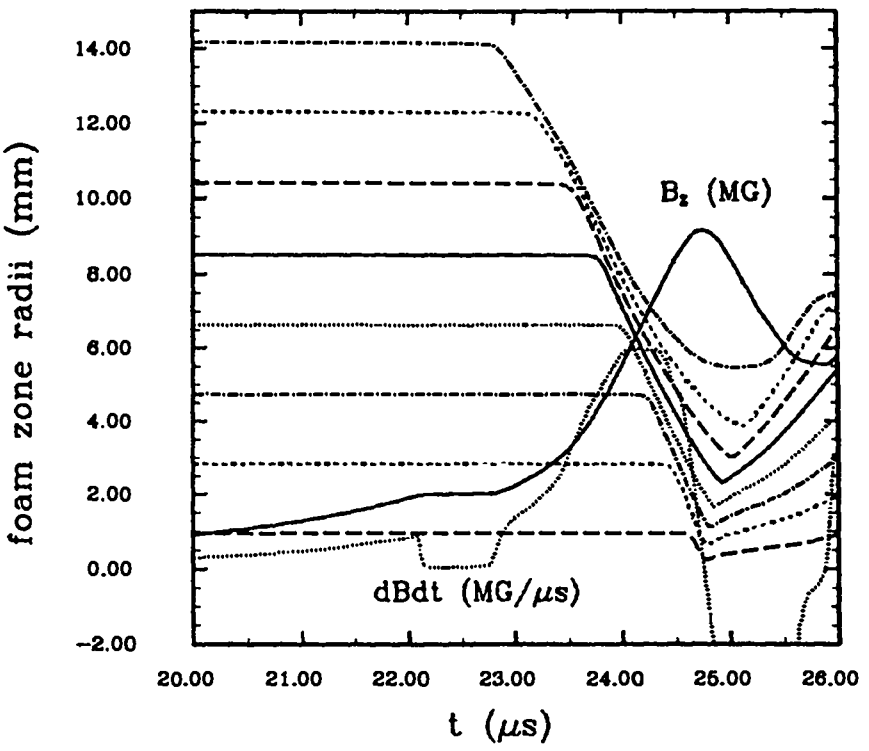


Fig. 7. Selected Lagrangian zone boundaries in the foam cryostat plus the magnetic field and its time derivative from a RAVEN simulation.

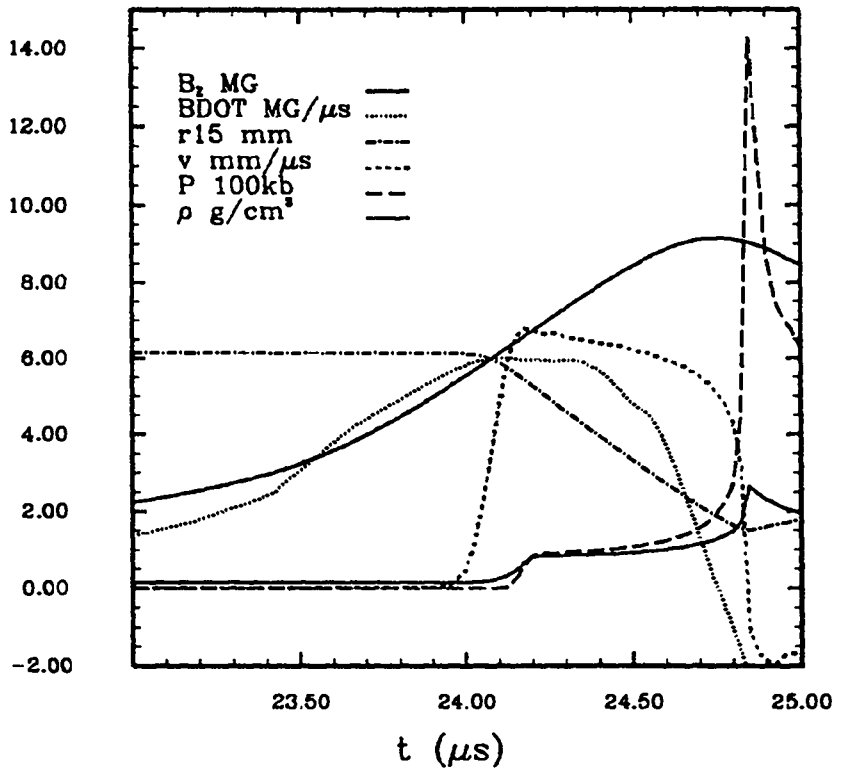


Fig. 8. Time history of the Lagrangian zone intially nearest 6-mm radius in the foam cryostat.

material sample — for instance, frozen deuterium or hydrogen. Only small magnetic fields penetrate through the cryostat to the sample during compression by megagauss fields. Figure 9, extracted from a RAVEN simulation, displays a 1D representation of a hydrogen-filled capsule implosion. Predicted peak pressure in the hydrogen exceeds 10 Mb; however, isentropic conditions are not perfectly maintained in the calculation.

Summary

Collaborations with Russian scientists on the production of ultra-high magnetic fields provide three exciting opportunities. First, these (above ground) experiments will access energy densities which are difficult to realize except in underground tests. Second, the Russian effort in this field is extensive. They have more people, more time, and more money invested in explosive pulsed power and high-field physics than anyone else in the world; we will benefit from their experience as a result of the collaboration. Finally (and this is a political statement reflecting the belief of the authors), the best way to deal with "enemies" is to convert them to friends; and the best way to become friends is to work together towards a mutually beneficial goal. Scientists from Los Alamos and Arzamas-16 will lead our respective countries towards friendship and a more stable peace through this endeavor.

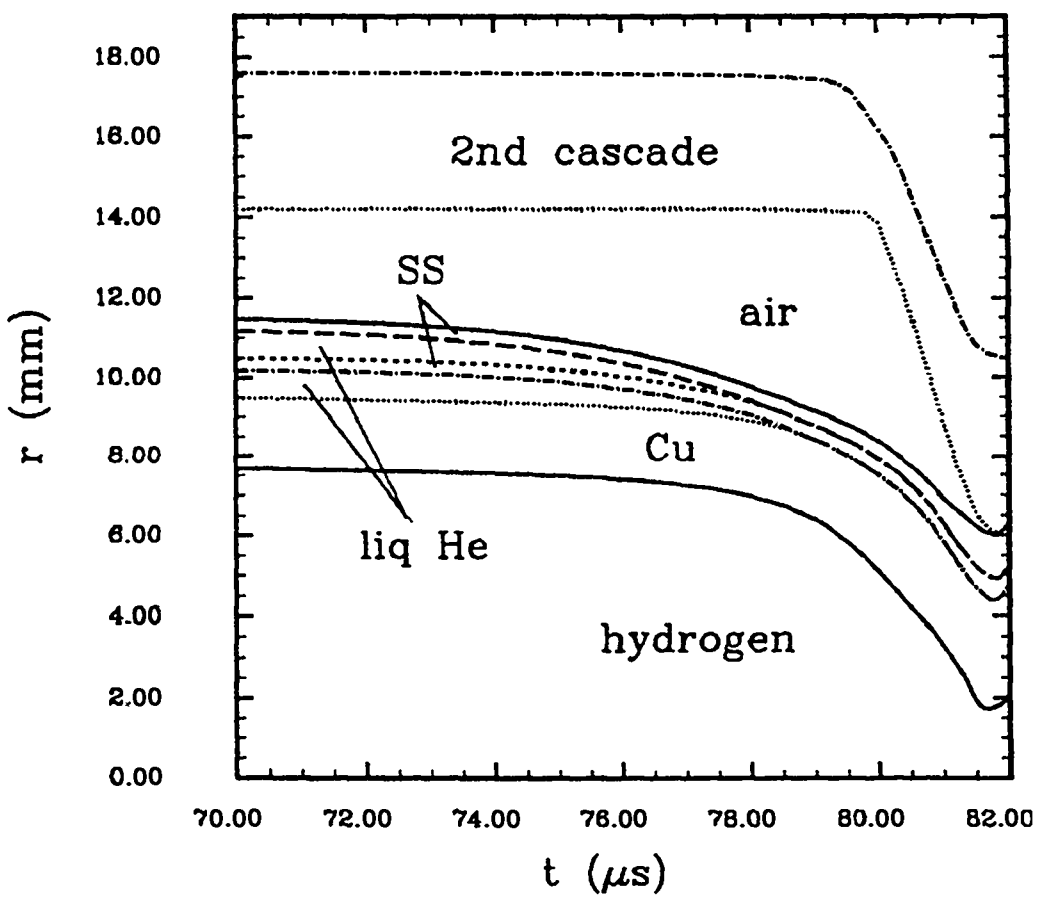


Fig. 9. Interface positions of 2nd cascade and central cryostatic sample container from RAVEN simulation of a possible isentropic compression experiment driven by COMP-B

References

1. Pavlovskii, A. I., "Ultra-high Magnetic Fields Cumulation," in *Megagauss Fields and Pulsed Power Systems*, ed. by Titov, V. M. and Shvetsov, G. A., (Nova Science Publishers, Inc., New York, 1990), p. 1.
2. Fowler, C. M., Caird, R. S. and Garn, W. B., *An Introduction to Explosive Magnetic Flux Compression Generators*, Los Alamos Scientific Laboratory, Los Alamos, NM, UC-34, LA-5890-MS (1975).
3. Pavlovskii, A. I., Karpikov, A. A., Dolotenko, M. I., and Mamyshev, V. I., "Dynamic Characteristics Analysis of a Ultra-High Magnetic Field Cascade Magnetocumulative Generator (MC-1)," in *Megagauss Fields and Pulsed Power Systems*, ed. by Titov, V. M. and Shvetsov, G. A., (Nova Science Publishers, Inc., New York, 1990), p. 21.
4. Pavlovskii, A. I., Kolokolchikov, N. P., Dolotenko, M. I., Bykov, A. I., Karpikov, A. A., Mamyshev, V. I., Spirov G. M., Tatsenko, O. M., Markevtsev, I. N., and Sosnin, P. V., "Production of 15-MG Magnetic Fields in Cascade Ultrahigh Field Generators (MC-1)," in *Megagauss Fields and Pulsed Power Systems*, ed. by Titov, V. M. and Shvetsov, G. A., (Nova Science Publishers, Inc., New York, 1990), p. 29.
5. Fowler, C M., Garn, W. B. and Caird, R. S., "Production of Very High Fields by Implosion," *J. Appl. Phys.*, **31**, 588 (1960).
6. Caird, R. S., Garn, W. B., Thomson, D. B. and Fowler, C. M., "An Explosive-Driven High-Field System for Physics Applications," *J. Appl. Phys.*, **35**, 781 (1964).
7. Caird, R. S., Garn, W. B., Thomson, D. B. and Fowler, C. M., "A Cylindrical Explosive Flux-Compression System," in proceedings of the Conference on Megagauss Magnetic Field Generation by Explosives and Related Experiments, (Frascati, Italy, September 21-23, 1965), p. 101.
8. More, R. M., Lawrence Livermore National Laboratory, Livermore, CA, UCRL-84991 (March 1981).
9. Lee, Y. T. and More, R. M., *Phys. Fluids*, **27**, 1273 (1984).
10. Pavlovskii, A. I., Bykov, A. I., Dolotenko, M. I., Karpikov, A. A., Kolokolchikov, N. P., Mamyshev, V. I., and Tatsenko, O. M., Limiting Value of Reproducible Magnetic Field in Cascade Generator MC-1," in *Megagauss Technology and Pulsed Power Applications*, ed. by Fowler, C. M., Caird, R. S., and Erickson, D. J., (Plenum Press, New York, 1987), p. 159.
11. Fowler, C. M., Caird, R. S., Edeskuty, F. J., Lund, C. M. and Mills, R. L., "Nearly Isentropic Compression of Materials by Large Magnetic Fields: A Survey," in *Proceedings of the International Symposium on Intense Dynamic Loading and its Effects*, (Sichuan University Press, Chengdu, China, 1992).
12. Pavlovskii, A. I., Karpikov, A. A., Mamyshev, V. I., Bykov, A. I., Dolotenko, M. I. and Egorov, N. I., "Analysis of Metal Tube Compression by Ultra-high Magnetic Field Pressure in Cascade MC-1 Generators," in *Megagauss Fields and Pulsed Power Systems*, ed. by Titov, V. M. and Shvetsov, G. A., (Nova Science Publishers, Inc., New York, 1990), p. 163.

This report has been reproduced directly from the
best available copy.

It is available to DOE and DOE contractors from the
Office of Scientific and Technical Information,
P.O. Box 62,
Oak Ridge, TN 37831.
Prices are available from
(615) 576-8401.

It is available to the public from the
National Technical Information Service,
US Department of Commerce,
5285 Port Royal Rd.,
Springfield, VA 22161.

Los Alamos
NATIONAL LABORATORY
Los Alamos, New Mexico 87545

Reference 10

HYDROTEST H-1668: TEST OF AN EXTEX INITIATOR AND COMP B DRIVER FOR THE RUSSIAN MC-1 FLUX COMPRESSION GENERATOR

by

M. Christian

DX-15 Shock Wave Physics Group

Los Alamos National Laboratory
Los Alamos, New Mexico 87544

DX-15:GR-94-1

February 1, 1994

Distribution:
S. Younger, NW/ICFA, MS E527
R. Day, DX-DO, MS P915
L. Hatler, ESA-2, MS C920
J. Boettner, DX-13, MS P940
M. Fowler, DX-15, MS C970
DX-15, Group Report File, MS C970

HYDROTEST H-1668: TEST OF AN EXTEX INITIATOR AND COMP B DRIVER FOR THE RUSSIAN MC-1 FLUX COMPRESSION GENERATOR

ABSTRACT

A series of MC -1 Russian flux compression generator tests planned for TA-39 required a preliminary experiment to check performance of the Los Alamos explosives with the Russian hardware. The goal was to insure a smooth, uniform, and energetic implosion of the cylindrical generator's large first stage, which also produces the initial magnetic flux. Results of RMC photography of a partial hemicylindrical mock-up of the device showed a highly convergent implosive launch of a surrogate liner when Russian initiator blocks loaded with XTX-8003 explosive were used to detonate the thick Composition B driver.

I. INTRODUCTION

Rather appealingly compact, the MC-1 generator's first stage uses ten foam blocks filled with extrudable explosive to initiate the surface of an HE ring (ϕ300 mm $\times$ ϕ152 mm $\times$ 183-mm L), which in turn implodes a hollow cylindrical armature made of many insulated copper wires suspended in a nonmetallic matrix. The Russian HE is a mix of equal parts RDX and TNT, somewhat less energetic than our Comp B variety, which is 60% RDX and 40% TNT. In the historic joint tests planned for the team of Arzamas-16 and Los Alamos scientists, several of the MC-1 generators were to be fired at TA-39's firing point AC88 in December 1993, representing a marriage of Russian hardware and diagnostics on the one hand and Los Alamos explosives and diagnostics on the other. Director S. S. Hecker would observe after the initial experiment how gratified we all were that the first test of a Russian implosion device on American soil would be of such a friendly nature and carried out with our permission.

Of course, the impracticality of rapidly shipping anything but inert parts from Russia to Los Alamos provided the impetus for us to verify that the Los Alamos HE

substitutes would be hydrodynamically acceptable, and we also needed practice hand loading XTX-8003 (also referred to as Extex) into the Russian Initiator Blocks (RIBs). Although there were several alternatives to choose from, we decided on a simple framing camera experiment as an ideal way to check the performance of the initiation system and Comp B in imploding a substitute material for the Russian composite armature.

II. PROCEDURE

While simple mechanical, elevated temperature, and adhesive compatibility tests were being conducted on the RIBs, Task Order 45554 was written by WX-3 for machining of the H-1668 Comp B hemicylinder and assembly of components. A cylinder of an even more energetic HE-PBX 9501 was tentatively requested under Task Order 45548 for a special MC-1 test. This T. O. also provided for Comp B cylinders and assembly of devices for the entire MC-1 Test series, but was contingent on success with H-1663. Meanwhile, Stan Marsh of M-6 ran a hydrocode calculation to verify that a hemicylindrical mock-up initiated with only three RIBs would give us a representative look at the central RIB's convergence zone. During the launch of the surrogate liner material, which we had decided would be 6061-T0 aluminum (fully annealed, zero temper), the camera view would necessarily be restricted to the liner portion below the center RIB. With this arrangement, the liner would function as a blast shield and preserve optical access to its central region. The camera pictures would allow us a means of looking for hints of destructive perturbations or anomalies attributable, perhaps, to a detonation irregularity or local instability justifying further scrutiny. Armed with tidy calculational confirmation of expectations, we began to complete the proposal for the rotating mirror camera (RMC) test to be performed at TA-15's firing point R306.

The 7.0-mm-thick surrogate liner was fabricated from 6061-T6 extruded aluminum tubing by John Horne of the M-1 Branch Shop at TA-15-R313, and then furnace annealed to the T0 condition. Mass of the finished part was 1.22 kg. With a 3.5-mm-square step machined into each long edge, the hemicylindrical liner had an inner surface finish of at least 0.8 μm. For camera recording purposes, the inner cylindrical surface was ink marked with an 11 $\times$ 22-mm grid. Snugly fitting the liner's step-jointed

edges was a box frame of aluminum that held semicircular discs of Plexiglas against the liner's two ends and provided a mounting surface for the large, rectangular, camera-viewing window of Plexiglas. Marked with centerlines, the window's inner free surface was 93.4 mm from the longitudinal centerline running the full length of the liner's inner surface. The two Plexiglas end caps were drilled so that helium could be injected into the liner cavity to defeat the early formation of a luminous gas shock. In retrospect, a vacuum would have been far better than helium because the calculated shock strength in the liner was well beyond 350 kb, and enough to insure an implosion accompained by strong local heating of the helium.

The Comp B cylinder prepared for H-1668 was first cut into halves lengthwise. One piece was further modified with a 12.7-mm × 45° chamfer along the two inner edges that would otherwise be in hard contact with the joint region of the aluminum liner and box frame. This relief prevented prompt penetration of the step-joint area by moderating the pressure discontinuity where the detonation wave abruptly ends. Recorded mass of the finished Comp B part was 7.99 kg. Inked registration lines were marked on both ends of the Comp B hemicylinder to simplify the attachment of the three RIBs on the outer surface and the installation of six ionization switches against the inner surface.

After the RIBs were cleaned, a stepped hole for a Dynasen Inc. Model CA-1040 brass/Teflon ionization pin (ϕ0.8 mm, with protruding central copper electrode ϕ0.25 mm) was drilled near each short edge of the RIB. The holes were drilled perpendicular to the RIB's flat surface and located 23.4-mm transversely by 77.0-mm longitudinally from block center, but were diagonally opposed. The RIB's central spotface was slightly enlarged with a flat end mill to a diameter appropriate for the SE-3 detonator. Holes for the detonator mounting hardware were also added. Next the RIBs were hand loaded with XTX-8003 (about 30 g for each RIB) by Robert Montoya, M-1 (TA-16-340), and then radiographed. The larger voids were repaired, and the completed RIBs were air dried overnight at room temperature. After a thin plastic cover was carefully glued into place, the ionization pins were installed flush against the inner curved surface.

To prepare the Comp B half cylinder for assembly the six, thin, Kapton/copper, ionization switches were glued into place against the inner radius; sensing area of each switch was 10 mm from the HE face. Circumferential location was determined by the angle between the central cutting plane and a radial line to the projected point of intercept with the tip of the ionization pin above in each RIB. The original intent was to have six pin and switch pairs to record relative detonation wave transit irregularities if the liner implosion was not satisfactory. Next, small plastic shims 0.13-mm thick were positioned at either end of the Comp B's inner surface, urethane 7200 adhesive was prepared and painted onto the Comp B, the liner was then pressed into place, excess adhesive wiped off, and a weight was applied to help preserve the uniformly thin and void-free glue layer during the adhesive's overnight cure. Because the ends of the liner had been kept free, however, the liner rotated about 2.6° and translated about 3.5 mm before the adhesive cured. At the top end of the Comp B, the liner was inset 3.5 mm (protruded 3.5 mm less) and rotated counterclockwise 2.6°. Alignment marks on the ends of the Comp B half cylinder were re-inked so that installation of the RIBs would preserve their registration relative to the ink grid on the liner's free surface. Subsequent bonding of the RIBs to the Comp B, with the use of urethane 7200 and carefully applied pressure in an assembly jig, did accomplish that goal. Fast-setting epoxy was used to glue the aluminum box frame to the liner. The final assembly step was to install in each RIB an SE-3 detonator with companion 460-mm-long 31-L cable.

III. FIRING ARRANGEMENT

After delivery to TA-15 firing point R306 on October 28, 1993, the assembly was positioned with cylindrical axis vertical and fixed into place on a rigid foam pad, as the close-up view of the device in Fig. 1 shows. A helium injection hose enters at the top (hidden below is an air exhaust hose), the grid-marked liner is easily seen through the Plexiglas window or cover plate, two timing fiducials (SE-1 bridgewire heads) are taped into place at the lower front of the assembly for proper camera viewing, two small diamonds of yellow tape highlight the location of the horizontal centerline that is inside the Plexiglas cover plate, and reflective poster board wings extend right and left along

the surface of the firing table. Figure 2 shows a near view of the back or RIB-side of the assembly with protective wrapping in place, ionization pins protruding with cables routed to the left, and three ionization switch leads connected to cables at the top of the assembly and taped against the upper end of the liner. Figure 3 is a distant view of the assembly as photographed above the turning mirror (foreground) for the RMC, showing argon flashes positioned for best illumination. The black bundle of cables on the ground to the right attaches to the ionization pins and foil switches.

IV. RESULTS

The synchronous, 70-mm-format, 25-lens RMC (Cordin Mod 120A) was operated at an interframe time of 1.0 μs, allowing an exposure time per frame of about 250 ns. Helium purge of the liner cavity required low-pressure gas flow for at least 20 minutes before firing. A four-channel (1.75-μF/channel), TSD-26, capacitor-discharge firing unit operating at 2.5 kV was used to simultaneously fire the SE-3 detonators in parallel through 14-m-long Type C cables. The camera delay was set to allow several static frames to be recorded before first motion of the liner. Figures 4–6 are enlargements of selected frames of the camera record and show the following:

Frame 7 (Fig. 4), time about 29.9 μs after firing unit discharge: Shock reflection from the liner free surface has occurred and the liner has just begun to move. Black centerlines on the liner surface cross at the location of the detonator center for the middle RIB, the Russian part of main interest in this picture sequence. As mentioned previously, the grid lines on the liner form rectangles 11 $\times$ 22 mm. Easily seen at the top of the picture is the highly uniform zonal expansion of Comp B decomposition products from detonation wave interaction regions. Just below the helium injection hose, the bright arc marks the location of the unchamfered upper edge of the Comp B on the outer surface of the liner. At the lower left of the frame, light from the first timing fiducial is visible.

Frame 9 (Fig. 5), time about 31.9 μs after firing unit discharge: Launch of the liner was highly symmetrical, free of perturbations, and remarkably convergent in the area

beneath the central RIB. The middle portion of the liner has moved about 5.5 mm in 2.0 μs. The strong convergent shock in the helium has heated the gas and it has become luminous, effectively front-lighting the aluminum liner.

Frame 13 (Fig. 6), time about 35.9 μs after firing unit discharge: The shocked helium continues to increase in brightness, reflecting much light from the bare (uninked) portions of the liner. Curvature of the central region of the liner is still highly cylindrical and smooth, with some lag becoming obvious to the extreme left and right as rarefactions take their toll. The center of the liner has moved more than 23-mm total, and velocity is about 4 mm/μs.

Although perfect simultaneity was the goal, detonation-wave arrival in the Comp B surface at the locations of the six coaxial pins in the RIBs ranged from 19.95 to 20.10 μs after firing signal, a rather surprisingly tight spread of only 0.15 μs. Considering the location of the pin relative to the nearby transition zone from XTX-8003 to Comp B, and allowing about 1.5 μs for the detonator's transit time, we can estimate the transit time of the RIB as somewhat less than 18.0 μs. Timing consistency of the RIBs was truly laudable, which may be attributed to Robert Montoya's skill and the forgiving design of the Russian part. Less remarkable simultaneity is to be expected of the two sets of three foil ionization switches, if only because of their asymmetric locations relative to the RIB ends and the printed-circuit switch's inherently more erratic response compared to that of a pin. Indeed, the switch performances offer neither pleasant surprise nor crushing disappointment. Comfortingly close, the average arrival times of the top and bottom sets were 27.38 μs and 27.42 μs, respectively. Time spread for the former was 0.67 us, while that of the bottom set was 0.16 μs. We were heartened by the averages and less so of the spreads, but the reassuring confirmatory evidence of the RMC pictures was agreeably complemented by the pin and foil switch data.

V. CONCLUSION

The combination of the XTX-8003-loaded RIB and the closely fitting Comp B charge functions very effectively as a large-area cylindrical lens with stable convergent

flow characteristics ideally suited for MC-1 generator applications. On the strength of these test results, cylindrical HE charges (four Comp B and one PBX 9501) and hand-loaded RIBs were ordered for the entire shot series, with every confidence of proper performance. The RIB detonators were fired in parallel for this experiment, as is customary here. The favorable outcome reinforced our assertion that the ten RIBs in the final assemblies would perform satisfactorily when fired in parallel, although the Russians typically fire them in series using a high-voltage (60-kV) firing unit.

ACKNOWLEDGMENT

In addition to those named specifically in this report, the author also wishes to thank WX-3 (now ESA-2) colleagues Larry Hatler, Doug Hemphill, Bart Olinger, and Jack Markham for shepherding the entire collection of test hardware through procedural review, fabrication, inspection, and assembly with artful efficiency regardless of a heartless deadline; M-2 (now DX-11) colleagues Daniel Salazar, for expert installation of foils and pins with little advance notice, and Ron Boat, for an entire suite of framing camera services; and M-4 (now DX-13) colleagues Rick Lohsen, for transforming hasty and abbreviated instructions into memos, shop orders, and timing/firing procedures, Lee Chavez, for providing his usual variety of services in fielding the experiment, and Jay Boettner, for expeditiously overseeing and verifying control room preparations and recovering/analyzing transient recorder data with his usual flair.



Fig. 1. Front view of the H-1668 firing assembly at

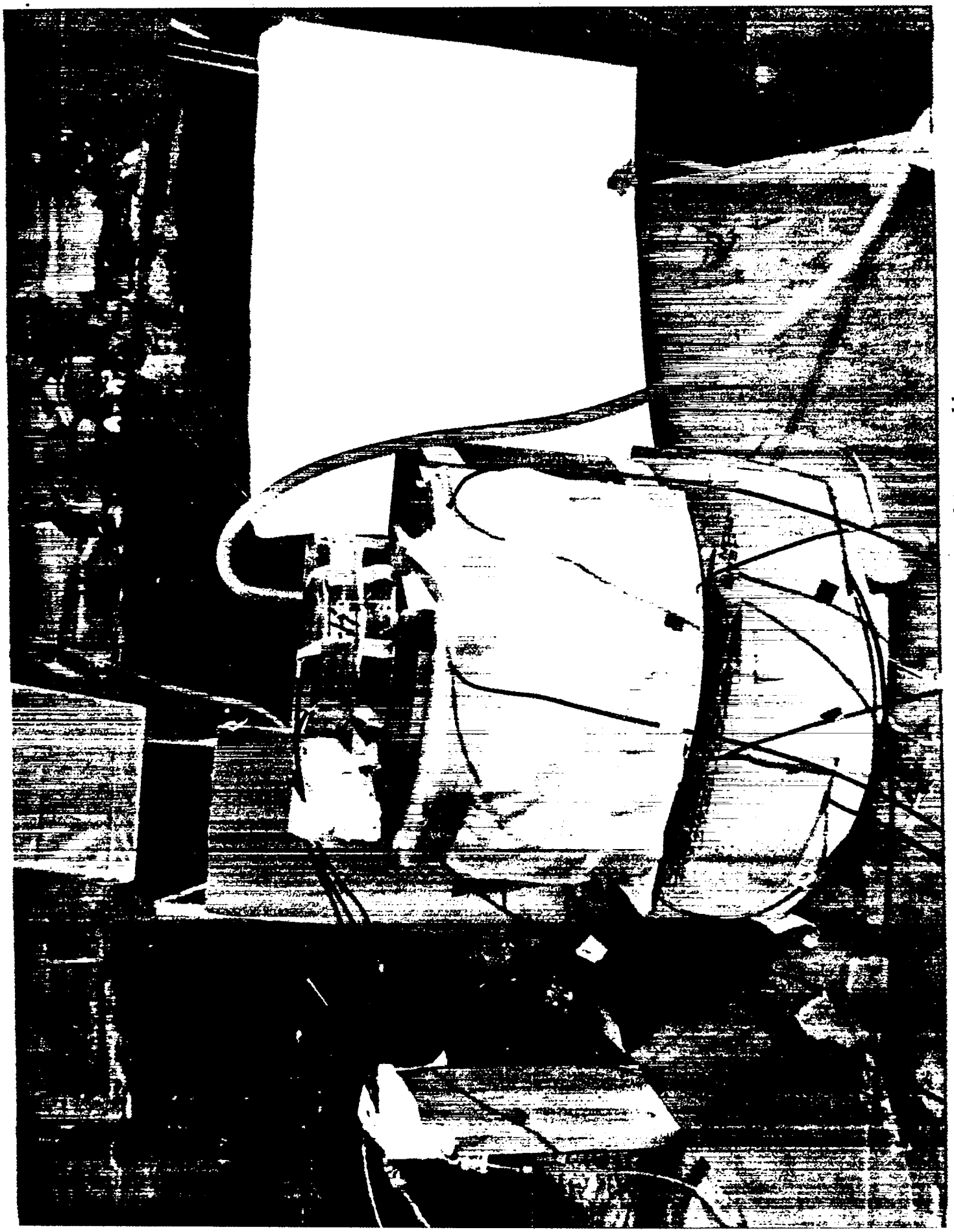


Fig. 2. Rear view (RIB-side) of the firing assembly.



Fig. 3. View of firing assembly from the RMC

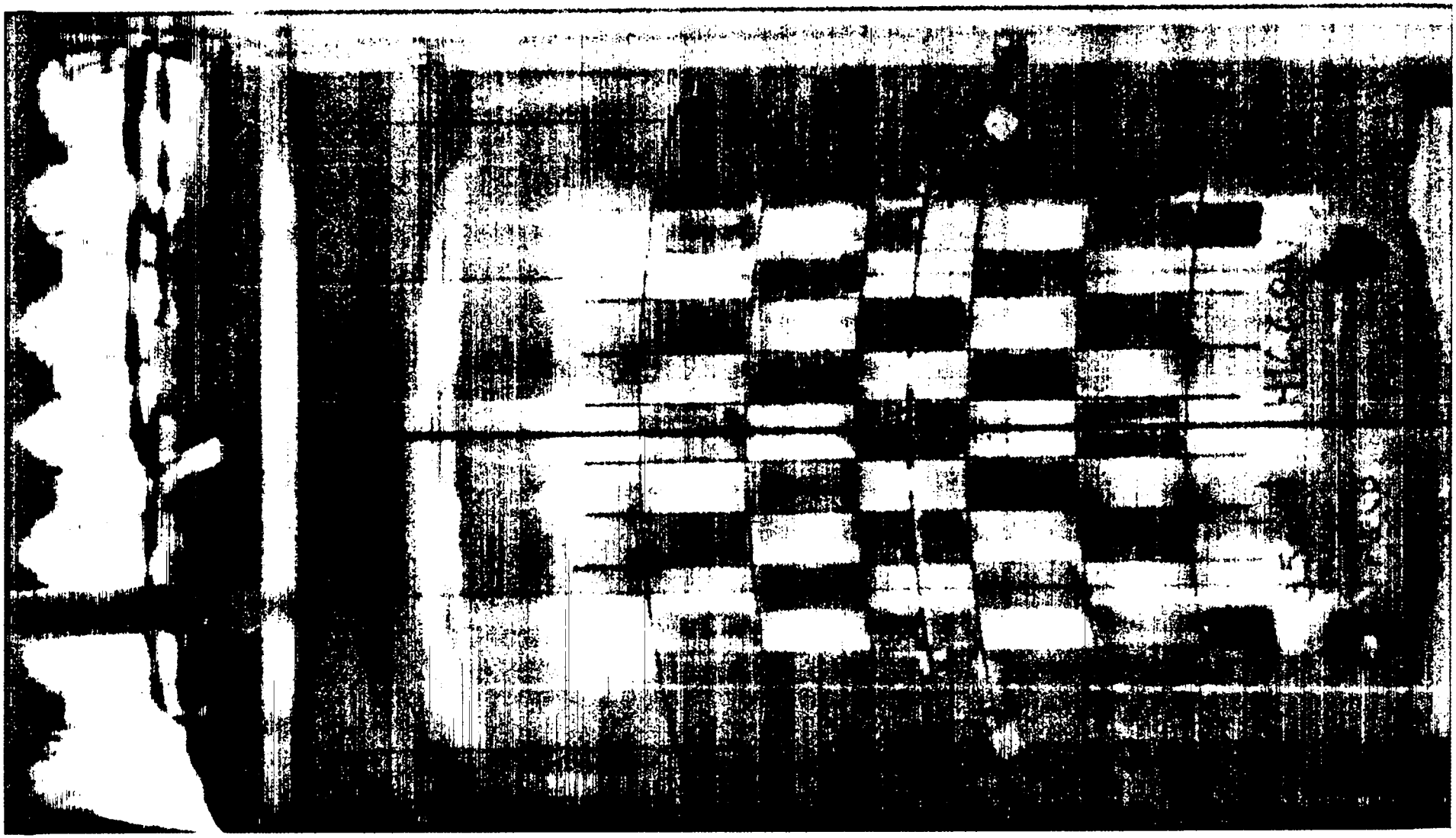


Fig. 4. Frame seven of the camera record.

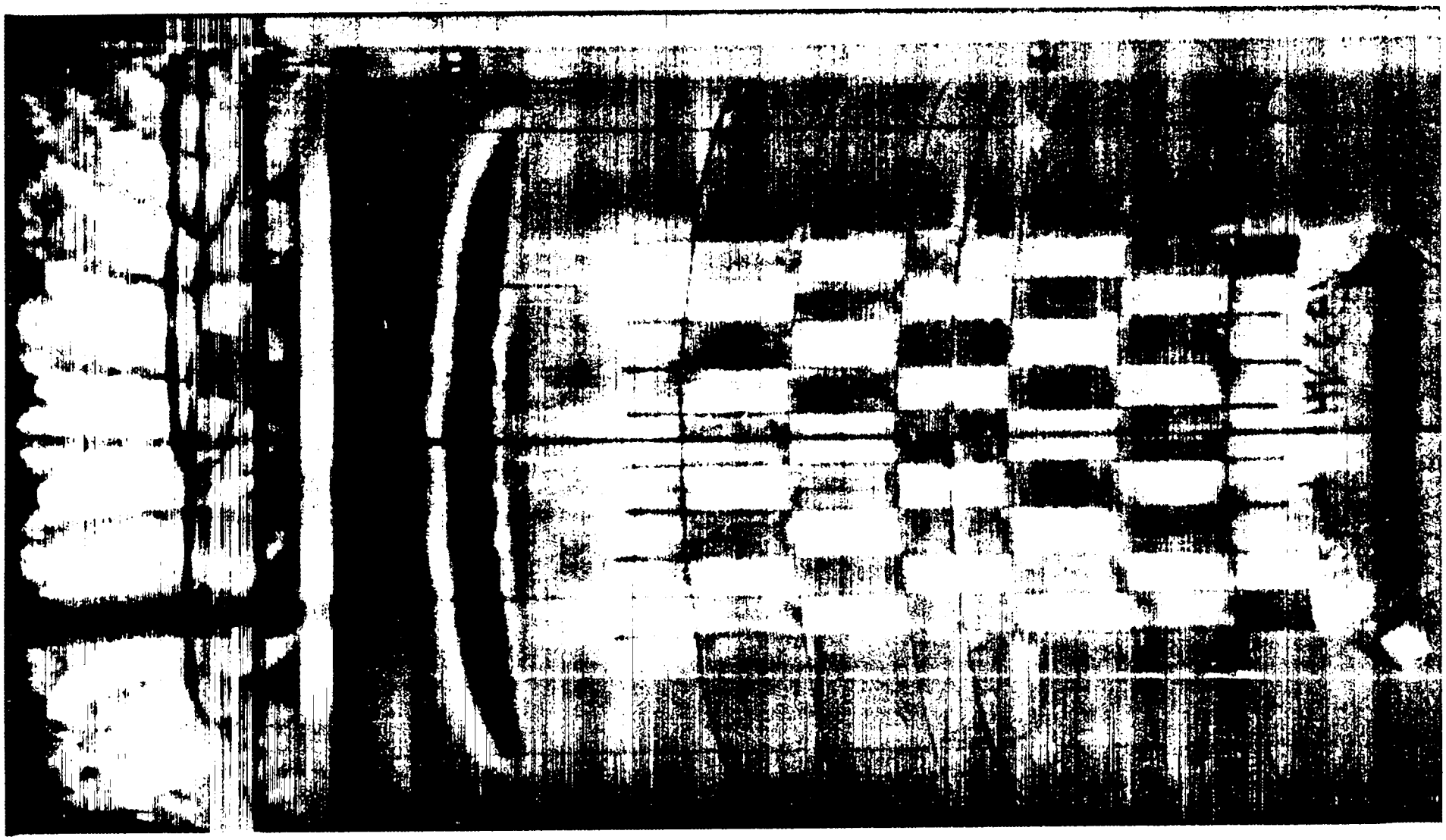


Fig. 5. Frame nine of the camera record.

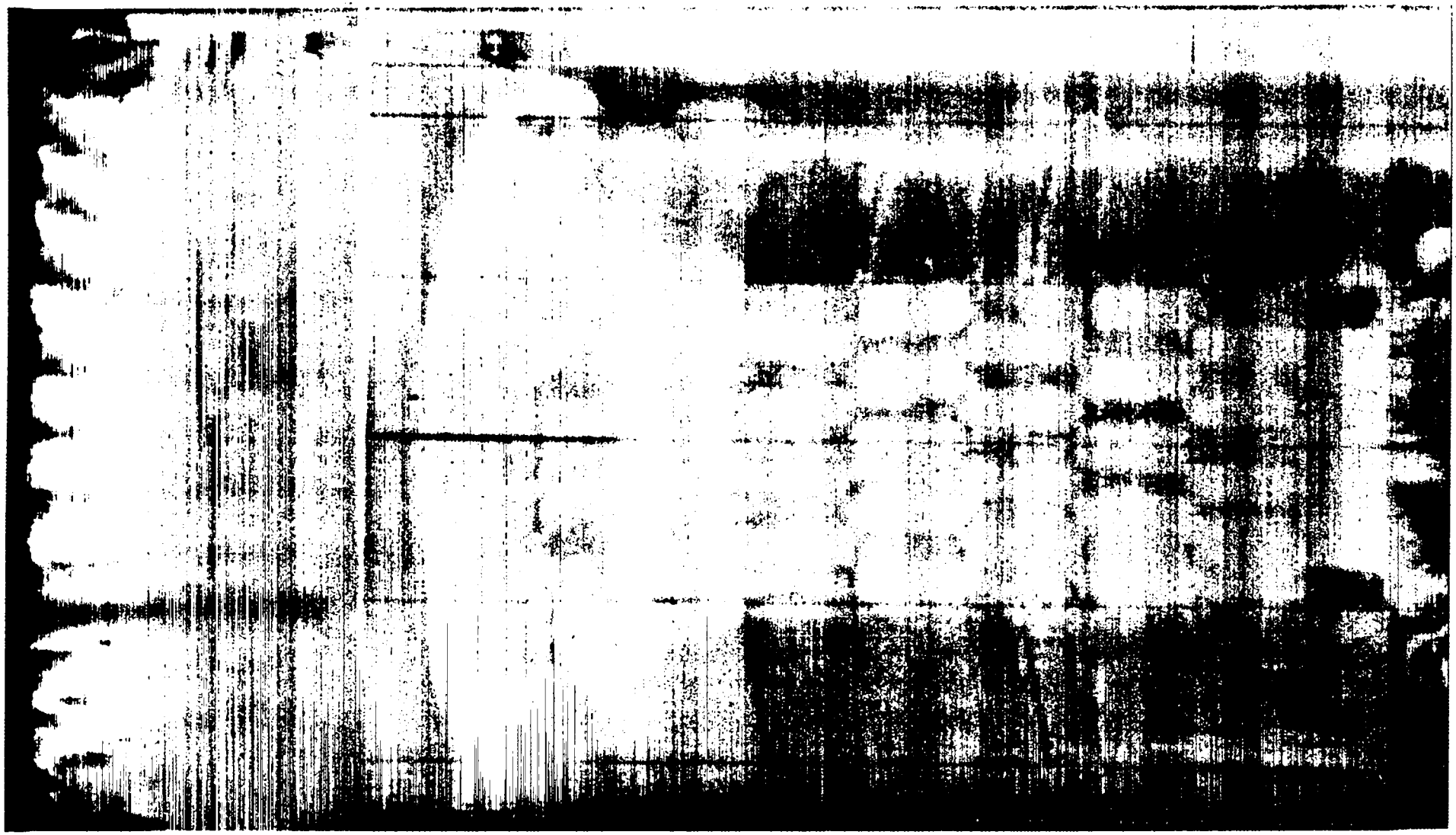


Fig. 6. Frame thirteen of the camera record.

Faraday Magnetic Field and Current Measurements

Lynn Veeser

Shot MC1-1
(3 Cascades)

Set-up for magnetic field diagnostics. On this shot we tried to make a careful comparison of the magnetic field diagnostics, optical and inductive, so that on subsequent experiments we could rely on one of them should there be a partial failure or, if space limitations required, should we be limited to fielding only one magnetic sensor. Here we describe the optical sensors. We fielded three field measurements: a lead-doped "flint" glass Faraday rotation sample, such has been fielded on many of the Russian experiments in the past; and two quartz crystals, for direct comparison to past American Faraday rotation current diagnostics, usually made directly in a low-birefringence, single-mode quartz optical fiber.

The principle of the Faraday diagnostic is that polarized light moving in the direction of a magnetic field will undergo rotation of its polarization direction if it is in a suitable medium, such as glass. The rotation angle is proportional to the line integral of the magnetic field in the medium, i,e, the longitudinal magnetic field times the path length, and the rotation constant is the Verdet constant. We tried in this experiment to define the length of the Faraday rotation medium carefully, placing very thin plastic polarizers on either end of the sample and measuring the modulation of the transmitted light. To make the system practical to field, we used 100-μm-diam-core fiber optics to carry the light to and from the sample, and we tried to place the sample in the center of the magnetic field to minimize fringing effects.

The glass samples were similar in their assembly and operation. The assembly details are described in a separate report by Bruce Marshall. Of prime consideration was the need to fit everything into a small ceramic tube for physical protection. A 1-mm-diam graded-index lens at the end of the fiber collimated the light beam just in front of the sample. Attached to each end of the sample was a plastic polarizer, which was made very thin to avoid excessive Faraday rotation in the plastic. A second lens collected the light into another fiber, which led back to the bunker. For alignment and protection from handling and stray light during

the experiment, the sample, polarizers, lenses, and fiber ends were assembled together and then pulled into a ceramic tube of dimensions 2.0 mm inner diam, 4.0 mm outer diam, and 300 mm length. To shield the fibers from external light, we pulled them into an opaque buffer, about 1 m long, that covered the fibers but left the sensor itself uncovered.

On this shot we struggled somewhat to keep the diagnostics inside a diameter of about 9-mm. As the inner cylindrical cascade stage of the MC1 implodes, it is slowed by forces from the magnetic pressure and from the material being compressed. We wished to restrict the tubes and other diagnostic hardware to the smallest possible volume at the center to allow the cascade to implode with minimal restriction to give the largest possible magnetic field. The three ceramic tubes were placed touching each other in a triangle. (This configuration has a radius of about 4.3 mm since the tubes are 4.0 mm in diam.) Outside the tubes, in one of the three outer recesses, went an optical fiber, approximately 1 mm in diam, to measure the current flowing in the MC1. This diagnostic is described below. Inductive probes went in the other two cavities.

The flint glass sample was 4.04 mm long. Polarizers about 0.02 mm thick were attached to the ends at a relative polarization angle of 45 deg, so that with no magnetic field present, half of the maximum light was transmitted. The Verdet constant, measured in Russia for samples of identical doping and for 632.8-nm-wavelength light, was 0.0526 min/(cm Oe), or 354 deg/MGauss for a 4.04-mm-long sample. The calibration work is unpublished, and its accuracy is about 0.5 %.

The quartz samples were 25.1 cm in length. An average of the published Verdet constant measurements for fused quartz for 632.8-nm-wavelength light is 0.0126 min/(cm Oe), which gives 527 deg/MGauss for the 25.1-mm-long sample. We assume that the constant varies inversely as the square of the wavelength to estimate it for other wavelengths. The polarizers were 0.13 mm thick and consisted of a very thin layer of polarizing material between two plastic layers. The polarizers on the quartz samples were at 22.5 degrees relative to each other. This angle was chosen because we had originally intended to pass laser light through the sample from both directions simultaneously. To the approximation that the wavelengths were identical, the two signals would then be in quadrature. Since the Faraday rotations are in the same absolute direction, one beam polarization rotates toward its polarization analyzer

and one rotates away. In the time available to set up this feature, we were unable to make it work, however, because we could not find a pair of lasers with wavelengths close together that did not experience laser noise when light from one of the lasers entered the other. Thus we ended up using only one light beam per sample.

One quartz sample and the flint sample were operated with HeNe laser light of 633 nm wavelength. Although the light from the lasers in the bunker is polarized, it becomes scrambled in the multimode fiber leading to the experiment so that about half of it passes through the polarizer and enters the sample. We had no problem getting plenty of light through the samples and back to the detectors in the bunker. The second laser was operated with an 818-nm diode laser. This laser failed shortly before the shot and did not return data.

Magnetic field results. Figure 1 shows the magnetic field measurements for the flint and quartz sensors. There is a difference of several per cent in the scale factors for the two data sets. We believe this difference is not caused by calibration differences, but we are in the process of calibrating the flint and quartz Verdet constants relative to each other to verify this belief. Relative calibrations can be done much more accurately than absolute. More likely the scale difference in the results is from position differences inside the MC1 or fringe-field effects caused by the different sensor lengths. An average of the two measurements gives a field of 9.0 MGauss when the probes were destroyed.

Set-up for the current measurements. The generator current was measured with a Faraday rotation fiber that formed a closed loop that went along the axis of the generator (inside the inner cascade, outside of the three ceramic tubes holding the magnetic field sensors) and around the ends and the outside of the MC1. In this way it enclosed the current path as a Rogowski belt would. The fiber was single mode optical fiber, which had been twisted at 40 twists/m to remove any linear birefringence. Its Verdet constant for a single-turn loop around a closed current path is 277 degrees/MA for 633 nm light and 154 degrees/MA at 834 nm.

The polarized light was provided by a diode laser of wavelength 834 nm. It was battery powered and was enclosed in an EMI-shielded box and placed on the firing point behind a blast shield a few meters from the generator.

Polarization analysis was done in a small cube, about 4 cm on a side, in which were contained the optics and polarizers. Fiber optic connectors, position adjustment fixtures, and collimating lenses allowed quick, easy attachment of the input and two output fibers. The cube had a half-wave plate and a non-polarizing beam splitter at the input, from which emerged two roughly equal light beams. These beams continued through infrared polarizing plastic films oriented at 45 degrees relative to each other to put the beam signals in quadrature. The polarization-analyzed light beams from the polaroid films were then lens-coupled into multimode optical fibers that led from the optics cube, near the laser, to the recording bunker. At that point optical receivers detected the light, and the resulting electrical signals were recorded on digitizers. Shortly before the shot the half-wave plate was rotated so that one signal (designated COS) was at its maximum, leaving the other (denoted SIN) at about half of maximum power level.

The optical receivers were photodiode-based, amplified electro-optical converters. Their bandwidth is from DC to 200 MHz, and their output gain is 50 mV/μW, linear to a maximum of 1 V output. Silicon photodiodes in them respond to wavelengths from about 400 to a little over 1000 nm. An optical filter of bandwidth 10 nm and roughly centered on the laser wavelength removed nearly all of the stray light.

Results of the current measurements. Only the COS signal returned data on this shot, and the fringes were poorly defined, with peaks that were only five digitizer sample units higher than the valleys. Apparently the laser output intensity dropped just before the shot, after the digitizer sensitivities had been set to match the receiver output. Instead of analyzing the data in our usual manner, which is to divide SIN by COS and calculate the arctangent, we calculated the current from the one good signal. For this particular signal, where there are many fringes and where it is known (from the magnetic field data) that there are no current reversals, the accuracy is hardly compromised by the lack of quadrature information. The current measurement from the current sensor is shown in Fig. 2. Because of fringing effects, the field in the center of the generator is not exactly proportional to the current, particularly at early times, when the diameter of the inner cascade is large.

Shot HTBF

For this experiment, a two-stage Los Alamos design, we used a single flint glass sensor to measure the magnetic field. The flint was 4.03 mm long, and its assembly and set-up were as described for shot MC1-1. Only the single ceramic tube was used. Since this shot was intended mainly as a test of the microwave diagnostics for the superconductor experiments to be done on the following MC1 tests, much of the diagnostic volume was devoted to the microwave experiment. No current measurement was made. Figure 3 shows the magnetic field v. time. It appears that the sensor followed the field to its maximum of 140 T and perhaps just slightly beyond before breaking.

Shot MC1-2
(3 Cascades)

This experiment was undertaken to concentrate on producing and diagnosing the highest possible magnetic field before losing the sensors. We used a single magnetic field sensor, a flint glass sample 4.03 mm long, centered in a ceramic tube of about 2-mm ID and 4-mm OD. Again, as on shot MC1-1, a fiber to measure the current and inductive probes to measure the field were all fastened to the outside of the tube, but diagnostics were kept to the absolute minimum.

Figure 4 shows the magnetic field v. time. For comparison the field obtained on shot MC1-1 is also included, but its time is shifted 2.89 μs later to account for the fact that on MC1-2 the crowbar time was later by that amount. It is apparent that the more energetic high explosive used on MC1-2 produced a faster implosion and a larger final magnetic field, 10.8 MGauss.

Figure 5 shows the current from the shot. As on MC1-1, the imploding cascade destroyed the fiber before the flint sample. Both of the quadratured channels returned good data.

Shot MC1-3
(2 Cascades)

This experiment attempted to use the diagnostic geometry of shot HTBF to measure the conductivity of a superconductor sample in the higher MC1 magnetic fields. Thus the cryostat, with a single flint sensor, 4.03 mm long, and the microwave diagnostics, was used. A fiber in the cryostat measured the current. The significant data were the microwave transmission and reflection as a function of the magnetic field. These data are shown in the section describing the microwave experiment. The field itself was similar to that on MC1-1, except it stopped increasing around 5 MGauss.

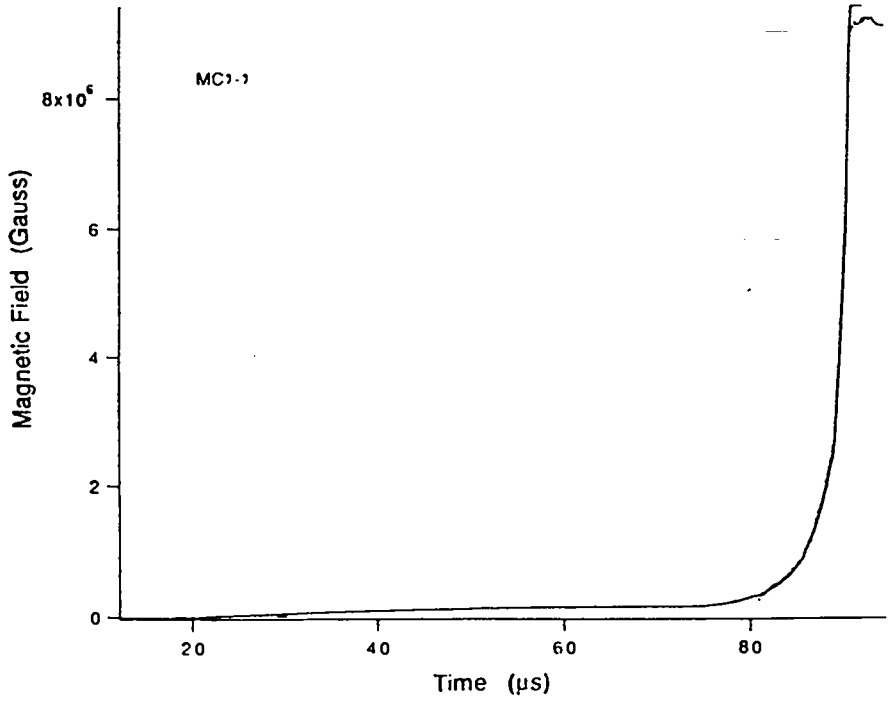
Shot MC1-4
(2 Cascades)

This experiment was a repeat of MC1-3 but at a different temperature. The diagnostics were similar: microwaves, a 4.02-mm-long flint glass, and a fiber. Again the magnetic field results are presented in the microwave section. On this shot the laser for the Faraday current fiber failed shortly before the shot, and no current measurement was obtained.

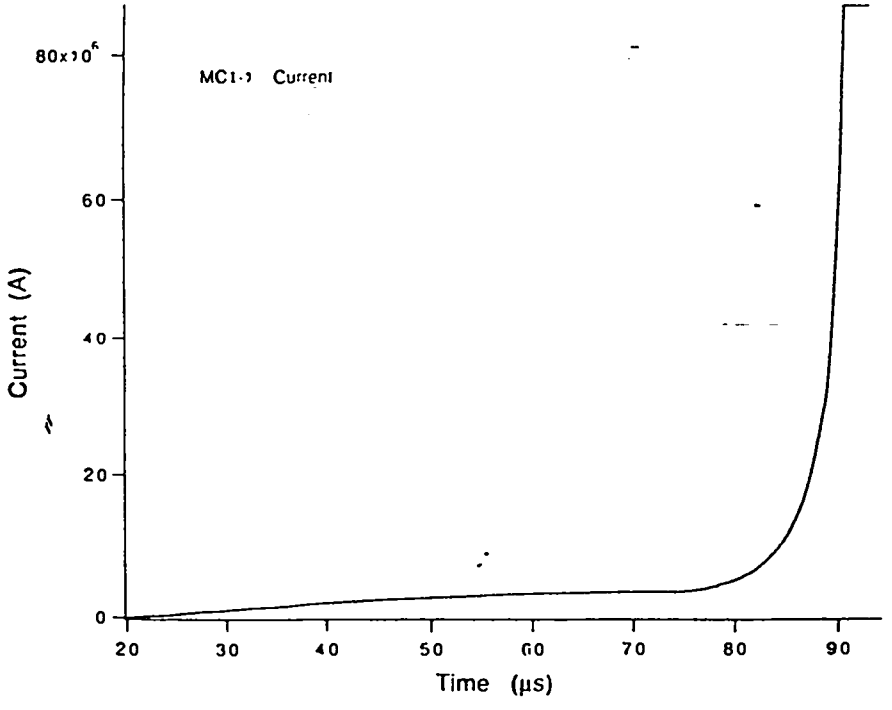
Shot MC1-5
(2 Cascades)

On this shot we fielded a 0.93-mm-thick CdS sample in place of the flint glass. The intent was to measure the CdS Faraday rotation as a function of field, but there was room for only one optical probe. Since the Faraday rotation becomes non-linear at high fields in CdS, we relied on the inductive probes to determine the field. To maximize the non-linearity in the Faraday rotation, we used a shorter-wavelength laser, a HeNe laser operating at 543 nm. We went to considerable effort to try to transmit

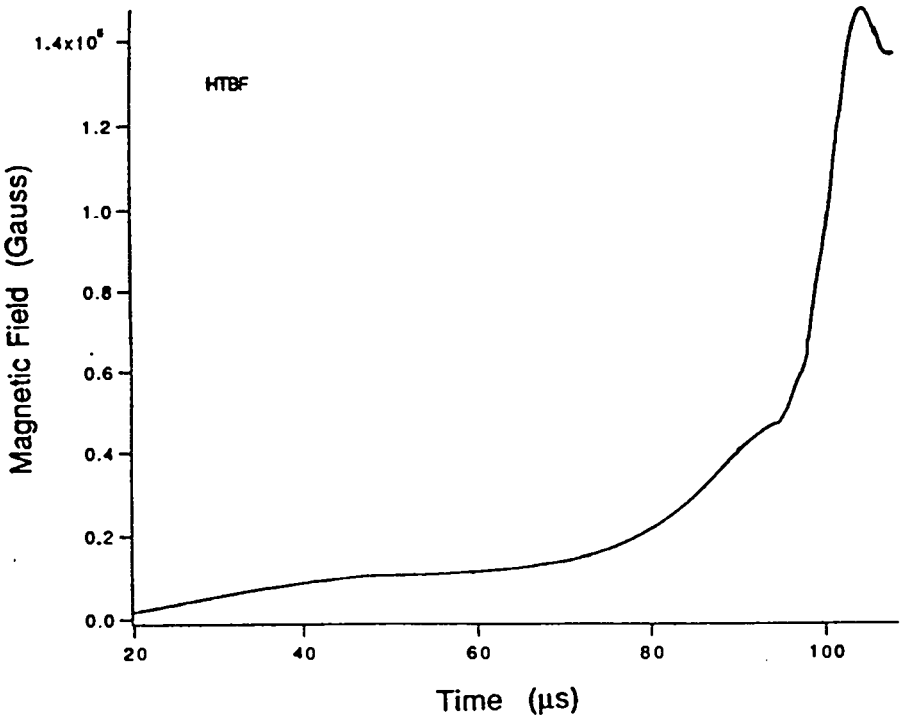
light from two lasers (the other was the 633-nm-HeNe from the flint glass sensor from the previous shots) simultaneously through the sample, this time with both beams travelling in the same direction to avoid the reflection problems. However the losses involved in using the required directional couplers were too high, and we had to abandon the red laser to obtain better data from the green one. Figure 6 shows the Faraday rotation v. time.



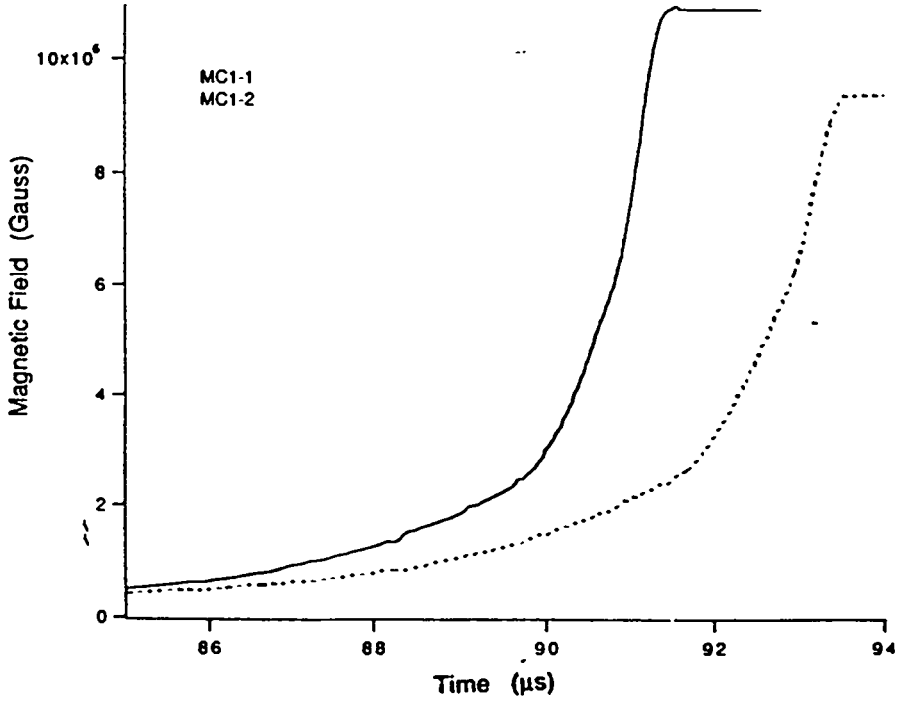
1) Faraday rotation measurements of the magnetic field for shot MC1-1. The solid line shows the flint glass results and the dashed line shows the results for a quartz sensor.



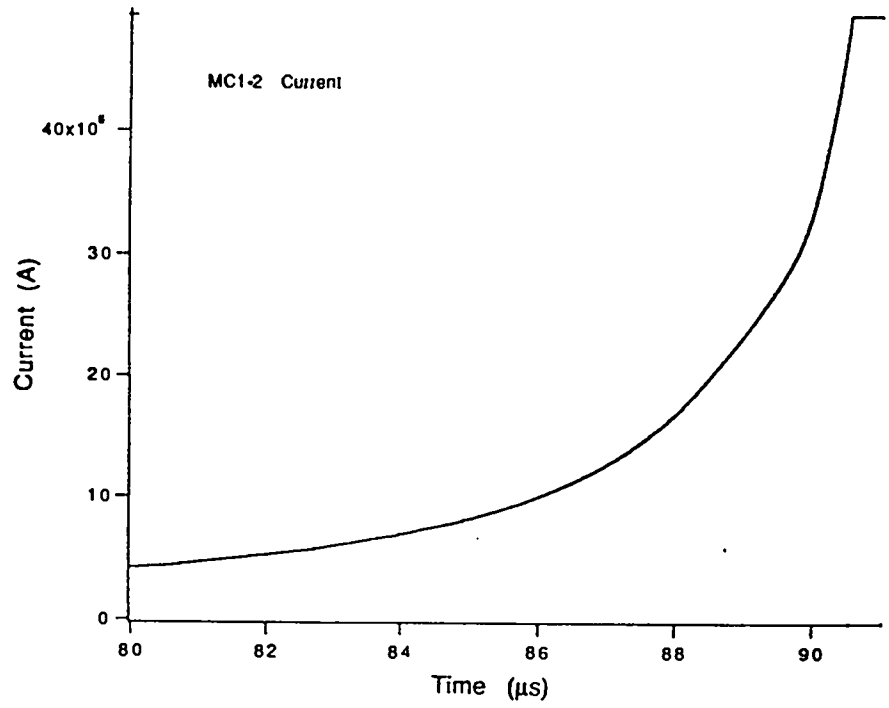
2) Faraday rotation measurements of the current from shot MC1-1.



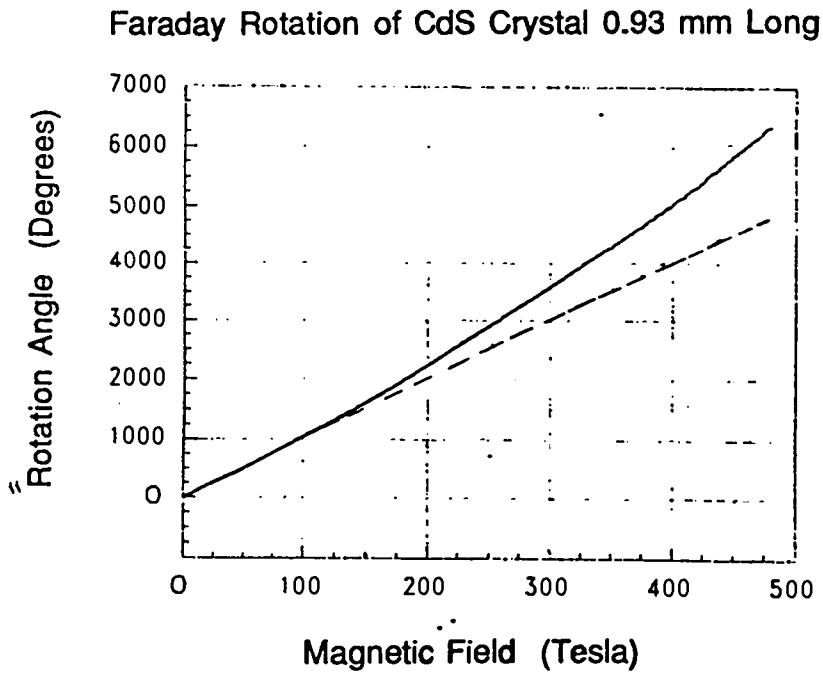
3) Faraday rotation measurements of the magnetic field for shot HTBF.



4) Faraday rotation measurements of the magnetic field from shot MC1-2. For comparison with the Comp-B-loaded shot, MC1-1, the dashed line shows the data of Fig. 1 delayed by 2.89 μs so that the times after detonation are the same. The higher explosive energy of 9501 is demonstrated by the faster implosion and higher final field in shot MC1-2.



5) Faraday rotation measurements of the current in shot MC1-2.



6) Faraday rotation in CdS (curve) v. magnetic field for shot MC1-5. The dashed straight line is drawn to help show the deviation from linearity at high fields.

Report on Faraday Sensors Supplied to P-14 for Magnetic Field Compression Experiments, November - December 1993

Bruce Marshall, EG&G SBO

Abstract

A total of nineteen Faraday effect magnetic field sensors were delivered to P-14 for the magnetic flux compression experiments. Three different active media were used: fused silica, lead glass, and cadmium sulfide. The sensors performed satisfactorily. A new method proposed for obtaining quadrature outputs was unsuccessful, probably due to reflections in the system. The schedule did not allow a thorough evaluation of the idea. We anticipate that more Faraday sensors will be needed in 1994. The fabrication will be transferred to EG&G LVAO.

Summary of sensors delivered to P-14

Qty	Faraday material	Length, mm	Wavelength, nm	Polarizer		
				Type	Thickness, μm	Angle, °
6	SiO_2	25.0 ±0.25	830	HN-7, 3 layer	125	22.5
6	Pb glass	4.02 ±0.02	633	HN-42	20	45
5	SiO_2	12.0 ±0.12	830	HN-7	40	0
2	CdS	0.93 ±0.02	488 543	OFS-270-2	20	0

In addition, we have components for two more CdS sensors, but are postponing assembly until we receive HNP'B polarizing material, which should be the best choice for the blue region.

Introduction

A number of magnetic field sensors were required for the joint P-14 / Russian magnetic field compression experiments. The technology of Faraday magnetic field sensors is well known. However, the experimental constraints coupled with a tight schedule made the present requirements somewhat more difficult to meet.

The fields to be measured were on the order of 10 megagauss; therefore, the sensors were made relatively short to achieve low sensitivity. To prevent Faraday rotation in the

downleads from affecting the measurement, we placed the polarizers immediately adjacent to the sensor rods. To minimize Faraday rotation in the polarizers, we stripped the protective layers off of the polaroid filters and used only the 25 micron thick polarizing layer.

No conductive materials were allowed. There was also concern about electrical breakdown or conduction by any plastics. The bodies of the sensors were made of MACOR machineable ceramic. The polarizers were epoxied to GRIN lenses and air gaps of several millimeters was maintained between the polarizers and the sensor rod. The sensor rod was mechanically supported without epoxy.

The sensors were to be placed in 2 millimeter inside diameter ceramic tubes that were mounted in the generator. This required that we use 1.0 millimeter diameter GRIN lenses instead of 1.8 mm or 2.0 mm, resulting in relatively poor collimation. Most of the laser diodes and receivers available for the experiment use 100 micron fibers. A smaller fiber on the sensor would have improved the collimation and coupling efficiency of the sensor while incurring excess loss at the interface with the 100 micron fiber. I chose to use 100 micron fiber on the sensors because the alignment would be less critical. The only time when the collimation became a significant problem was on the 25 mm long fused silica sensors, where some of the marginal rays reflected off of the side of the rod. However, the effect only caused a reduction in the extinction ratio to about 50:1. On the shorter sensors, it was not a problem.

On some of the tests, the sensors would be used at near liquid helium temperatures ($\sim$4 K). Therefore it was important to match expansion coefficients of the materials as much as possible and minimize the thickness of the epoxy joints. The sensors were designed so that they would probably still function even if the epoxy joints failed.

A number of Faraday materials were considered, including lead glass, SF 57 glass, zinc selenide, fused silica, and cadmium sulfide. As the experimental plan solidified, the list was narrowed down to 4 mm long lead glass, 12 mm and 25 mm long fused silica, and 1 mm long cadmium sulfide.

The Russians supplied six pieces of lead glass 1 mm diameter by 4 mm long. We cut and polished Ensign Bickford 1 mm fiber for the fused silica rods, leaving the hard plastic cladding on the 25 mm rods for strength, but removing it from the 12 mm rods to eliminate plastic. Max Fowler supplied a piece of CdS 6 mm diameter by 1 mm thick with polished surfaces. From this, we cut four pieces 1.35 mm diameter for the sensors.

We used Polaroid HN-42 polarizers for the lead glass sensors which operated at 633 nm and Polaroid HN-7 for the fused silica sensors, which operated at 830 nm. For the cadmium sulfide, operating at 488 nm, we used OFS-270-2 manufactured by American Hoescht, because it gives good extinction in the blue.

Quadrature outputs would be desirable since it would improve the quality of the data. To achieve this, I proposed a system using bidirectional light paths with polarizers at 22.5°. This would allow us to get quadrature outputs while retaining the small size of the sensor.

This idea was tried on the confidence tests using the 25 mm fused silica sensors, but the signal levels were very small with a large DC background. It is not clear what caused the problem, but it may be due to feedback into the lasers or non-optimized bandpass filters. Also, the 25 mm sensors have the lowest transmission due to the long path length. It would be worth investigating this idea more carefully before the next series of experiments begins.

Preliminary design - 25 mm long SiO_2 rods

For the preliminary confidence tests at 1 to 2 megagauss, we built 6 sensors with 25 mm long fused silica rods using the design shown in figure 1. The design of these sensors differed from the later ones in that the rod was not enclosed in a ceramic tube because of the difficulty in drilling so great a distance. Instead, each end of the rod was inserted a few millimeters into a ceramic tube containing the GRIN lens. The polarizers were epoxied to the sensor rod and oriented at 22.5°. The sensor rod was made from 1 mm Ensign-Bickford optical fiber, and the hard plastic cladding was left on the rod for strength. The excess insertion loss of this design was about 8 dB.

There were several problems with the 25 mm design. The polarizers were attached directly to the sensor rod. Epoxy was in contact with the sensor rod both to hold the polarizers on and to attach the collimator tubes to the rod. More fragile sensor materials would require continuous support over their entire length. Since all of the remaining sensor rods were at most 12 millimeters long, continuous tubes would be practical. Therefore, we changed the design for the remaining sensors.

Final Design

Figure 2 shows the final design used for the 4 mm long sensors. The 12 mm and 1 mm sensors were similar to the 4 mm, with the length of the space for the sensor rod adjusted appropriately. The main difference between the final design and the preliminary one is that, in the final design, there is no epoxy touching the sensor rod and the polarizers are mounted on the GRIN lenses.

As can be seen in Figure 2, two ceramic tubes are used, one of which has space for the sensor rod to be inserted. A GRIN lens with polarizer attached is epoxied into each tube, and a cleaved fiber mounted in a glass capillary tube is aligned to the GRIN lens and epoxied in place. After the sensor rod is inserted, the two ceramic tube assemblies are joined, rotationally aligned, and epoxied. The sensor rod is mechanically retained by the ceramic tubes and separated from the polarizers and epoxy by several millimeters of air space.

Suggestions for improvement

A number of improvements should be considered before fabricating more sensors. First, the technique for aligning the collimators is pretty crude, although it worked well enough for this

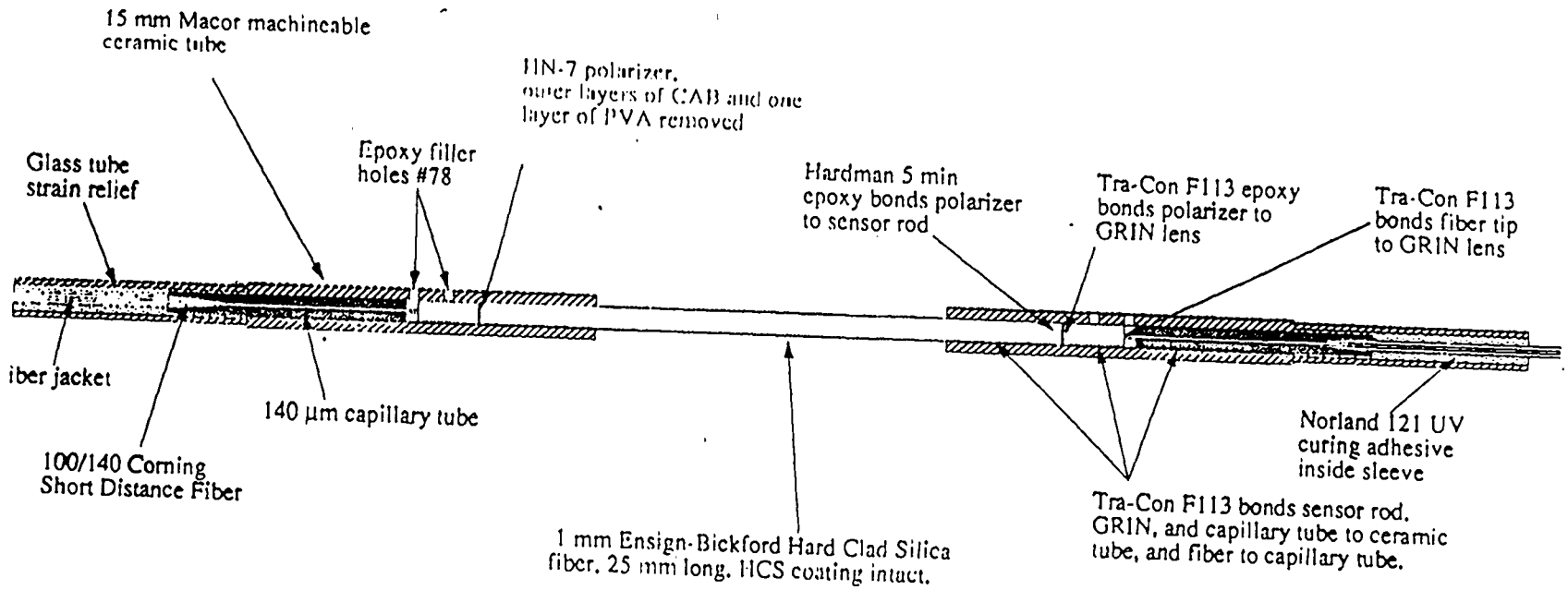
application. Better positioners would allow a more conventional approach. It might be worthwhile to conduct a literature search on techniques for assembling GRIN lens fiber collimators.

A better procedure for cleaning the polarizers needs to be developed. I think that it would help to mount the material on a frame so that it could be handled more easily. It might be necessary to use a clean room, or at least a clean bench. A portable punch that could be placed in a clean environment would probably help. If we could clean the polarizers, punch them out, and attach them to the GRIN lenses in a clean environment, we would be able to produce a better quality product. However, the dirt problems I encountered seem to be only cosmetic, and the only real effect of it was to produce a lot of reject polarizers.

The Hardman 5-minute epoxy used to attach the polarizers to the GRIN lenses might be replaced by a UV curing adhesive. This would take some of the pressure off of the assembly procedure. However, we must be certain that the UV adhesive does not cause any problems.

The TraCon F-113 epoxy requires an overnight cure. Since there are several gluing steps, this increases the assembly time. I was unable to find another adhesive that had low viscosity and room temperature cure as well as a faster cure time.

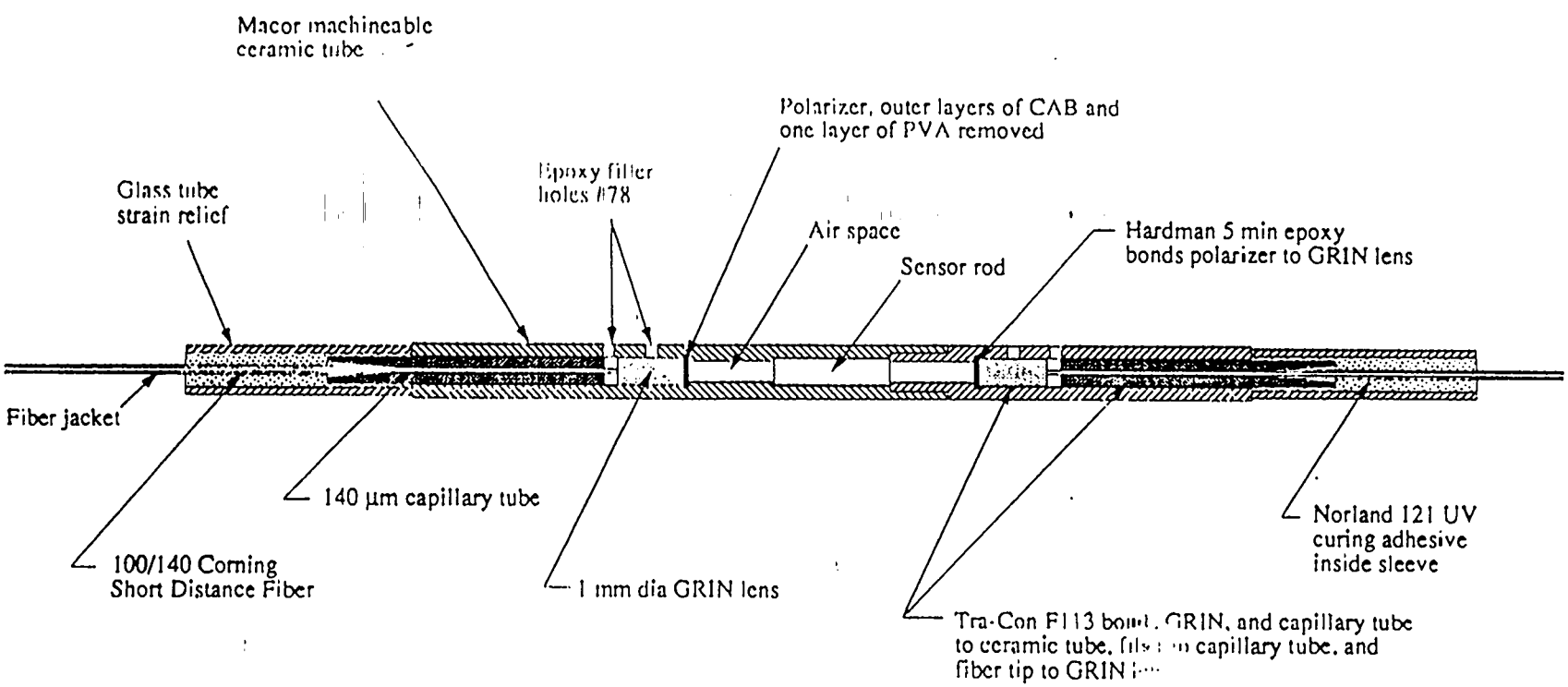
Figure 1. Faraday Sensor Using 25 mm Fused Silica Rod and GRIN Lenses, Split Tube



file: 25 mm split tube assembly final

Figure 2. 4 mm Sensor, Final Design

The sensor rod is held in place mechanically.
The nearest epoxy is about 2 mm away, and the polarizers are about 4 mm away.



file: 4 mm assembly final

94 Ghz Interferometer

William D. Zerwekh, DX-15
Los Alamos National Laboratory

ABSTRACT This paper describes a 94 GHz interferometer that was used to measure the change in complex impedance in a thin-film, high temperature superconductor (YBCO) when under the influence of an extremely high pulsed magnetic field.

INTRODUCTION In the fall of 1993, a series of experiments was planned to characterize the response of thin-film (1500 nm) YBCO (Y123) superconductors to high (500 T) pulsed (600 ns final doubling time) magnetic fields. These experiments were intended to identify the field at the commencement of magnetic vortex unpinning and the field at saturation of vortex migration. In view of the extreme B and dB/dt involved in these experiments, no sensor coils or hollow metallic waveguide could be used. Therefore measurement signals were to be inserted and collected via dielectric waveguide. The magnetic fields were to be produced using MC-1 generators provided by a team of Russian scientists from Arzamas-16. This generator is a cylindrical implosion system, and the diameter of the implosion shock at a field of 500 T is approximately 12 mm. To keep the imploding shock from unduly modifying the propagation of the evanescent wave around the dielectric waveguide, a maximum wavelength of 4 mm was indicated. Due to atmospheric attenuation characteristics, a frequency of 94 GHz was chosen. Because of the losses involved in the large length of WR-10 waveguide necessary to provide standoff from the explosive used in the MC-1 flux compression generators, 60 dB of gain was required. Since the generators produce a severe EMP environment, the bulk of the gain must be supplied at a frequency well above bandwidth of the EMP energy. Due to previous experience with interferometers at 8 GHz, this frequency was chosen as the intermediate frequency.

CIRCUIT DESCRIPTION Two sources of RF are required for this interferometer (Figs. 1 & 2), one at 8 GHz and the other at 86 GHz. The 8-GHz source is provided by a CW Synthesizer and a TWT Amplifier located at a protected remote location. The output of the synthesizer is set to establish the proper power level at the input of the interferometer chassis. The 86 GHz is provided by a Gunn diode oscillator mounted on the chassis.

The output of the Gunn is split, and half is filtered to remove spurs and fed to the up converter mixer. The output of the up converter is filtered to remove the residual 86 GHz and fed through an isolator to prevent reflected signals from affecting the RF supply performance. It is then fed through a 10 dB coupler which returns the reflected signal to a down converter mixer. The RF is then sent to the HTSC sample. The transmitted signal returns through a second waveguide to the second down converter. The second half of the Gunn output is split again and used as the local oscillator (LO) for the down converters.

The outputs of the down converters are amplified by 40 dB and sent to the quadrature phase detectors at 8 GHz. Note that the same sources are used for both up and down conversion, so that the down conversion is coherent with the up conversion, and jitter in the oscillators results in phase noise only at frequencies above that corresponding to the path length difference in the interferometer.

The reflected and transmitted phase detectors are identical. Each IF signal is split in phase and fed to the RF ports on a pair of mixers. The 8-GHz LO signal is split 90° out of phase and fed to the LO ports. The IF ports, therefore, yield quadrature encoded phase information, indicating the phase of the reflected and transmitted signals at the HTSC film. These signals are boosted an additional 20 dB for transmission to the diagnostic chamber at the experimental facility. The signal-to-noise ratio of the reflected channel is greater than 40 dB and the signal-to noise-ratio of the transmitted signal is greater than 100 dB, measured at the IF output of the down converters.

EXPERIMENTAL SETUP The interferometer was placed behind a steel blast shield and surrounded with blast protection to isolate it from the explosives used in the MC-1 generator. Approximately 3 m of WR-10 was used to route the output (and reflected input) to a position 50 cm from the generator. The waveguide was terminated in a standard gain horn. A 50-cm piece of Teflon dielectric waveguide was shaped to fit into the horn, with the dielectric extending 2-3 mm into the straight section. The end of the dielectric was tapered 30° to provide a smoother transition. The other end of the dielectric waveguide was imbedded in the cryostat that held the sample. Another piece of dielectric waveguide extended from the opposite end of the cryostat and, making the same transition to metal waveguide, carried the transmission signal to the other port on the interferometer. The total round trip waveguide loss was approximately 25 dB.

The sample was arranged between the ends of the two dielectric waveguides so that the RF would impinge on the YBCO film. However, as much as half of the signal was transmitted around the sample, limiting the sensitivity of the transmission signal. The reflection signal sensitivity was in turn limited by stray reflections in the waveguide and in the experiment.

CONCLUSION The interferometer successfully produced data which was used to establish the temperature variation of the upper critical field for these superconductor samples.

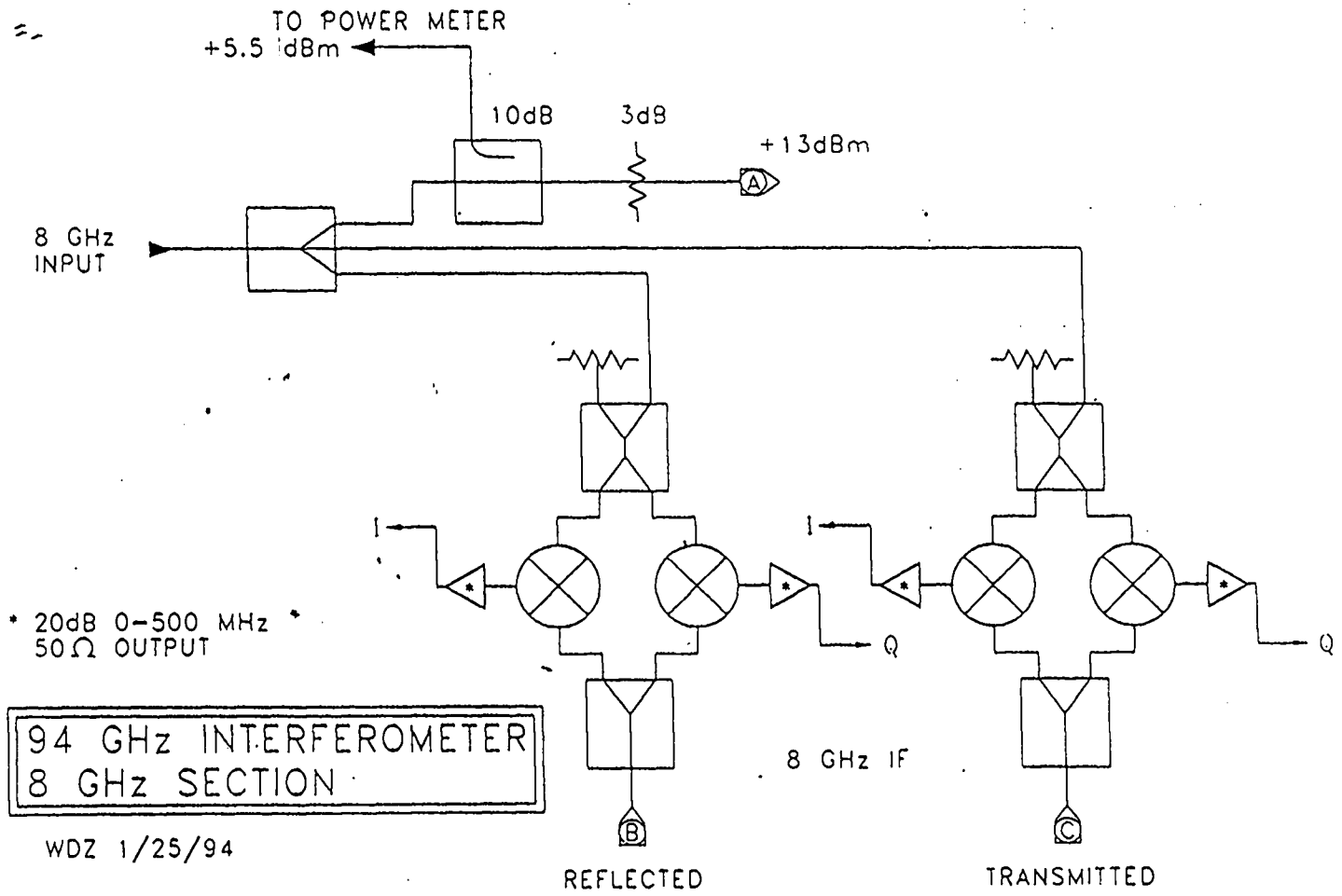


Figure 1. 8 GHz Section

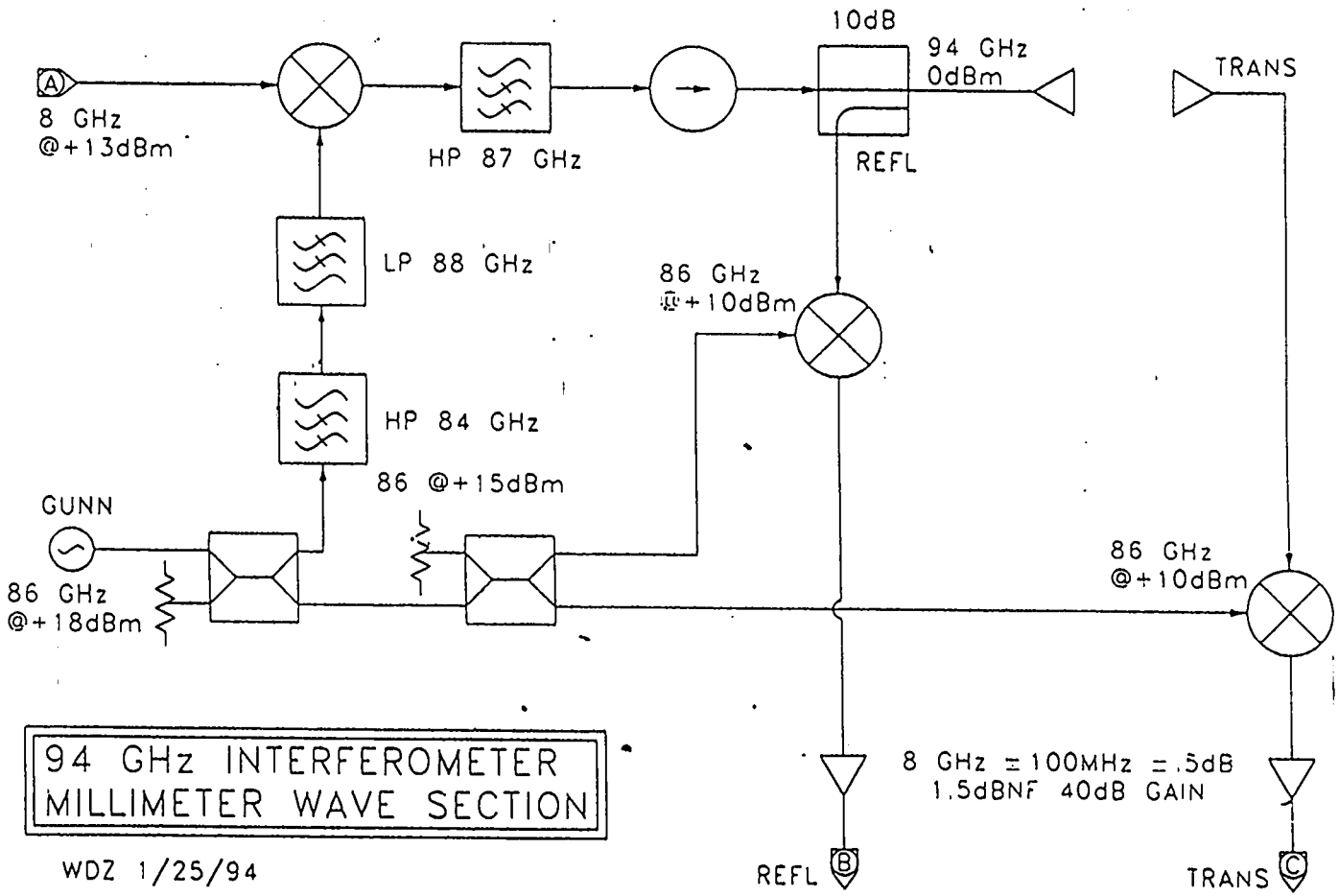


Figure 2. Millimeter Wave section

LA-UR-94-2197

Title: **Complex Microwave Conductivity of $YBa_2Cu_3O_7$ in Magnetic Fields up to 500 T**

Authors: J.D. Goettee, Yu. B. Kudasov, W.D. Zerwekh, A.I. Bykov, M.I. Dolotenko, C.M. Fowler, B.L. Freeman, J.C. King, N.P. Kolokolchikov, W. Lewis, B.R. Marshall, B. Papatheofanis, V.V. Platonov, P.J. Rodriguez, M.G. Sheppard O.M. Tatsenko and L.R. Veeser

Submitted to: M^2S-HTSC IV Fourth International Conference on Materials and Mechanisms of Superconductivity, High Temperature Superconductors, Grenoble, France, 5-9,,July 1994: (Proceedings to be published as a special issue of Physics C, edited by P. Wyder)

Jeffrey D. Goettee
Mail Stop E536
Los Alamos National Laboratory
Los Alamoa, New Mexico, 87545, USA
Phone: 505-665-0264, FAX: 505-665-4311

Complex Microwave Conductivity of $YBa_2Cu_3O_7$ in Magnetic Fields Up to 500T‡

J. D. Goettee[a], Yu. B. Kudasov[b], W. D. Zerwekh[a], A.I. Bykov[b], M. I. Dolotenko[b], C. M. Fowler[a], B.L. Feeman[a], J.C. King[a], N. P. Kolokolchikov[b], W. Lewis[c], B. R. Marshall[c], B. J. Papatheofanis[a], V. V. Platonov[b], P.J. Rodriguez[a], M. G. Sheppard[a], O.M. Tatsenko[b], and L. R. Veeser[a]

[a]Los Alamos National Laboratory, Los Alamos, NM 87545 USA
[b]All-Russian Scientific Research Institute of Experimental Physics, Arzamas-16, Russia 607200
[c]EG&G Energy Measurements, 130 Robin Hill Rd., Goleta, CA 93117 USA

We have measured the complex conductivity of thin films of $YBa_2Cu_3O_7$ (YBCO) superconductor down to temperatures of 4K and magnetic fields up to 500T. The highly oriented films were probed by 94 GHz radiation, with the external magnetic field applied perpendicular to the c-axis. As discussed below, these measurements allowed us to assign a value of 340 ± 40 T for the upper critical field at T=0. The measurements were recently carried out at the pulsed field facility of the National High Magnetic Field Laboratory at Los Alamos using both Russian and American magnetic flux compression generators.

Epitaxial thin films (100 nm) of YBCO have been used to measure the upper critical field for the magnetic field, **B**, perpendicular to the c-axis. A 94 GHz interferometer recorded amplitude and phase information for transmission and reflection of the sample. These signals were analyzed to give the high frequency, complex conductivity of the superconducting film.

Two kinds of high field generators were used in the experiments: the Russian MC-1[1] generator that can generate fields in excess of 1000 T by cylindrical implosion, and the Los Alamos strip generator[2] that produces fields up to 250 T, but in a relatively large, fixed volume. In both systems a modest initial magnetic field is generated (usually from a capacitor bank) in a large area conductor, part or all of which is overlaid with explosives. When the explosives are detonated the initial magnetic flux is forcibly driven into a smaller area. The magnetic fields therefore increase since the flux contained in the system is approximately conserved in the time scales involved in the compression process.

Cooled helium gas or liquid helium was flowed though a foam-plastic cryostat to control the sample temperature, Figure 1. The cryostat supported the sample and wave guide, two Si diodes for temperature monitoring, and both inductive and Faraday rotation probes for field measurement.

An interferometer, centered at 94 GHz, was used to measure the high frequency transmission and reflection. This data was then used to determine the high frequency complex conductivity of the YBCO, after Ref. 3. The microwave radiation was carried by standard

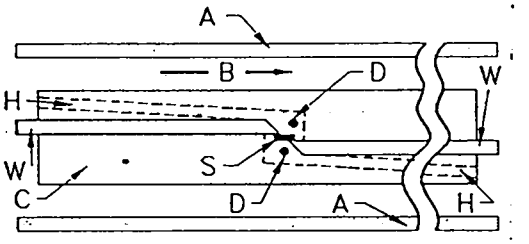


Figure 1. Schematic of the diagnostics inside the MC1 generator. A is the imploding liner, B is the magnetic field direction, C is the cryostat, D are the temperature-sensing diodes, H is the helium cooling channel, S is the sample, and W is the dielectric waveguide. The inductive and Faraday magnetic field probes are near D.

WR-10 waveguide up to the high field region, where it was replaced by rectangular (2 mm x 3 mm) dielectric waveguide. The small guide

‡ Work supported by the U.S. Department of Energy

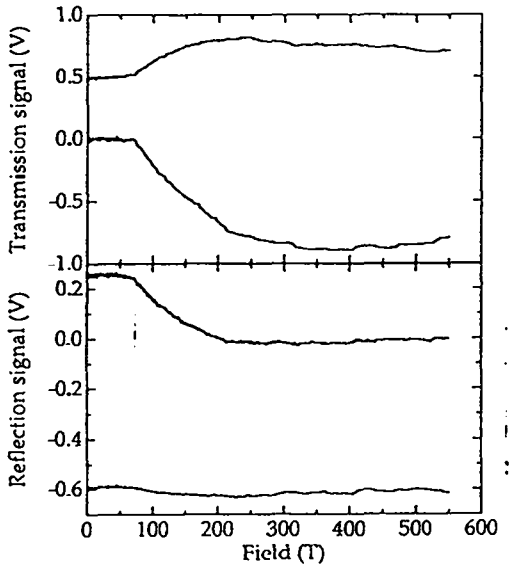


Figure 2. Measured microwave transmission and reflection signals from the 4 K experiment.

dimensions and thus the high frequency were required by space limitations in the cylindrical field generators. The use of common metallic guide was prevented because the sizable **B** fields would destroy the conductor.

Figure 2 shows the transmission and reflection signals of the shot at T = 4 K with amplitude and phase information preserved. The conductivity, $\sigma = \sigma' + i\,\sigma''$, at these high fields is dominated by the vortex dynamics in the superconductor. The probing radiation is at a high enough frequency so that there is a sizable contribution from both the real (σ') and imaginary (σ'') parts of the conductivity. We assume the vanishing of σ'' signifies the end of the superconducting state. Figure 3 shows the conductivities calculated[3] from the data of Figure 2. We assign the value 340±40 T as the field at which σ'' goes to zero and plot this value on Figure 4. (The temperature error bars arise from a temperature rise estimate of ≤ 10 K.) The higher temperature data points shown with appropriate error bars in Figure 4 define a high temperature slope, $dB_{c2}(Tc)/dT \approx -12$ T/K. Our low temperature limit is far below 650 T, the value predicted from the high temperature slope[4].

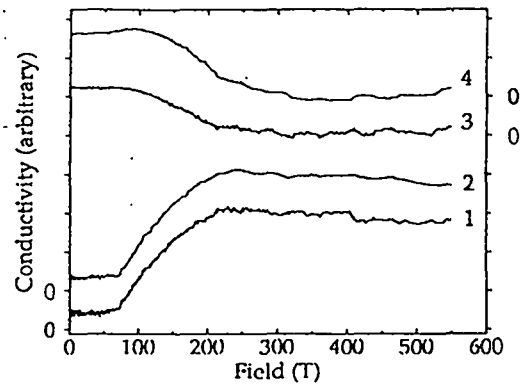


Figure 3. Curves (1) and (3) show, respectively, the real and imaginary conductivities determined from the reflection signals. Curves (2) and (4) give values from transmission signals.

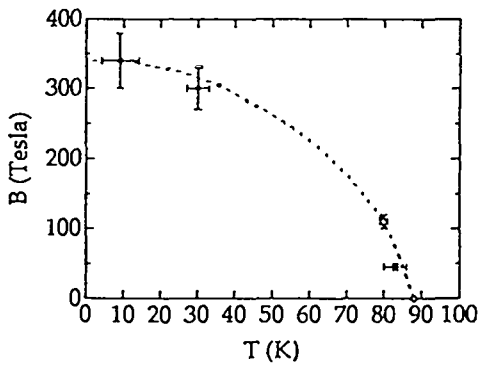


Figure 4. Measured values of B (points), the upper critical magnetic field in the superconductor YBCO, as a function of temperature. The one open point is from earlier work.

REFERENCES

1. A.I. Pavlovskii, *et al.*, Megagauss Physics and Tech., ed. P.J. Turchi (Plenum Press, New York 1980) p.627.
2. C.M. Fowler et al.., Physics in High Magnetic Fields, eds. S. Chikazumi and N. Miura, (Springer, Berlin, 1981) p.54.
3. A.J. Basovich, *et al.*, Phys. Lett. A 163, 322 (1992).
4. N.R. Werthamer, E. Helfand, and P.C. Hohenberg, Phys. Rev. 147, 295 (1966).

NONLINEAR FARADAY EFFECT IN CDS SEMICONDUCTOR IN AN ULTRAHIGH MAGNETIC FIELD

V. V. Druzhinin, O. M. Tatsenko, A. I. Bykov, M. I. Dolotenko,
N. P. Kolokol'chikov, Yu. B. Kudasov, V. V. Platonov, C. M. Fowler,
B. L. Freeman, J. D Goettee, J. C. King, W. Lewis, B. R. Marshall,
B. J. Papatheofanis, P. J. Rodriguez, L. R. Veeser, and W. D. Zerwekh

A significant nonlinearity in the angle of rotation of the polarization plane was observed in CdS at wavelengths of 494-633 nm in the presence of high magnetic fields (0.5-5 MG). The onset of nonlinearity also depended on sample temperature. An optical absorption study with probe wavelength of 494 ± 6 nm revealed an increase in optical transmission associated with a splitting of the conduction band. Dispersion, field and temperature curves indicate a low conduction electron mass $m_e = 0.3\ m_0$. A numerical calculation and interpretation of the observed effects was carried out using band theory. The optical and magnetooptical properties of semiconducting crystals of CdS were studied, reviews of which are presented in.[1,2]

This article describes joint American-Russian experiments to study the optical and magnetooptical properties of CdS in ultrahigh magnetic fields to ~7 MG.

The study of CdS semiconductor was carried out in two kinds of high field systems: the MC-1 generator[3] at temperatures of 100 and 300 K at various wavelengths: 441, 495, 544 and 633 nm and as is discussed later, in a strip generator,[4] at a temperature of 6.5 K over a continuum of wavelengths. The CdS sample had two parallel, polished faces perpendicularly oriented to the C-axis which was, in turn, parallel to the magnetic field, a thickness of h = 0.93 mm, and a transmission spectrum with an absorption band edge in the neighborhood of 510 nm (300K) and 500 nm (100 K).

The optical and magnetooptical properties of CdS semiconductors have a host of interesting characteristics, among which the following can be identified:

1. A large refractive index n = 2.4 in the red spectral region and 3-4 in the region near the absorption edge (blue-green);

2. The manifestation of nonlinearity in the Faraday effect with megagauss fields, which increases with shorter wavelengths and has an upward curving character. In comparison, the majority of other compounds which manifest nonlinearity, exhibit a downward curving slope;

3. An anomalously high positive Verdet coefficient V = 0.5-2 min/cm G in the 500-630 nm spectral region;

4. A shift in the edge of the intrinsic absorption band under the effect of a magnetic field toward shorter wavelengths.

All these characteristics were experimentally observed in magnetic fields to 2 MG.[1] The results of the present joint experiments corroborate the observed effects in magnetic

fields to 7 MG. Thus, at a probe wavelength of 544 nm and T = 100 K, the nonlinearity of the Faraday effect starts to show up visibly in magnetic fields of 1 MG, and at a wavelength of 633 nm and T = 300 K, in fields of 5 MG. Simultaneously with the Faraday effect, the transmission of light through a CdS sample was measured at a probe wavelength of 494 nm ($\Delta\lambda = \pm 6$ nm). With the zero field absorption edge at about 510 nm, initially no light was transmitted. It was noted, however, that when the magnetic field reached a value of ~7.3 MG, a transmitted signal was observed through the CdS sample, which indicated a shift of the absorption band edge to the blue spectral region.

Most of the optical and magnetooptical properties of CdS mentioned above, have been experimentally observed for a relatively long time[1] but have not, to date, been adequately explained. This study proposes a microscopic-phenomenological theory which qualitatively and quantitatively explains these characteristics. The fundamental mechanism for interpreting the optical properties of CdS is based on the calculation of two contributions to the high frequency dielectric susceptibility which are due to a diamagnetic transition into the conduction band and a paramagnetic transition between the valence band and the bottom of the conduction band.

The general formula which describes the dispersion of the refractive index in the absence of a magnetic field has the form:

$$n = \sqrt{\frac{3 + 8\pi N\beta}{3 - 4\pi N\beta}} \tag{1}$$

where N is the molecular concentration of CdS per unit volume; and β is the polarization tensor which is written in the form:

$$\beta = \sum_{m=1}^{n} \frac{2e^2 R_{KM}\omega_{KM}}{\hbar(w_{KM}^2 - \omega^2)} \tag{2}$$

Here R_{KM} is the matrix element between the ground ψ_K and excited ψ_M states; e is the electron charge; ω is the probe frequency and ω_{KM} is the transition frequency.

For the above-mentioned reasons, the summation in Eq. (2) is divided into two basic components having the transition frequencies:

ω_{01} - an indirect transition into the conduction band and,
ω_{02} - an interband transition, that mainly determines the optical properties of CdS.

The subscript 0 here and below refers to value in the absence of a magnetic field. The existence of these transitions verify and corroborate the structure of the energy band in CdS semiconductors, which is shown in Fig. 1.[5]

Thus the value for $4\pi N\beta$ in Eqs. (1) and (2) can be written in the form:

$$4\pi N\beta = \frac{C_1}{\omega_{01}^2 - \omega^2} + \frac{C_2}{\omega_{02}^2 - \omega^2} \tag{3}$$

where C_1 and C_2 are the constants of Eq. (2) and are equal to

$$\frac{4\pi N\beta 2e^2 R_{oi}\omega_{0i}}{\hbar} \; ; \; i = 1,2$$

Substituting the known values[6] $N = N_A\rho/M = 2 \times 10^{22} cm^{-3}, R_{oi} = 2.9 \times 10^{-8} cm$ we find $C_1 = 61 \times 10^{30}$ sec^{-2}; $C_2 = 0.4 \times 10^{30}$ sec^{-2}. With these values from Eq. (3) we obtain the following results: far from the absorption edge, the contribution of Eq. (3) which corresponds to the dispersion curve for the refractive index (Eqs. (1) and (2)) is dominated by the first component due to the large value of C_1. In the region near ω_{02} (the edge of the intrinsic absorption band) the second component also becomes significant. Figure 2 shows the dispersion curve $n(\omega)$ calculated from Eqs. (1–3) with the above values of C_1,C_2 and the values ω_{01} and ω_{02} given in the caption of Fig. 1. As is shown in Fig. 2, the calculated curves are in good agreement with the experimental values, which argues for the validity of the selected model.

The presence of an interband (paramagnetic) contribution to the high frequency susceptibility explains not only the strong increase in n in the region near the intrinsic absorption edge ($\omega_{02} \sim 4 \times 10^{15}$ rad/sec), but also the characteristics of the Faraday effect, specifically the dispersion of the Verdet coefficient and nonlinearity of the Faraday effect.

As a result of the dispersion of the refractive index, it is possible to predict a Faraday effect composed of two basic contributions. This means that the Verdet coefficient for CdS has the following form:

$$V = V_g + V_n \tag{4}$$

Here, V_g is the diamagnetic (positive) component, resulting from the transition $\Gamma_{15} \rightarrow X_1$ with a frequency of $\omega_{01} \simeq 6.64 \times 10^{15}$ rad/sec, and V_n is the paramagnetic (negative) component, resulting from the interband transition $\Gamma_{15} \rightarrow \Gamma_1$ with frequency $\omega_{02} \cong \omega_{g0} \cong 4 \times 10^{15}$ rad/sec.

As known earlier from experimental data,[1] the edge of the absorption band shifts in a magnetic field toward shorter wavelengths. It is possible to predict the frequency of this transition as it shifts in a magnetic field from:

$$\omega_g = \omega_{g0} + \omega_c/2 \tag{5}$$

where $\omega_c = eH/m^*C$ is the cyclotron frequency and m* is the effective mass determined from the extent of the band splitting of the Landau levels.

The dispersion curves for the diamagnetic and paramagnetic components differ. Based on classical predictions, they may be written in the form: $V_g = \text{const} \bullet F_n(\omega) f_1(\omega)$ where $F_n(\omega) = \frac{1}{n}\left(\frac{n^2+2}{3}\right)^2$ is a factor giving the functional dependence of V_g on the radiation frequency through the refractive index, and $f_1(\omega) = \omega_{01}\omega^2/(\omega_{01}^2 - \omega^2)^2$ is the characteristic function for the diamagnetic Faraday effect.

As for the paramagnetic component,

$$V_n = -\text{const}' \bullet F_n(\omega) \bullet f_2(\omega) \text{ where } f_2(\omega) = \frac{w^2}{(\omega_g^2 - \omega^2)} \tag{6}$$

Thus, the Verdet coefficient clearly shows a nonlinear functional dependence on ω which is shown in Fig. 3.

From Fig. 3 it is apparent that the model used and experimental data agree quantitatively. The resulting paramagnetic component can be associated to a large degree with

both the interband transition and exciton states.[7] While a definitive understanding of its characteristics requires additional data, it can still be said that the presence of a minus sign indicates significant splitting of the ground state.

In addition to the dispersion curve for the Verdet coefficient, we can show from Eq. (6) that there is also a functional dependence of the Verdet coefficient on magnetic field, specifically a functional dependence of the paramagnetic component. Let us consider this dependence, the resulting nonlinearity of the Faraday effect, its magnitude and shape. The Verdet coefficient increases with a growth in the magnetic field. While the diamagnetic component V_g does not depend significantly on the magnetic field, the paramagnetic contribution V_n does, through the field dependency of the bandgap edge Δ_g. From Eq. (6) we obtain this change Δ V:

$$\Delta V = \Delta V_n = \text{const}' \bullet F_n(\omega) \frac{2\omega^2 \omega_{g0}}{(\omega_{g0}^2 - \omega^2)^2} \Delta\omega_g \qquad (7)$$

where $\Delta\omega_g = \text{eH}/2\text{m}^*\text{m}_0 C$ determines the shift of the lower Landau sub-level toward shorter wavelengths under the influence of a magnetic field.

From Eq. (7) it follows that ΔV and thus the Verdet coefficient depends upon the magnetic field. The nonlinearity of the Faraday effect in high magnetic fields is thus due to an increase in the energy of the forbidden band through $\Delta\omega_g$ and is associated with a decrease in $|V_n|$. It is also seen from Eq (7) that with an increase in probe radiation frequency, the non-linear Faraday effect increases and can be observed in increasingly weaker fields. Figures 4 and 5 show experimental data and curves calculated from Eq. (7) and exhibit good agreement between the results.

A few additional calculations were carried out. According to the experimental results of[1] for a field of 1.9 MG, $\Delta\lambda_g = 63$ A, or $\Delta\omega_g = 0.035$ eV (5.36×10^{13} rad/sec) which means that the effective mass m^*, expressed in electron mass units is equal to:

$$m^* = \left(\frac{2\Delta\omega_g m_0 C}{eH} \right)^{-1} = 0.312 \quad .$$

This result may be compared with the experimental values.[2]

$$m_p = (0.3 - 0.36) m_0 \qquad m_e \simeq 0.2 m_0$$

The growth in the Verdet coefficient ΔV was calculated from Eq. (7) based on the dependence of the Faraday effect on magnetic field for a probe wavelength of 517 nm in a magnetic field up to 1.2 MG (Fig. 4). For $\Delta\omega_g = 3.38 \times 10^{13}$ rad/sec, H = 1.2 MG, and $\omega = 3.64 \times 10^{15}$ rad/sec; $\Delta V \doteq 0.1$ min/cm G, which is in good agreement with the experimental value.

Thus, in an external ultrahigh magnetic field (with a strongly nonlinear Faraday effect), an interband paramagnetic component arises which has a significant effect on the value of the refractive index, its dispersion, and on the value of the Verdet coefficient, its dispersion and its dependence on field. The value of the paramagnetic component, itself, depends on exciton states, the precise identification of which requires further experimentation.

REFERENCES

1. C. M. Fowler, "Megagauss Field Applications," Informal report, LA-5065-MS, Los Alamos, New Mexico 87544, C. M. Fowler, Science 180, 1973, 261.

2. F. Herlach, "Strong and Ultrastrong Magnetic Fields and Their Applications," (Springer-Verlag, 1985).

3. A. I. Pavlovskii, N. P. Kolokolchikov, O. M. Tatsenko, A. I. Bykov, M. I. Dolotenko and A. A. Karpikov, in Megagauss Physics and Technology, ed. P. J. Turchi (Plenum Press, New York, 1980) p. 627.

4. C. M. Fowler, R. S. Caird, D. J. Erickson, B. L. Freeman and W. B. Garn in Physics in High Magnetic Fields, eds. S. Chikazumi and N. Miura (Springer, Berlin, 1981) p. 54.

5. I. M. Tsidil'kovskiy, "Electrons and Holes in Semiconductors," (Möskva, Nauka, 1972).

6. Reference for R_{oi} (below Eq. 3) and $\omega_{01,2}$ given in Fig.1 caption to be supplied by Olga.

7. I. Bosware, A. K. Lidiard, Proc. Roy. Soc. 269A, 1962, 125.

8. I. Uohida, J. Phys. Soc. of Japan 22, No. 3, 1967, 720-778.

Fig. 1

Structure of the energy bands in CdS semiconductors.[5] The frequency $\omega_{01} = 6.64 \times 10^{15}$ rad/sec (4.37 eV) corresponds to the transition $\Gamma_{15} \rightarrow X_1; \omega_{02} = 4.05 \times 10^{15}$ rad/sec (2.66 eV) to the transition $\Gamma_{15} \rightarrow \Gamma_1$. T = 100 K.

Fig. 2

The calculated (dashed lines) dispersion $n(\omega)$. Δ - experimental values[1], n_1 diamagnetic, n_2 - paramagnetic components (first and second contributions in Eq. (2)).

Fig. 3

Dispersion curve for the Verdet coefficient in CdS in weak magnetic fields. Δ are experimental data,[1] the dashed lines are calculated; V_g, V_n are the respective diamagnetic and paramagnetic components. The solid line represents the sum of the dashed components.

Fig. 4

Dependence of the angle of rotation of the polarization Θ on magnetic field H for various wavelengths in semiconducting CdS.[1,2] The crystal was 1.15 mm-thick. The dashed lines are linear extrapolations from low field data; • - calculated; Δ - experimental

Fig. 5

Dependence of Θ on H for CdS from the joint American-Russian experiments. Crystal thickness was 0.93 mm. Solid lines, calculated; dashed lines, linear extrapolations from low field data; Δ, LANL data; •, Arzamas-16 data.

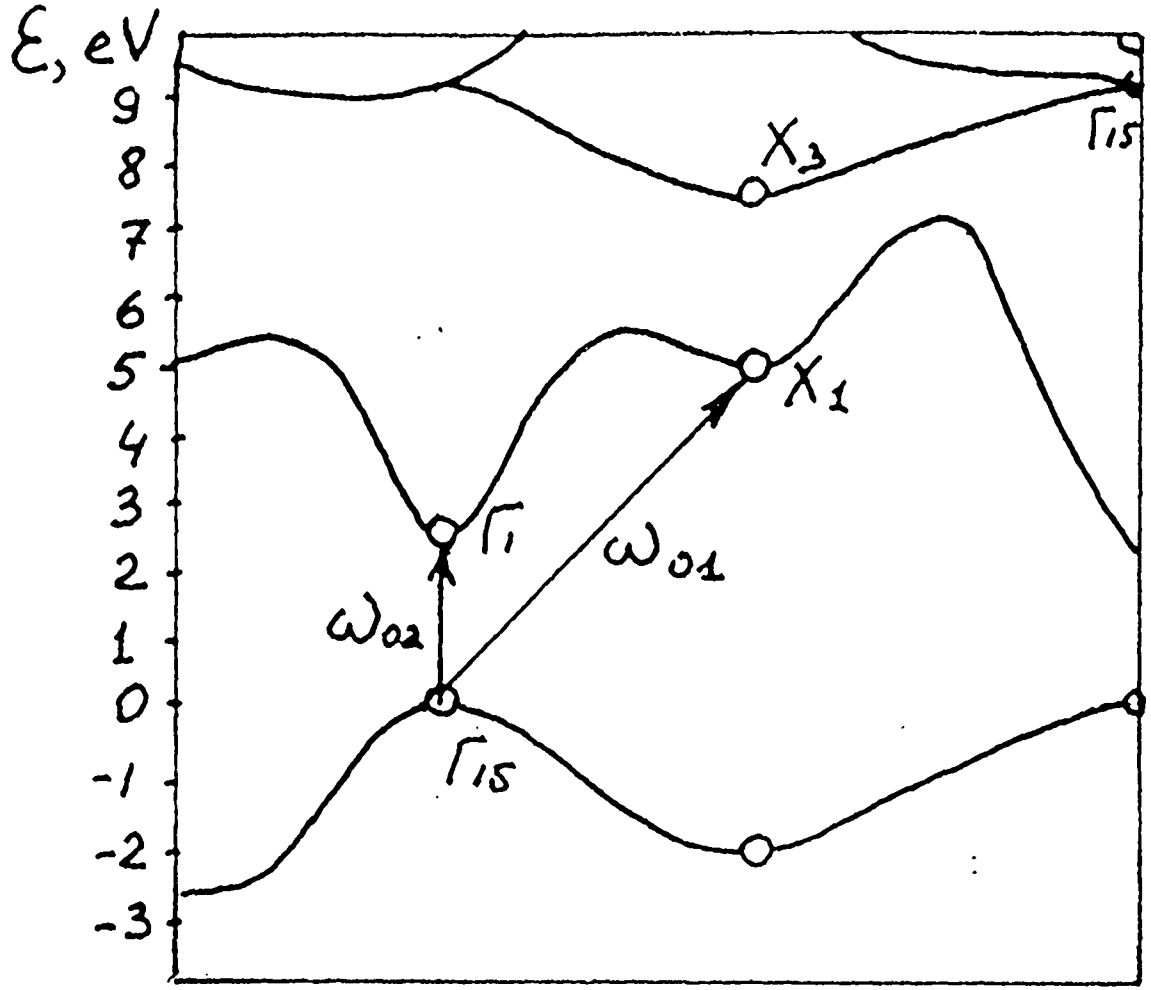


Fig 1.

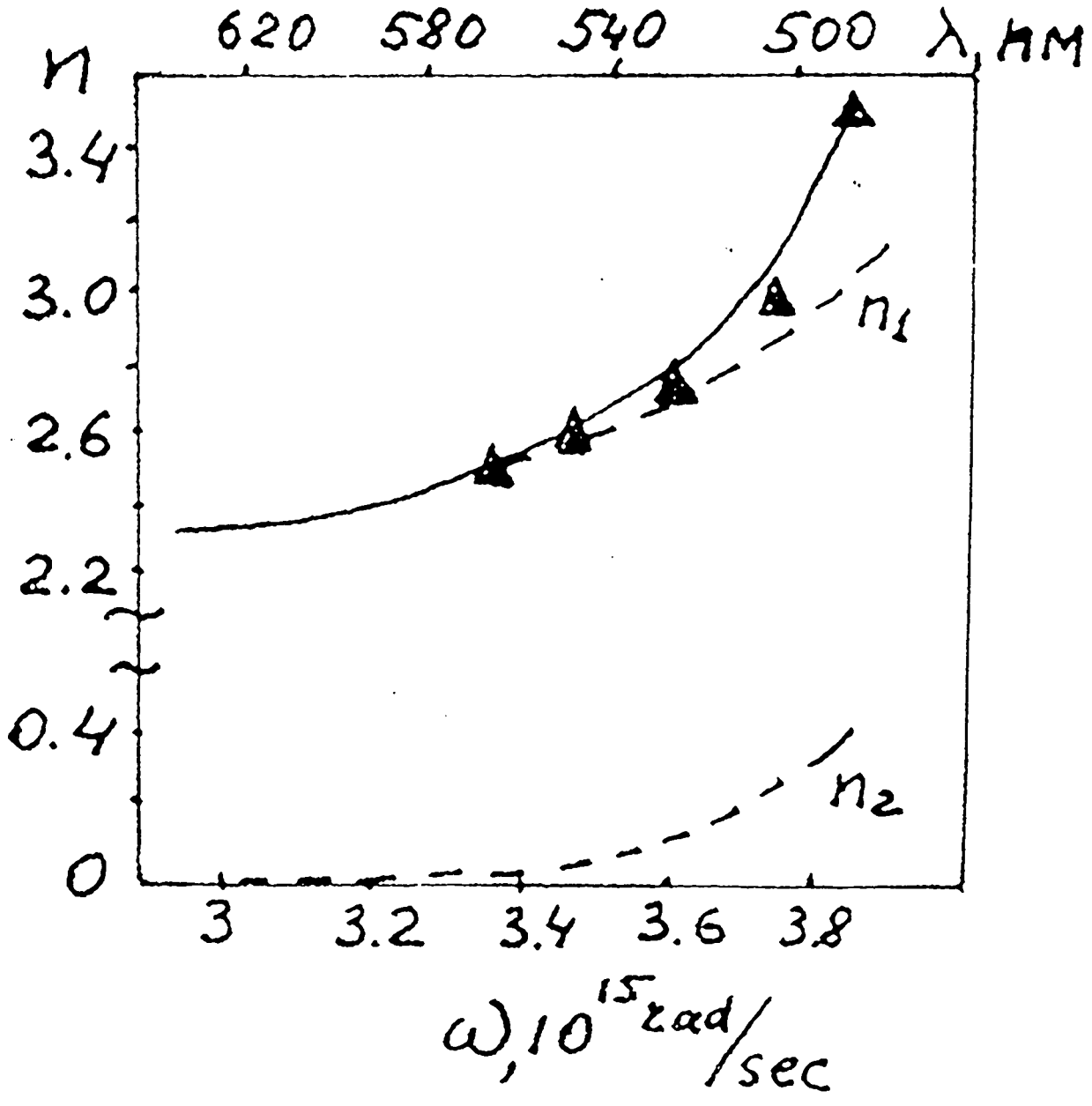

620
580
540
500
λ, нм
n
3.4
3.0
2.6
2.2
0.4
0
n1
n2
3
3.2
3.4
3.6
3.8
ω, 10^15 rad/sec

Fig. 2

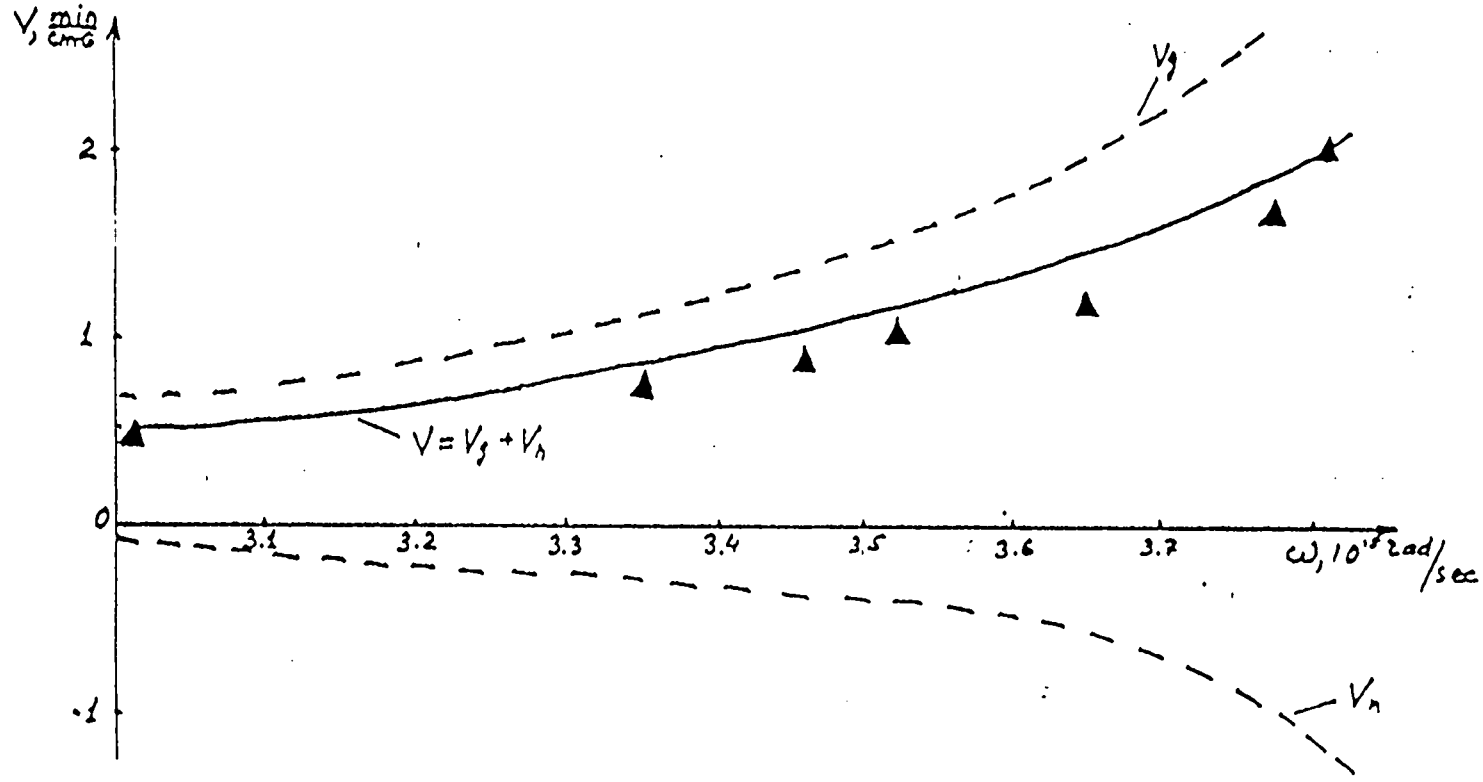


Fig 3

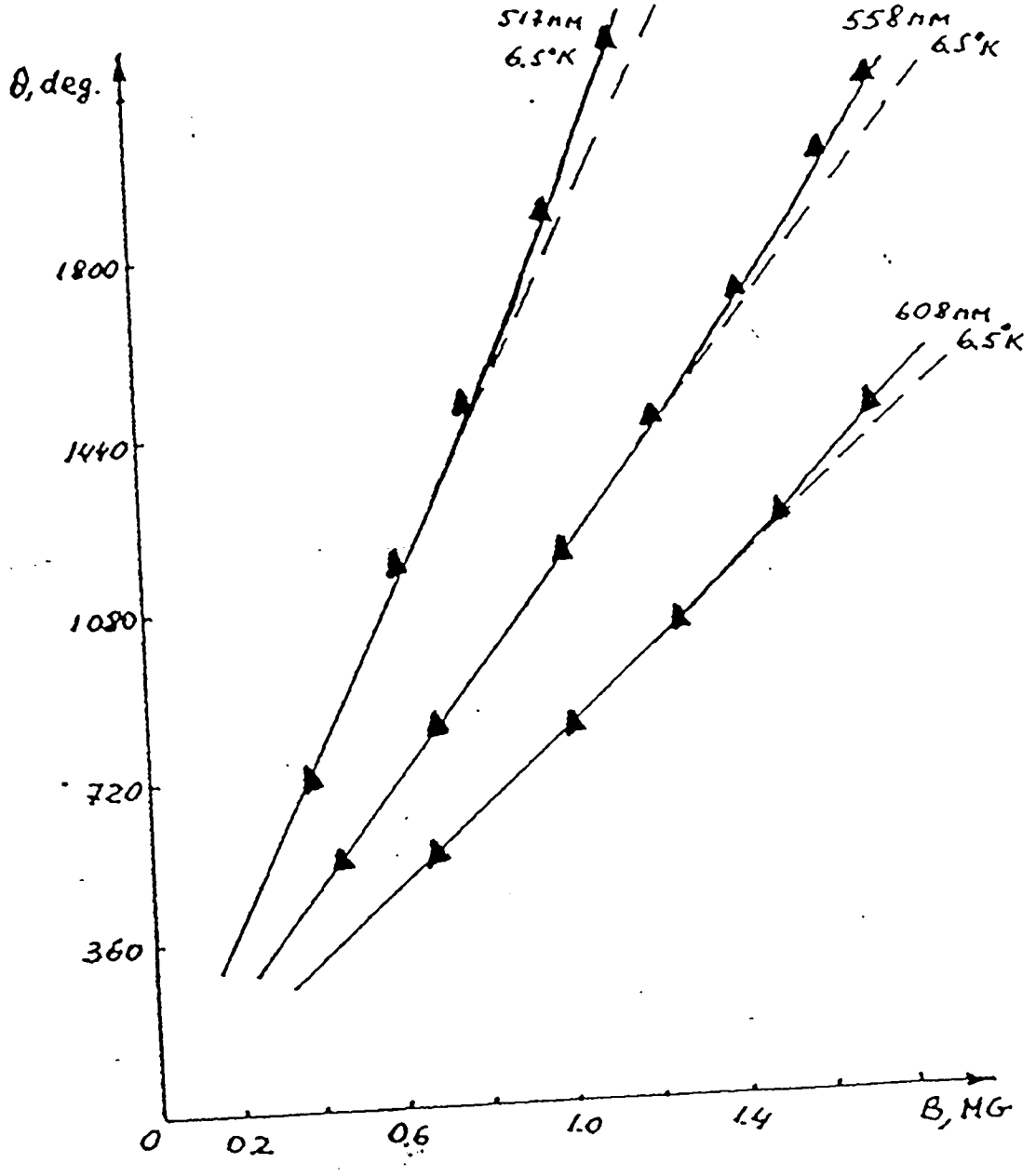

θ, deg.
1800
1440
1080
720
360
0
0.2
0.6
1.0
1.4
B, MG
513nm
6.5°K
558nm
6.5°K
608nm
6.5°K

Fig 4

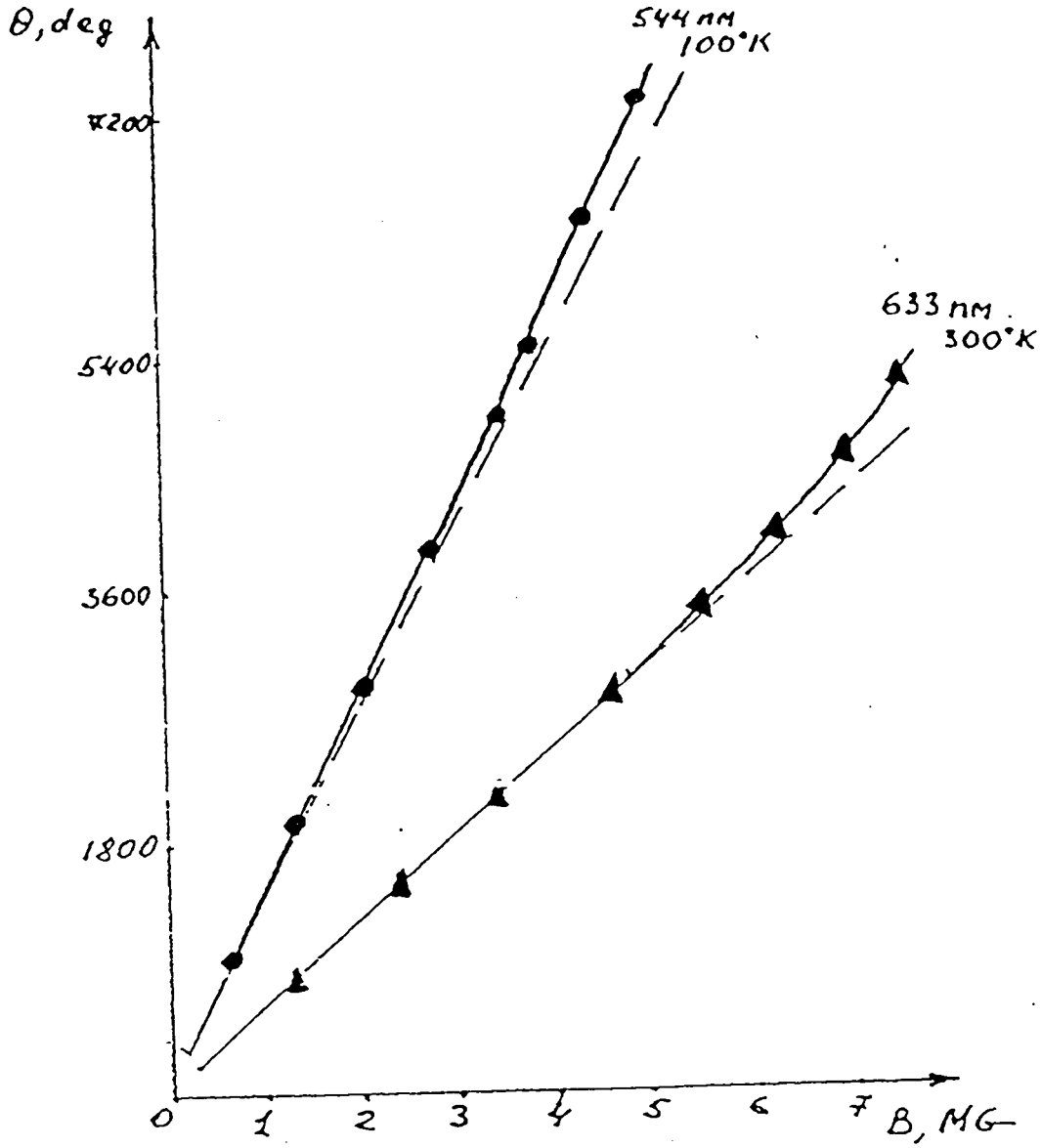


Fig 5

LOS ALAMOS NAT'L LAB.
LIB. REPT. COLLECTION
RECEIVED

'94 SEP 27 PM 10 57